Author's response to reviewer comments for Tomsche et al. (2018)

-Reviewer 1:

The EMAC model, on the other hand, has a much coarser resolution of 2.8x2.8 degrees and 90 levels. Unfortunately the EMAC simulation used is not described in detail, leaving open some important questions: Is EMAC used in an offline CTM mode? If this is the case, what is the model then driven by? Or, in other words: Do both models, the Lagrangian as well as the Eulerian model "see" the same background atmosphere?

What kind of vertical velocity was used for the EMAC simulation? Another important point of course would be the initialization of the model, the length of the simulation and whether a certain spin-up time was necessary.

Since during the analysis of the data results from both models were used simultaneously (e.g. footprints and emission data) or observations of tracers obviously transported upward by convection are compared to distributions modified by vertical transport in EMAC, a more detailed description of the model setup would be very helpful. A very interesting diagnostic in this context would e.g. be the vertical transport time of tracers emitted from the surface to reach the 200 hPa level in EMAC.

Author:

We thank the reviewer for pointing out the lack of information regarding the model simulation. Here additional details are given, also added to manuscript.

Authors changes in manuscript:

P5-6 L30-9: The EMAC model was not run in an offline CTM mode, as the radiation calculations were based on simulated GHGs concentrations. Nevertheless, the model was weakly nudged towards ECMWF ERA Interim data (Jeuken et al., 1996) and therefore reproduced very similar dynamics to the ECMWF model (although not binary identical). The simulation is an extension of simulation RC1SD-base-10 (Jöckel et al. 2016) so to cover the full OMO campaign. Few changes to the original simulation have been applied (i.e. increased South Asia SO_2 emissions and reduced lightning NO_x), as described in Lelieveld et al. (2018). Although the simulation is the continuation of a well evaluated experiment, the simulation was running from March 1st, 2015 so to give time to the SO_2 and NO_x to balance to the new emissions (i.e. 4 months spin up time). Only the data from July and August 2015, which covers the field campaign is actually used. The EMAC model is a hydrostatic model and the convective transport is parameterized (Ouwersloot et al. 2015, Tost et al. 2006). Indication of the vertical transport time in EMAC can be found in Krol et al. (2018), where also a comparison with model of similar complexity is shown.

-Reviewer 1:

The derivation of threshold values for CO and CH_4 to distinguish between the inside of the monsoon anticyclone and the outside by using vertical profiles for NH and SH background and AMA leads to the question, why profiles over Egypt are considered as influenced by AMA and profiles over Cyprus are not. At least a look at the figures showing the different AMA modes (figures 18 to 21) would lead to a different expectation. But this is just judged by visual measure (and only on 204 hPa), so if there are distinct differences between profiles at these locations, the authors would be well advised to please show them. Since the classification of profiles influences the threshold values, this question may be quite important for the further analyses.

Author:

In the classification of the profiles used for the calculation of the Northern hemisphere background and AMA-influenced air masses, respectively, and not only the geographical location but also the meteorological context have been accounted for. The profiles over Egypt were sampled during the second double anticyclone mode, with the westerly part of the anticyclone extending over Egypt. Profiles over Paphos were obtained over a longer period, representing background conditions but partly also AMA-influenced air masses. We calculated the NH background with and without profiles over Paphos. For profiles only over Oberpaffenhofen and Etna the average CH_4 mixing ratio is 1871.2±9.2 ppbv and for profiles over Oberpfafffenhofen, Etna, and Paphos the CH_4 average is 1863.4±14.0 ppbv. Thus the profiles with and without Paphos profiles agree within their standard deviation. Due to a better statistics, we used the NH background profile including profiles over Paphos.,

Authors changes in manuscript:

P7 L5-7: As observed, the CO and CH_4 profiles measured during OMO indicate different altitude distributions depending on the geographical location and partly also on the meteorological situation, especially for Paphos and Egypt. Profiles over Egypt were measured when the AMA extended over this region. Profiles over Paphos were sampled during periods with and without the AMA being positioned over Cyprus.

-Reviewer 1:

The observations shown for the case study for flight 19 indicate a highly structured CO and CH_4 distribution in the vicinity of the AMA boundary region. The distributions simulated by EMAC matches the observations only very roughly. In particular the CH_4 values are underestimated significantly. By looking at the horizontal and vertical distributions one gets the

impression that the vertical transport of the model is probably too weak. This may have several reasons: First, the vertical velocity may be too slow, e. g. the processes leading to strong updraft (namely convection) are too weak or insufficiently parameterized, or second, the numerical horizontal diffusion implied by the coarse grid resolution dampens the strong updraft plumes (approximately above 500 K). Adding horizontal wind as contour lines to the cross sections could shed some light on this problem. The included lines of potential temperature already point into this direction.

Author:

Indeed, the referee is correct in mentioning a possible too low transport of methane and carbon monoxide as a reason for underestimation in the upper troposphere. As shown by Krol et al. (2018), EMAC seems to have a weaker transport of surface tracers than other models. Both reasons suggested by the referee are possible, and it is difficult (if not impossible) to really distinguish the real reason for the underestimation of the transport. Nevertheless we would like to notice that for the comparison of CO with the model, the results are in line with other literature studies at such resolution (e.g. Baret et al., 2016). Horizontal wind components are added to the cross sections in figures 9-12, in detail: eastward wind component in cross sections along a longitude and northward wind component in cross sections along a latitude.

Authors changes in manuscript:

P11 L13-18: The simulated CO pattern, especially the enhanced values over Oman, fits well to the observed CO mixing ratios along the flight track. The EMAC model underestimates CH_4 and CO in the upper troposphere. As shown by Krol et al. (2018), EMAC seems to have a weaker transport of surface tracers than other models. There are two potential reasons for that, but it is difficult to distinguish them. First, a too slow vertical velocity, thus the convective updraft is too ineffective, or second, the numerical diffusion implied by the coarse resolution restricts the updraft too strong. Nevertheless we would like to notice that for the comparison of CO with the model, the results are in line with other literature studies at such resolution (e.g. Baret et al., 2016).

Horizontal wind components are added to the cross sections in Figures 9-12 (P35-41)

-Reviewer 1:

However, although the EMAC distributions may be consistent within the model, these effects may lead to a too small AMA region, when defined by an observational-based CH_4 threshold. A dynamical shape of the AMA could be gained by using

geopotential height or stream function. In this context I would suggest to add some contour lines to the figures displaying the horizontal CO and CH_4 distribution including the threshold values and lower values to give a better visual feedback of the AMA and its position relatively to the flight tracks.

Author:

In Figures 7,8, 18-21 and also in Figures 22 and 23 now contour lines are added for the CH_4 threshold (1879.8 ppbv) and the CH_4 background (1859.4 ppbv) values according to the calculation of the CH_4 threshold in section 3.1. In the horizontal CO distribution also the CH_4 threshold is added. Now the position of the AMA is easier to identify with respect to the flight tracks.

Authors changes in manuscript:

Figures 7,8,(P31-32), 18-21 (P42-45), 22 (P47),23 (P48)

-Reviewer 1:

A comparison between footprints of last PBL contact derived from 10 day backward trajectories from FLEXPART and the surface emissions from EMAC could be much more efficient, when footprints would be graphically added to the surface emission charts.

Author:

Footprint is now added as white contour lines for the number of particles per grid cell = 2 to the surface emission charts for CH_4 and CO (Figures14 and 15).

Authors changes in manuscript:

Figure 14,15 (P38 and P 39)

-Reviewer 1:

The analysis with respect to the different AMA modes defined by the CH4 distribution of the EMAC simulation leads to very interesting results, which are almost impossible to interpret from the values of table 2 without the knowledge of the

flight tracks and the position of the AMA. Probably one could use the distance not to the anticyclonic centers but to the boundaries of the anticyclones.

Author:

In Table 2 we add a column for the relative position to the AMA, which is quite descriptive. As most of the flight tracks are in and outside the AMA a more detailed geographical location with respect to the AMA can be realized better in a graphical way. Thus we added for each flight in the supplement the CH_4 threshold (1879.8ppbv) for the AMA-influence and the background value (1859.4ppbv) as contour lines in the EMAC CH_4 and CO distributions as already done in the manuscript, e.g. Figure 7 and 8 for flight 19. In these plots the position of the flight track with respect to the AMA is more obvious.

Authors changes in manuscript:

Column added in table 2.P46

Table 2: In situ CO and CH_4 for the four different anticyclone situations. Differentiation between AMA and background for each flight between 300-140 hPa.

meteorological situation	flight no.	date	position relative to AMA	in situ at 300-140 hPa							
				CO [ppbv]				CH_4 [ppbv]			
				background	sigma	monsoon	sigma	background	sigma	monsoon	sigma
double anticyclone	#8	21.07.2015	partly in the western AMA	67.8	8.7	89.8	7.4	1847.1	12.3	1898.6	7.8
	#9	25.07.2015	in the western AMA	83.1	9.4	94.5	6.1	1870.0	11.4	1913.7	16.7
	#10	28.07.2015	in the western AMA	76.1	16.4	91.4	5.1	1856.4	24.8	1896.4	12.4
	#11	01.08.2015	partly in residuals of the AMA	92.8	6.8	108.6	4.5	1823.5	21.0	1889.0	4.8
				80.0	10.3	96.1	5.8	1849.3	17.4	1899.4	10.4
central mode	#12/13	06.08.2015	in outflow region	78.6	33.3	117.3	22.2	1827.4	26.8	1893.5	9.8
	#14	08.08.2015	in background south of the AMA	76.3	8.0			1788.2	9.2		
	#15/16	09.08.2015	at the south western edge	77.5	12.0			1812.6	34.3		
	#17/18	10.08.2015	at the south eastern edge and in outflow region	76.5	7.9	98.3	7.8	1832.0	19.5	1909.3	15.0
				77.2	15.3	107.8	15.0	1815.1	22.5	1901.4	12.4
Tibetan mode	#19	13.08.2015	at the western edge of the AMA	74.7	10.4	99.4	13.8	1848.0	16.3	1907.3	20.8
	#20	15.08.2015	at the western edge of the AMA					1855.2	11.6	1905.2	13.9
	#21	18.08.2015	in and outside the AMA	87.9	16.3	104.8	9.8	1853.0	12.9	1917.1	20.6
				81.3	13.4	102.1	11.8	1852.1	13.6	1909.9	18.4
double anticyclone	#22	23.08.2015	at the western edge of the western AMA					1857.0	8.2	1927.9	22.6
	#23	25.08.2015	at the western edge of the western AMA	65.7	12.4	93.8	7.6	1855.9	8.5	1926.4	21.0
	#24	27.08.2015	outside the AMA					1853.7	14.6	1889.1	8.8
				65.7	12.4	93.8	7.6	1855.5	10.4	1914.4	17.5

-Reviewer 1:

The last case study focusing on an outflow event tracked with trajectories and probed twice within 4 days seem to give better agreement with EMAC results (again only judged by visual measure). Maybe an additional figure showing observed and simulated tracer distributions would complement this very interesting manuscript.

Author:

According to the suggestion of the reviewer the CO and CH_4 distributions along the flight track as a time line are added in Figures 24 and 25. The trace gas mixing ratios (observed and simulated) show clear enhancement due to the outflow event for both flights (flight 12/13 and flight 17/18). The outflow regions are marked in grey in the Figures. Additionally, we add in the manuscript the average CO and CH4 mixing ratios calculated from EMAC for the outflow periods for both flights (flight 12/13: CO=112.2±1.2 ppbv and CH_4=1891.7±1.2 ppbv and flight 17/18: CO=90.8±3.1 ppbv and CH_4=1864.6±5.9 ppbv) for a better comparison with the measured data in the outflow.

Authors changes in manuscript:

Figures 24 and 25 added to manuscript P49

P17 L18-22: In the air mass CO and CH_4 mixing ratios increased to 117.3±22.2 ppbv and 1893.5±9.8 ppbv, respectively (background: CO=78.6±33.3 ppbv and CH_4=1827.4±26.8 ppbv), which can be seen in Figure 24. The second probing of this air mass took place at August 10 (flight 17/18, Figure 23) over the Red Sea yielding mixing ratios of 94.2±6.8 ppbv and 1903.7±19.2 ppbv. This corresponds to the increase at around 12-13 UTC in Figure 25.

P17 L25-28: Comparing the EMAC simulations with the in situ data along the flight tracks (Figure 24 and 25), the trends for the outflow agree. The EMAC average mixing ratios for CO and CH_4 are 112.2±1.2 ppbv and CH_4=1891.7±1.2 ppbv for flight 12/13 and 90.8±3.1 ppbv and CH_4=1864.6±5.9 ppbv for flight 17/18, respectively. Thus also the values agree within their standard deviation beside CH_4 in flight 17/18, where the outflow is underestimated by the model.

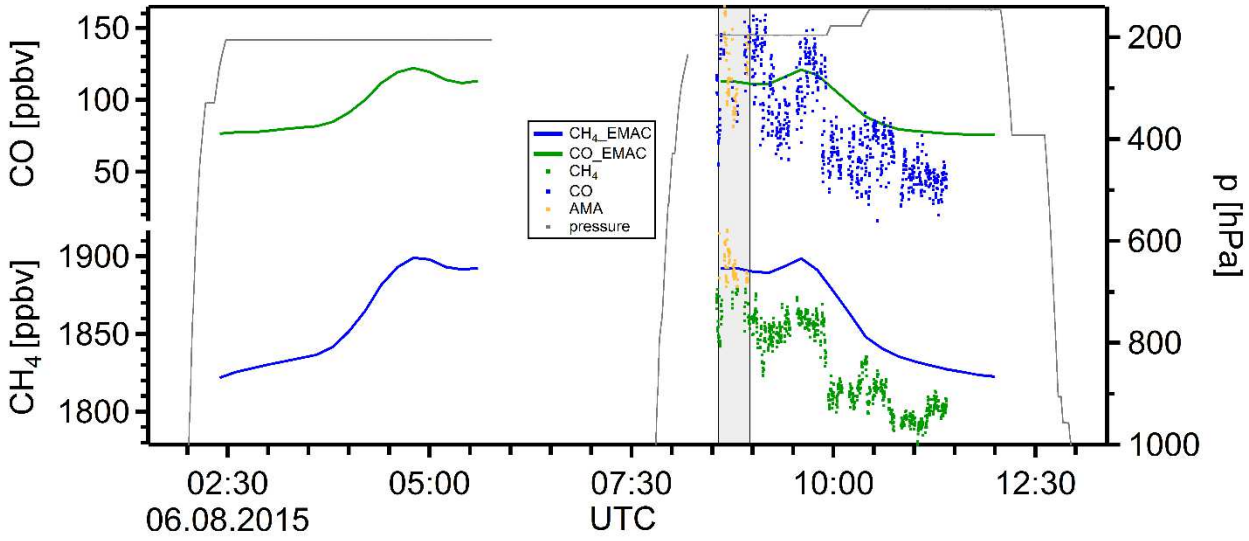

Figure 24: Flight 12/13 (August 6, 2015) in situ CH_4 and CO data and EMAC results along the flight track, as well as the flight altitude. The AMA is colour coded by CH_4>1879.8 ppbv. Outflow region is marked in grey.

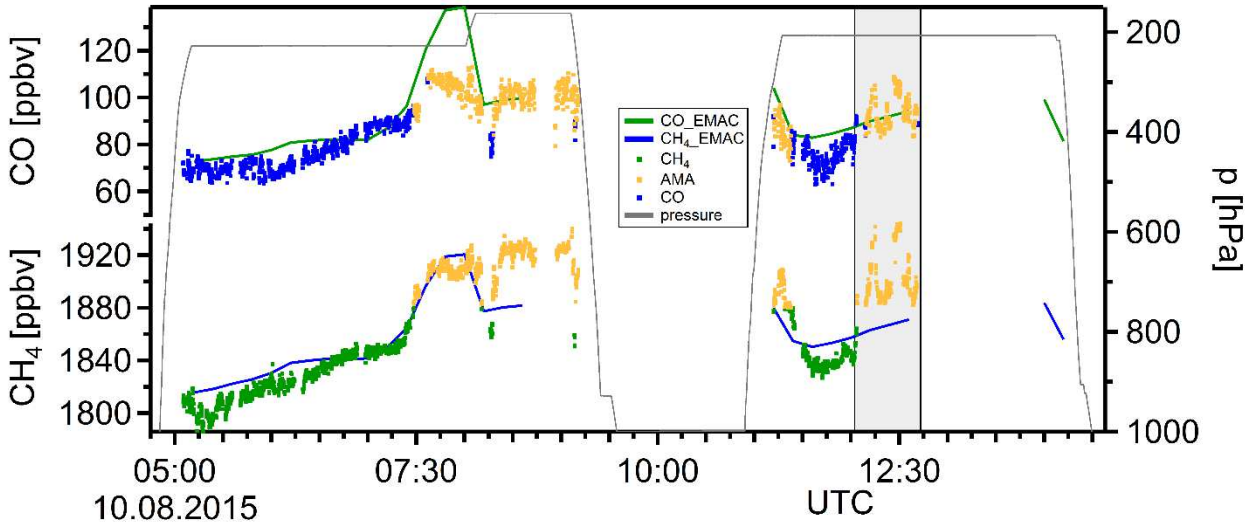

Figure 25: Flight 17/18 (August 10, 2015) in situ CH_4 and CO data and EMAC results along the flight track, as well as the flight altitude. The AMA is colour coded by CH_4>1879.8 ppbv. Outflow region is marked in grey.

-Reviewer 2:

The goal of this study is not clearly stated. Is it to explore transport pathways inside the anticyclone or in the vicinity? For instance, flight 19 suggests the measurements took place outside the anticyclone based on the

boundaries estimated from the model simulations (Fig. 7 & 8). I think it is important to clarify the goal of this study and explain different transport pathways separately.

Author:

The goal of the present study is to understand the transport pathways from the source regions into the upper troposphere via the convective uplift into the AMA and further within the UT, especially towards the southern and western areas of the AMA. The transport pathways in the UT include the transport along the edges of the AMA, the circulation in the AMA where air masses are trapped and the transport across the AMA edges, and the outflow out of the anticyclone due to instabilities in the strong circulation. For instance, flight 19 took place outside and at the western edge of the AMA, which is now better visible in Figures 7 and 8 due to addition of a contour line for the CH_4 threshold.

Authors changes in manuscript: Adapted Figures 7 and 8

P2-3 L32-3: The measurement campaign OMO (Oxidation Mechanism Observations) took place in July/August 2015 with the German High Altitude and Long range (HALO) research Aircraft, performing flights at altitudes between 11 km and 15 km over the above-mentioned regions to investigate the dynamics and atmospheric chemistry in the upper troposphere over five weeks during the monsoon season.

-Reviewer 2:

In introduction, brief background of the Asian monsoon anticyclone and its role in chemical transport in the UTLS region should be mentioned first. Then why in-situ measurements are so valuable but challenging and limited should be mentioned along with pros and cons of other data sources, including, satellite measurements. The purpose of utilizing two separate models should be emphasized. The key factors of OMO field campaign should be included with proper citations as well. Additionally, the goal of this paper and why this paper is unique compared to previous work should be mentioned clearly.

Author:

The introduction is reorganized according to the suggestions of the reviewer.

We used the EMAC model simulations to extend our view on trace gas distributions from the regional scale along flight tracks to a global scale, i.e. horizontal and vertical trace gas distributions, and also to separate different AMA modes. With the second model (FLEXPART) we calculated back trajectories to investigate the emission sources and the transport pathways from the source regions, via the convection into the AMA in the upper troposphere and further westward towards the flight tracks. Thus the back trajectories are mainly used for dynamical processes.

Authors changes in manuscript:

P1-3 L27-21: The Asian monsoon anticyclone (AMA) is an annual, large-scale weather phenomenon in the upper troposphere and lower stratosphere during the boreal summer. It is enclosed by the westerly subtropical jet in the north and the easterly jet in the south and extends over southern Asia and the Middle East up to the Mediterranean. It is formed by diabatic heating in the South Asian monsoon region (Gill, 1980, Hoskins and Rodwell, 1995). The anticyclone is a strong and nearly closed circulation system, which is variable in strength and location (Hsu and Plumb, 2000, Popovic and Plumb, 2001, Garny and Randel, 2013, Ploeger et al., 2015). The strong winds at its edges act as transport barrier for chemical constituents in the upper troposphere. Stratospheric tracers, like ozone, show generally lower concentrations inside the AMA than outside (Park et al., 2008, Randel and Park, 2006). Tropospheric tracers, like CO and CH_4, are uplifted to the upper troposphere by the strong monsoon convection. These chemical constituents can be trapped in the anticyclone, change the atmospheric chemistry in the upper troposphere and lower stratosphere and clearly signify the monsoon influence (Park et al., 2007). The signature of the anticyclone has been identified from different measurement platforms, like satellites and aircrafts. Airborne measurements are rare and limited in time and space but resolve small scales. For example, the in-service airborne projects CARIBIC (Civil Aircraft for the Regular Investigation of the atmosphere Based on an Instrument Container; e.g. Schuck et al., 2012, Rauthe-Schöch et al., 2016) and IAGOS-MOZAIC (IAGOS (In-service Aircraft for a Global Observing System) and MOZAIC (Measurements of OZone by Airbus In-service aircraft); Barret et al., 2016, Dethof et al., 1999) reported trace gas measurements in the Asian monsoon region. In addition aircraft campaigns investigated the Asian monsoon during the aircraft campaign MINOS (Lelieveld et al., 2002, Scheeren et al., 2003) and the Earth System Model Validation (ESMVal) campaign (Gottschaldt et al., 2017). In contrast, satellite data cover a larger spatial area and can be used for long term measurements, nevertheless they are limited to their overpassing track and they have a coarse resolution. The obscured view from clouds during the South Asian monsoon additionally restricts the satellite view (e. g. Ojha et al., 2016), which requires long-term averaging in time and should be complemented by in situ measurements. Satellite data for different trace gases, like H_2O (Park et al., 2004, Randel and Park, 2006), CO (Li et al., 2005, Park et al, 2008) and CH_4 (Park et al., 2004), show the vertical and horizontal extension of the AMA and are generally in agreement with model simulations (e.g. Pan et al., 2016, Nützel et al., 2016, Bergman et al., 2013). To improve model outputs and satellite data retrievals, airborne measurements are necessary,

A more physically motivated criterion to distinguish between the AMA and its surrounding in the upper troposphere is the potential vorticity (PV) (e.g. Ploeger et al., 2015, Garny and Randel, 2013). In the anticyclone PV values on isentropic surfaces are lower than outside. Therefore, a maximum in the PV gradient can be used to identify the horizontal transport barrier associated with the AMA. However, applying the PV criterion is not straightforward since PV values in the AMA increase during the monsoon season and decrease from the extra-tropics towards the tropics, which limits its usefulness. Nevertheless, it is quite helpful in combination with trace gas distributions from in situ and satellite measurements.

During the aircraft campaign MINOS the outflow of the AMA was investigated over the eastern Mediterranean basin (Lelieveld et al., 2002, Scheeren et al., 2003), while during the Earth System Model Validation (ESMVal) campaign a single flight was performed from Male/Maldives to Larnaca/Cyprus in September 2012 that intersected the AMA at an altitude of 150 hPa (Gottschaldt et al., 2017). In situ airborne measurements in the region of the Mediterranean, the Arabian Peninsula, and the Arabian Sea during the monsoon season are still limited, even though the AMA impacts these regions either by its extension or via outflow. Here we present results from an aircraft mission, which focuses on the AMA between the Indian Ocean and the Mediterranean. The measurement campaign OMO (Oxidation Mechanism Observations) took place in July/August 2015 with the High Altitude and Long range (HALO) research Aircraft, performing flights at altitudes between 11 km and 15 km over the above-mentioned regions to investigate the dynamics and atmospheric chemistry in the upper troposphere over five weeks during the monsoon season.

The present study focuses on the measurements of CH_4 and CO, which document long-distance transport of air pollution, as these species have extended lifetimes of 8-9 years (CH_4, Lelieveld et al., 2016) and 2-3 months (CO,

Xiao et al., 2007). These trace gases can be used to identify emission sources from the surface as they are co-emitted with other pollutants. They have both natural and anthropogenic sources. Major CO sources are anthropogenic and emitted via combustion processes of fossil fuel, biomass, and domestic fuel. Its natural sources are mainly from vegetation and oceans, but they are minor (Pandis and Seinfeld, 2006). CH_4 is also emitted by combustion of fossil fuel and biomass (Khalil, 2000). Further sources are rice cultivation and ruminants, but also swamps and flood areas. For wetlands, the uncertainty in CH_4 emissions is still a large concern in atmospheric chemical transport models (Bloom et al., 2017, and references there in). In South Asia anthropogenic emissions increase with a growing population and economic development (Rauthe-Schöch et al., 2016, Ohara et al., 2007). The observations of CH_4 and CO show zonal and meridional concentration gradients as well as vertical gradients in the upper troposphere, allowing to investigate the extent of the AMA. In order to differentiate background from AMA influenced air masses, we derived a CH_4 based threshold. Further, we compared our observations with EMAC model simulations, which extend the view on the trace gas distribution from a regional (along the flight tracks) to a global scale. To study the transport pathways we calculated back trajectories with the Lagrangian particle dispersion model FLEXPART along the flight tracks. With FLEXPART we gained a more detailed insight into the dynamics. We compared the back trajectories with observations of CH_4 and CO to distinguish between different transport pathways. Thus we also studied the origin of emissions within South Asia. Finally, we investigated the variability of the AMA over several weeks as the anticyclone changes its position, extent, and strength due to the monsoon dynamics.P3 L15-21: Further, we compared our observations with EMAC model simulations, which extend the view on the trace gas distribution from a regional (along the flight tracks) to a global scale. To study the transport pathways we calculated back trajectories with the Lagrangian particle dispersion model FLEXPART along the flight tracks. With FLEXPART we gained a more detailed insight into the dynamics. We compared the back trajectories with observations of CH_4 and CO to distinguish between different transport pathways. Thus we also studied the origin of emissions within South Asia. Finally, we investigated the variability of the AMA over several weeks as the anticyclone changes its position, extent, and strength due to the monsoon dynamics.

-Reviewer2:

Abstract of this paper should be a summary of what is shown in this work without including general statements. In the current form, most of the information exists without clearly stating what the goal of this paper is.

Author:

The abstract is revised.

Authors changes in manuscript:

P1 L6-22: The Asian monsoon anticyclone (AMA) is a yearly recurring phenomenon in the northern hemispheric upper troposphere and lower stratosphere. It is part of the South Asian summer monsoon system, and it has a clearly

observable signature due to vertical transport of polluted air masses from the surface to the upper troposphere by the monsoon convection. We performed in situ measurements of carbon monoxide (CO) and methane (CH_4) in the region of monsoon outflow and in background air in the upper troposphere (Mediterranean, Arabian Peninsula, Arabian Sea) by optical absorption spectroscopy on board the High Altitude and Long range (HALO) research aircraft during the OMO (Oxidation Mechanism Observations) mission in summer 2015. We identified the transport pathways and the origin of the trace gases with back trajectories, calculated with the Lagrangian particle dispersion model FLEXPART, and we compared the in situ data with simulations of the atmospheric chemistry general circulation model EMAC. CH_4 and CO mixing ratios were found to be enhanced within the AMA, the in situ data increased on average by 72.1 ppbv and 20.1 ppbv, respectively, originating in the South Asian region (Indio-Gangetic Plain, North East India, Bangladesh and Bay of Bengal). It appears that CH_4 is an ideal monsoon tracer in the upper troposphere due to its extended lifetime and the strong South Asian emissions. Furthermore, we used the measurements and model results to study the dynamics of the AMA over several weeks during the monsoon season, with an emphasis on the southern and western areas in the upper troposphere. We distinguished four AMA modes based on different meteorological conditions. During one occasion we observed that under the influence of dwindling flow the transport barrier between the anticyclone and its surroundings weakened, expelling air masses from the AMA. The trace gases exhibited a distinct fingerprint of the AMA, and we also found that CH_4 accumulated over the course of the OMO campaign.

-Reviewer2:

Section 2 (methods) should include general information about OMO field campaign, including its science goal. What other species were measured during the campaign? What were the science questions? Are there any references?

Author:

General information about the OMO mission are added in the manuscript in the method part in section 2.1 including references.

Authors changes in manuscript:

P3-4 L23-7: The Oxidation Mechanism Observation (OMO) aircraft measurement campaign focused on the self-cleaning capacity of the atmosphere in connection with the Indian summer monsoon. The mission took place in July and August 2015 with flight tracks in the upper troposphere (10-15 km) over the Mediterranean, the Arabian Peninsula, and the Indian Ocean (Figure 1). In South Asia the pollution emissions are growing and during the monsoon season they are uplifted into the upper troposphere. The pollution is partly removed by wet deposition or transformation into soluble gases, or they are involved in air chemistry and transported downwind of the sources. For a broad analysis of the efficiency of the self-cleaning mechanism a large variety of chemical compounds, like CH_4, CO, OH, HO_2, NO_y, SO_2, RO_2, H_2O_2, and total peroxides, were measured during the multi-institutional campaign,

involving the Max-Planck-Institute for Chemistry, Mainz, the Research Centre Jülich, the German Aerospace Center, the Research Centre Karlsruhe, and the universities of Bremen, Heidelberg, and Wuppertal. The main objectives were the oxidation processes and free radical chemistry, the efficiency of convective cloud transport and wet deposition, as well as long-distance transport of air pollution and impacts on air quality and climate change. The OMO mission comprised 111 flight hours during 17 flights. HALO was based alternately at Paphos (Cyprus) and on Gan (Maldives) with refueling stops at the airport of Bahrain. Further information about OMO can be found in Lelieveld et al. (2018) and on the webpage http://www.halo.dlr.de/science/missions/omo/omo.html.

-Reviewer 2:

Section 3.5 (AMA mode) should include discussions of bimodal mode of the monsoon anticyclone shown in Zhang et al. (2002) and Nützel et al. (2016). Also, it should be justified why it is necessary to have four modes instead of two. Is bimodal distribution of the anticyclone wrong?

Author:

A short discussion about bimodality of the AMA is now added I section 3.5.

Authors changes in manuscript:

P15 L8-17: Zhang et al. (2002) presented a bimodality of the AMA with a center position of the anticyclone over the Iranian or the Tibetan Plateau. During OMO we found both positions, which in line with the bimodality assumption. In contrast, Nützel et al. (2016) reported different center positions of the AMA in several models, but most of them did not simulate a preferred bimodality. Regarding the eastern anticyclones during the double anticyclones modes, the positions were in-between the Iranian and Tibetan Plateau (first mode) and in the fourth mode over the Tibetan Plateau. Consequently, they do not support a preferred bimodality. In Zhang et al. (2002) and Nützel et al. (2016) the Iranian and the Tibetan mode are further distinguished by parameters, like diabatic heating, rain patterns or areas of convection, which are out of scope in the present study. Here the focus is on the dynamics with respect to the trace gas distributions. The subdivision into four modes represents the dynamics of the AMA over the course of the campaign.

-Reviewer 2:

The abstract includes a few general statements, which makes abstract sound rather like introduction. For instance, L9-11 (However: : :expected) can be removed.

Author:

L9-11 Sentence is removed.

Authors changes in manuscript: P1, L9-11

-Reviewer 2:

P1, L7 – It is connected to -> It is part of the South Asian summer monsoon system

Author: This has been changed.

Authors changes in manuscript: P1, L7: It is part of the South Asian summer monsoon system

-Reviewer 2:

P1, L17-19 – Are those based on the in-situ measurements?

Author:

Yes, these values are representing the in situ data, but also the simulated data show increased mixing ratios with AMA-influence, as mentioned in section 3.4 The AMA during OMO. In situ increase 72.1 ppbv and 20.1 ppbv and EMAC increase 24.0 ppbv and 14.7 ppbv for CH_4 and CO, respectively.

Authors changes in manuscript:

P1, L14-15: the in situ data increased on average by 72.1 ppbv and 20.1 ppbv, respectively,

-Reviewer 2:

P1, L21 – areas within the upper troposphere -> areas in the upper troposphere

Author:

This has been changed.

Authors changes in manuscript:

P1, L19: areas in the upper troposphere

-Reviewer 2:

P2, L3 – Park et al. (2008) might be relevant here.

Author:

The reference has been added as it is relevant here.

Authors changes in manuscript:

P2, L2: Stratospheric tracers, like ozone, show generally lower concentrations inside the AMA than outside (Park et al., 2008, Randel and Park, 2006).

-Reviewer 2:

P2, L4 – within the strong: : :monsoon -> by the strong monsoon convection

Author:

This has been changed.

Authors changes in manuscript:

P2, L3-: to the upper troposphere by the strong monsoon convection.

-Reviewer 2:

P2, L5 – Park et al. (2007) might be relevant here.

Author:

The reference has been added as it is relevant here.

Authors changes in manuscript:

P2,L5: clearly signify the monsoon influence (Park et al., 2007)

-Reviewer 2:

P2, L9 – physical -> physically

Author:

This has been changed.

Authors changes in manuscript:

P2, L20: A more physically motivated criterion

-Reviewer 2:

P2, L17-18 – Full name for CARIBIC and IAGOS-MIZAIC should be provided here as well.

Author:

The full names are added.

Authors changes in manuscript:

P2, L7-10: CARIBIC (Civil Aircraft for the Regular Investigation of the atmosphere Based on an Instrument Container; e.g. Schuck et al., 2012, Rauthe-Schöch et al., 2016) and IAGOS-MOZAIC (IAGOS (In-service Aircraft for a Global Observing System) and MOZAIC (Measurements of OZone by Airbus In-service aircraft); Barret et al., 2016, Dethof et al., 1999)

-Reviewer 2:

P3, L1- It is also important to mention that there is a big uncertainty in source estimates of methane (Bloom et al., 2017 GMD and references there in).

Author:

The information has been added including the reference.

Authors changes in manuscript:

P3L9-11: Further sources are rice cultivation and ruminants, but also swamps and flood areas. For wetlands, the uncertainty in CH_4 emissions is still a large concern in atmospheric chemical transport models (Bloom et al., 2017, and references there in).

-Reviewer 2:

P3, L8 – 'variability of the AMA' can be explained more detail here.

Author:

A more detailed explanation is now added.

Authors changes in manuscript:

P4:L20-21: Finally, we investigated the variability of the AMA over several weeks as the anticyclone changes its position, extent, and strength due to the monsoon dynamics.

-Reviewer 2:

P4, L8 (section 2.2) – I assume the trajectory calculations are done backward. Where is the initialization location?

Author:

We calculated back trajectories and the initializations are along the flight tracks. The subtitle for section 2.3 is now "FLEXPART back trajectories".

Authors changes in manuscript:

P5 L8: 2.3 FLEXPART back trajectories

-Reviewer 2:

P5, L11 (section 2.4) – The reason why MODIS cloud top pressure is used is missing. Is this used as convective proxy?

Author:

Yes it is used as a proxy for the location of convection to compare the region with the calculated updraft of the back trajectories. This information is added in the actual section 2.5.

Authors changes in manuscript:

P6 L23-24: Cloud top pressure information is used as a proxy for convection. We compared the location of the convective clouds with the location of the uplift of the back trajectories simulated by FLEXPART. The cloud top pressure data are collected from the MODIS instrument on board of AQUA

-Reviewer 2:

P5, L28 – I would like to know if there are any in-situ measurements of methane and if so how the mixing ratios compare with them even over different regions in different season.

Author:

Yes, there are other in situ profiles. Lelieveld et al. (2002) measured profiles over the Mediterranean in summer 2001 during MINOS. They have observed enhanced CH_4 and CO values in the UT, especially during stronger influence from the AMA in the UT with CH_4 mixing ratios up to ca. 1890 ppbv. Bergamaschi et al. (2013) presented CH_4 profiles over the pacific in dependence of the latitude observed in 2009. The CH_4 mixing ratios decrease from the northern hemisphere to the southern hemisphere. The highest values are reported for the lower troposphere in the northern hemisphere (around 1882 ppbv). In the UT CH_4 increases towards the tropics to around 1800 ppbv.

Authors changes in manuscript:

P7 L10: is now the position for the authors answer in the manuscript.

-Reviewer 2:

P5, L30 – I have tried to find CO observations from satellite in Randel and Park (2006) but they seem to have used only ozone and water vapor.

Author:

The reference was wrong and the right one is Park et al. (2007).

Authors changes in manuscript:

P7,L12: Park et al. (2007) used CO observations from satellites and wind fields

-Reviewer 2:

P5, L31 – to identified -> to identify

Author:

This has been changed.

Authors changes in manuscript:

P7 L13: to identify monsoon influenced

-Reviewer 2:

P6, L8 -12 – This paragraph is not convincing to me without supporting material or references

Author:

The paragraph is rewritten including supporting material and references.

Authors changes in manuscript:

P7 L22-26: The observed CH_4 increase with height can be explained by the global circulation. . In the boundary layer CH_4 mixing ratios are influenced by turbulent mixing close to emission sources or by horizontal advection in remote places (Saito et al., 2013). At the surface the air at Gan is influenced by wind from southern directions with low CH_4 mixing ratios originating from the southern Indian Ocean. High altitude advection leads to interhemispheric transport (Saito et al., 2013) thus to transfer of higher CH_4 mixing ratios from the NH into the SH, which have been convectively uplifted from the boundary layer.

-Reviewer 2:

P6, L18 – This is in consistent -> This is consistent

Author: This has been changed.

Authors changes in manuscript:

P8 L1: This is consistent with the observed upper tropospheric increase of CO and CH_4 in the NH background profiles

-Reviewer 2:

L6, L20-22 – Do the mixing ratios of CO in the upper troposphere agree as well?

Author:

Park et al., 2008 reported CO MR in the UT (10-15km) of around 100ppbv in the AMA and 65-90 ppbv outside. We measured in 10-14km around 74.0±15.2 ppbv and outside of 71.2±10.0 ppbv. Park et al., 2008 defined the AMA by a CO threshold opposite to our CH_4 approach and in our profiles inside and outside events are included, only separated by their location, which leads to a smaller difference in the CO mixing ratios for background and AMA-influence in the UT.

Authors changes in manuscript:

P8 L1-5-6: CO mixing ratios in the upper troposphere inside the AMA (around 100 ppbv in 10-15 km) in comparison to air outside the AMA (65-90 ppbv in 10-15 km).

Reviewer 2:

P6, L30-31- Does this problem prevented from using the measurement or only degraded the data quality of CO measurements?

Author:

This problem only degraded the data quality of CO measurements.

Authors changes in manuscript:

P8 L14-15: is now the position for the authors answer in the manuscript.

-Reviewer 2:

P7, Eq. (1) – I think this threshold is somewhat subjective. At least it should be mentioned that this might introduce uncertainty in the analyses and also how sensitive the results are depending on the threshold values.

Author:

The threshold is a simple tool to distinguish between background air masses and air masses influenced by the monsoon. It is based on in situ measurements and it is subjectively chosen, however its application to the in situ data showed a reasonable differentiation. The threshold itself was not applied to the EMAC data along the flight tracks and in the histograms (Figures 16 and 17) as the model underestimated the in situ measurements. The in situ CO and

the EMAC data are distinguished into AMA-influence and background according to the time, when the in situ CH_4 was above or below the CH_4 threshold. Nevertheless the CH_4 threshold is represented in the EMAC horizontal trace gas distributions as a contour line for a better orientation of the AMA position. Consequently the analyses depend on the threshold. A change in the absolute value would increase or decrease the region which we assumed to be influenced by the monsoon.

Authors changes in manuscript:

P8 L22: In situ CH_4 mixing ratios

P8 L25-29: Further evaluation depends on the CH_4 threshold and thus the results are sensitive to it. Nevertheless also other compounds measured during OMO showed the isolation of the anticyclone in the UT (Lelieveld et al., 2018) which confirms the usefulness of CH_4. With a change in the absolute value the region which is supposed to be AMA-influenced will be either larger or smaller, thus the edge of the anticyclone would be differently defined but the whole dynamical process is not significantly changing.

-Reviewer 2:

P7, L28 – Does the difference between Scheeren et al. (2003) and this study agrees with the values in Zimmermann et al. (2018) quantitatively?

Author:

Zimmermann et al. (2018) calculated a CH_4 mixing ratio of 1781 ppbv for the upper troposphere between 2000 and 2006. The CH_4 values in Scheeren at al. (2003) are 1819±26 ppbv for North America/North Atlantic origin and 1882±21 oobv for South Asia origin. The value in Zimmermann et al. (2018) is a global average over seven years in contrast to the values of Scheeren et al. (2203), which represent only one summer month of northern hemispheric origin, thus not accounting for the lower southern hemispheric CH_4 mixing ratios. Zimmermann et al. (2018) increased the CH_4 mixing ratio due to additional CH_4 emissions starting in 2007 up to 1815 ppbv for 2015. In this study the CH_4 mixing ratio is in average 1866.4±43.0 ppbv.

Authors changes in manuscript:

P9 L21: is now the position for the authors answer in the manuscript.

-Reviewer 2:

P8, L13 – cloud top height pressure -> cloud top pressure (also in P10, L23)

Author:

This has been changed.

Authors changes in manuscript:

P10 L6: cloud top pressure

P12 L23: cloud top pressure

-Reviewer 2:

P8, L16-17 – This sentence should be revised for clarity.

Author:

The sentence is rewritten.

Authors changes in manuscript:

P11 L9-10: Matches were generally found over the Bay of Bengal, the Indo-Gangetic Plain, Bangladesh, the north easern region of India, and Myanmar. During the days when the back trajectories passed over central India, convection occurred also in this area, but the cloud top pressure was at a lower altitude than the height of the trajectories.

-Reviewer 2:

P8, L34 – high pressure -> anticyclonic

Author:

This has been changed.

Authors changes in manuscript:

P11 L27: the anticyclonic circulation

-Reviewer 2:

P9, L13 (Figs. 7 & 8) – Here, it looks like the flight path is outside the anticyclone based on the model simulations. The high values from the flight almost should be at the center of the anticyclone. I am not sure how to understand those comparisons.

Author:

We added contour lines for the CH_4 threshold (1879.8 ppbv) and the CH_4 background (1859.4 ppbv) value in Figure 7 and 8 according to the suggestion of reviewer 1. The flight track crosses the edge of the AMA with higher mixing ratios inside the AMA, which can be seen in the measured and the modeled data. The difference between the in situ and simulated values show that on a regional scale the model is not able to reproduce the reality with respect to the absolute values.

Authors changes in manuscript:

Figure 7 and 8(P31, P32) (P11 L8-9: is now the position for the authors answer in the manuscript.)

-Reviewer 2:

P15, L29 – Instead of 'these transport' describe specific transport processes here

Author:

A detailed description of the transport processes is added.

Authors changes in manuscript:

P1 L19-21: In the present work, we address the transport pathways, including the convective transport from the boundary layer into the UT, the circulation in the AMA, the transport at and across the edges of the AMA, associated with outflow events and further transport in the UT partly in connection with the jet streams.

Upper tropospheric CH_4 and CO affected by the South Asian summer monsoon during OMO

Laura Tomsche[1], Andrea Pozzer[1], Narendra Ojha[1], Uwe Parchatka[1], Jos Lelieveld[1], Horst Fischer[1]

[1]Department of Atmospheric Chemistry, Max-Planck-Institute for Chemistry, Mainz, 55128, Germany

Correspondence to: Laura Tomsche (laura.tomsche@mpic.de)

Abstract. The Asian monsoon anticyclone (AMA) is a yearly recurring phenomenon in the northern hemispheric upper troposphere and lower stratosphere. It is part of ~~connected to~~ the South Asian summer monsoon system, and ~~the circulation extends approximately across 20°-120°E and 15°-40°N longitude-latitude. It~~it has a clearly observable signature due to vertical transport of polluted air masses from the surface to the upper troposphere by the monsoon convection. ~~However, the transport pathways and the fate of pollutants in the upper troposphere are not yet fully understood. As pollution emissions in South Asia are increasing, changes in the chemical composition of the AMA can be expected.~~ We performed in situ measurements of carbon monoxide (CO) and methane (CH_4) in the region of monsoon outflow and in background air in the upper troposphere (Mediterranean, Arabian Peninsula, Arabian Sea) by optical absorption spectroscopy on board the ~~German~~ High Altitude and Long range (HALO) research aircraft during the OMO (Oxidation Mechanism Observations) mission in summer 2015. We identified the transport pathways and the origin of the trace gases with back trajectories, calculated with the Lagrangian particle dispersion model FLEXPART, and we compared the in situ data with simulations of the atmospheric chemistry general circulation model EMAC. CH_4 and CO mixing ratios were found to be enhanced within the AMA, the in situ -data increased on average by 72.1 ppbv and 20.1 ppbv, respectively, originating in the South Asian region (Indio-Gangetic Plain, North East India, Bangladesh and Bay of Bengal). It appears that CH_4 is an ideal monsoon tracer in the upper troposphere due to its extended lifetime and the strong South Asian emissions. Furthermore, we used the measurements and model results to study the dynamics of the AMA over several weeks during the monsoon season, with an emphasis on the southern and western areas ~~with~~in the upper troposphere. ~~For example, w~~We distinguished four AMA modes based on different meteorological conditions. During one occasion we observed that under the influence of dwindling flow the transport barrier between the anticyclone and its surroundings weakened, expelling air masses from the AMA. The trace gases exhibited a distinct fingerprint of the AMA, and we also found that CH_4 accumulated over the course of the OMO campaign.

1 Introduction

The Asian monsoon anticyclone (AMA) is an annual, large-scale weather ~~yearly recurring~~ phenomenon in the upper troposphere and lower stratosphere during the boreal summer. It is enclosed by the westerly subtropical jet in the north and the

Kommentiert [TL1]: The abstract is revised.

Kommentiert [TL2]: This has been changed.

Kommentiert [TL3]: Sentence is removed.

Kommentiert [TL4]: Yes, these values are representing the in situ data, but also the simulated data show increased mixing ratios with AMA-influence, as mentioned in section 3.4 The AMA during OMO. In situ increase 72.1 ppbv and 20.1 ppbv and EMAC increase 24.0 ppbv and 14.7 ppbv for CH_4 and CO, respectively.

Kommentiert [TL5]: This has been changed.

Kommentiert [TL6]: The introduction is reorganized according to the suggestions of the reviewer.

easterly jet in the south and extends over southern Asia and the Middle East up to the Mediterranean. It is formed by diabatic heating in the South Asian monsoon region (Gill, 1980, Hoskins and Rodwell, 1995). The anticyclone is a strong and nearly closed circulation system, which is variable in strength and location (Hsu and Plumb, 2000, Popovic and Plumb, 2001, Garny and Randel, 2013, Ploeger et al., 2015). The strong winds at its edges act as transport barrier for chemical constituents in the upper troposphere. Stratospheric tracers, like ozone, show generally lower concentrations inside the AMA than outside (Park et al., 2008, Randel and Park, 2006). Tropospheric tracers, like CO and CH_4, are uplifted to the upper troposphere by ~~within~~ the strong monsoon convection ~~of the monsoon.~~ These chemical constituents can be trapped in the anticyclone, change~~ing~~ the atmospheric chemistry in the upper troposphere and lower stratosphere and clearly signify the monsoon influence ~~(~~(Park et al., 2007)~~Park et al., 2007)~~. The signature of the anticyclone has been identified from different measurement platforms, like satellites and aircrafts. Airborne measurements are rare and limited in time and space but ~~they~~ resolve small scales. ~~There are~~For example, the in-service airborne projects CARIBIC (Civil Aircraft for the Regular Investigation of the atmosphere Based on an Instrument Container; e.g. Schuck et al., 2012, Rauthe-Schöch et al., 2016) and IAGOS-MOZAIC (IAGOS (In-service Aircraft for a Global Observing System) and MOZAIC (Measurements of OZone by Airbus In-service aircraft); Barret et al., 2016, Dethof et al., 1999)~~, which~~ reported trace gas measurements in the Asian monsoon region. In addition aircraft campaigns investigated the Asian monsoon~~, like~~ during the aircraft campaign MINOS (Lelieveld et al., 2002, Scheeren et al., 2003) and~~or~~ the Earth System Model Validation (ESMVal) campaign (Gottschaldt et al., 2017).~~Airborne measurements are rare and represent only on temporary and spacial restricted scales but resolve small scales.~~ In contrast, satellite data cover a larger spa~~e~~tial area and can be used for long term measurements, nevertheless they are limited to their~~represent mostly one~~ overpassing track~~flight time~~ and they have a coarse~~r~~ resolution. The obscured view from~~by~~ clouds ~~in~~during the South Asian monsoon ~~restricts~~ additionally restricts the satellite ~~data~~view (e. g. Ojha et al., 2016), which requires long-term averaging in time and should be complemented by in situ measurements. ~~Moreover, s~~Satellite data for different trace gases, like H_2O (Park et al., 2004, Randel and Park, 2006), CO (Li et al., 2005, Park et al, 2008) and CH_4 (Park et al., 2004), show the vertical and horizontal extension of the AMA and ~~which~~ are generally in agreement with model simulations (e.g. Pan et al., 2016, Nützel et al., 2016, Bergman et al., 2013). ~~Global models simulate the AMA as a dynamic pattern on a global scale, but a detailed resolution (e.g. the distribution and the absolute mixing ratios of trace gases) is more dependent on the grid size of the model itself, the parameterization of the convection, and the emission inventory.~~ To improve model outputs and satellite data retrievals, airborne measurements are necessary.

A more physically motivated criterion to distinguish between the AMA and its surrounding in the upper troposphere is the potential vorticity (PV) (e.g. Ploeger et al., 2015, Garny and Randel, 2013). In the anticyclone PV values on isentropic surfaces are lower than outside. Therefore, a maximum in the PV gradient can be used to identify the horizontal transport barrier associated with the AMA. However, applying the PV criterion is not straightforward since PV values in the AMA increase

Kommentiert [TL7]: The reference has been added as it is relevant here.

Kommentiert [TL8]: This has been changed.

Kommentiert [TL9]: The reference has been added as it is relevant here.

Kommentiert [TL10]: The full names are added.

Kommentiert [TL11]: This has been changed.

during the monsoon season and decrease from the extra-tropics towards the tropics, which limits its usefulness. Nevertheless, it is quite helpful in combination with trace gas distributions from~~, gained by~~ in situ and satellite measurements.

During the aircraft campaign MINOS the outflow of the AMA was investigated over the eastern Mediterranean basin (Lelieveld et al., 2002, Scheeren et al., 2003), while during the Earth System Model Validation (ESMVal) campaign a single flight was performed from Male/Maldives to Larnaca/Cyprus in September 2012 that intersected the AMA at an altitude of 150 hPa (Gottschaldt et al., 2017). ~~As mentioned above, trace gas distributions can be obtained from satellite data. However, the vertical and horizontal resolution of satellite data is coarse, in addition to the obscured view by clouds in South Asian monsoon (e. g. Ojha et al., 2016), which requires long-term averaging in time and should be complemented by in situ measurements. The in-service airborne projects CARIBIC (Civil Aircraft for the Regular Investigation of the atmosphere Based on an Instrument Container; e.g. Schuck et al., 20126, Rauthe-Schöch et al., 2016) and IAGOS-MOZAIC (IAGOS (In-service Aircraft for a Global Observing System) and MOZAIC (Measurements of OZone by Airbus In-service aircraft); Barret et al., 2016, Dethof et al., 1999) reported trace gas measurements in the Asian monsoon region. Moreover, during the aircraft campaign MINOS the outflow of the AMA was investigated over the eastern Mediterranean basin (Lelieveld et al., 2002, Scheeren et al., 2003), while during the Earth System Model Validation (ESMVal) campaign a single flight was performed from Male/Maldives to Larnaca/Cyprus in September 2012 that intersected the AMA at an altitude of 150 hPa (Gottschaldt et al., 2017).~~ In situ airborne measurements in the region of the Mediterranean, the Arabian Peninsula, and the Arabian Sea during the monsoon season are still limited, even though the AMA impacts these regions either by its extension or via outflow. Here we present results from an aircraft mission, which focuses on the AMA between the Indian Ocean and the Mediterranean. The measurement campaign OMO (Oxidation Mechanism Observations) took place in July/August 2015 with the ~~German~~ High Altitude and Long range (HALO) research Aircraft, performing flights at altitudes between 11 -km and 15 -km over the above-mentioned regions to~~and~~ investigate~~document~~ the dynamics and atmospheric chemistry in the upper troposphere over five weeks during the monsoon season.~~ HALO was based alternately at Paphos (Cyprus) and on Gan (Maldives) with refuelling stops at the airport of Bahrain. Flights were generally made at altitudes between 11 km and 15 km to investigate the upper troposphere.~~

The present study focuses on the measurements of CH_4 and CO, which document long-distance transport of air pollution, as these species have extended lifetimes of 8-9 years (CH_4, Lelieveld et al., 2016) and 2-3 months (CO, Xiao et al., 2007). These trace gases can be used to identify emission sources from the surface as they are co-emitted with other pollutants. They have both natural and anthropogenic sources. Major CO sources are anthropogenic and emitted via combustion processes of fossil fuel, biomass, and domestic fuel. Its natural sources are mainly from vegetation and oceans, but they are minor (Pandis and Seinfeld, 2006). CH_4 is also emitted by combustion of fossil fuel and biomass (Khalil, 2000). Further sources are rice cultivation and ruminants~~swamps and flood areas~~, but also swamps and flood areas~~rice cultivation and ruminants~~. For wetlands, t~~T~~he uncertainty in CH_4 emissions ~~from wetlands~~ is still a large concern in atmospheric chemical transport models

Kommentiert [TL12]: The goal of the present study is to understand the transport pathways from the source regions into the upper troposphere via the convective uplift into the AMA and further in the UT, especially towards the southern and western areas of the AMA. The transport pathways in the UT include the transport along the edges of the AMA, the circulation in the AMA, where air mass are trapped and the transport across the AMA edges and the outflow out of the anticyclone due to instabilities in the strong circulation. For instance flight 19 took place outside and at the western edge of the AMA, which is now better visible in Figures 7 and 8 due to addition of a contour line for the CH4 threshold.

Formatiert: Tiefgestellt, Unterschneidung ab 10 Pt.

(Bloom et al., 2017, and references there in). In South Asia anthropogenic emissions increase with a growing population and economic development (Rauthe-Schöch et al., 2016, Ohara et al., 2007). The observations of CH_4 and CO show zonal and meridional concentration gradients as well as vertical gradients in the upper troposphere, allowing to investigate the extent of the AMA. In order to differentiate background from AMA influenced air masses, we derived a CH_4 based threshold. ~~Additionally~~Further, we compared our observations with EMAC model simulations, which extend the view on the trace gas distribution from a regional (along the flight tracks) to a global scale. To study the transport pathways we calculated back trajectories with the Lagrangian particle dispersion model FLEXPART along the flight tracks. ~~and~~ With FLEXPART we gained a more detailed insight into the dynamics. We compared ~~them~~ the back trajectories with observations of CH_4 and CO to distinguish between different transport pathways. Thus we also studied ~~also~~ the origin of emissions within South Asia. ~~Furthermore~~Finally, we investigated the variability of the AMA over several weeks as the anticyclone changes its position, extent~~d~~, and ~~with respect to its position and~~ strength due to the ~~its~~monsoon dynamics.

2 Methods

2.1 OMO campaign

The Oxidation Mechanism Observation (OMO) aircraft measurement campaign~~mission~~ focused on the self-cleaning capacity of the atmosphere in connection with the Indian summer monsoon. The mission took place in July and August 2015 with flight tracks in the upper troposphere (10-15 km) over the Mediterranean, the Arabian Peninsula, and the Indian Ocean (Figure 1). In South Asia the pollution emissions are growing and during the monsoon season they are uplifted into the upper tropa~~tm~~osphere. The pollution is partly removed by wet deposition or transformation into soluble gases, or they are involved in air chemistry and transported downwind of the sources. For a broad analysis of the efficiency of the self-cleaning mechanism a large variety of chemical compounds, like CH_4, CO, OH, HO_2, NOy, SO_2, RO_2, H_2O_2, and total peroxides, were measured during the multi-institutional campaign, involving the Max-Planck-Institute for ~~Chemsitry~~Chemistry, Mainz, the Research Centre~~Forschungszentrum~~ Jülich ~~(FZJ)~~, the German Aerospace Centre~~(DLR)~~, the Research Centre Karlsruhe, and~~d~~ the universities of Bremen, Heidelberg, and Wuppertal. The main objectives ~~of OMO~~ were~~are~~ the oxidation processes and free radical chemistry, the efficiency of convective cloud transport and wet deposition, as well as long-distance transport of air pollution, and impacts on air quality and climate change. The OMO mission comprised 111 flight hours during 17 flights. HALO was based alternately at Paphos (Cyprus) and on Gan (Maldives) with refuelling stops at the airport of Bahrain. Further information about OMO can be found in Lelieveld et al. (218) and on the webpage **http://www.halo.dlr.de/science/missions/omo/omo.html**

Kommentiert [TL13]: The information has been added including the reference.

Kommentiert [TL14]: A more detailed explanation is now added.

Kommentiert [TL15]: We used the EMAC model simulations to extend our view on trace gas distributions from the regional scale along flight tracks to a global scale, i.e. horizontal and vertical trace gas distributions, and also to separate different AMA modes. With the second model (FLEXPART) we calculated back trajectories to investigate the emission sources and the transport pathways from the source regions, via the convection into the AMA in the upper troposphere and further westward towards the flight tracks. Thus the back trajectories are mainly used for dynamical processes.

Kommentiert [TL16]: General information about the OMO mission are added in the manuscript in the method part in section 2.1 including references.

Formatiert: Tiefgestellt, Unterschneidung ab 10 Pt.

Formatiert: Tiefgestellt, Unterschneidung ab 10 Pt.

Formatiert: Tiefgestellt, Unterschneidung ab 10 Pt.

Formatiert: Tiefgestellt, Unterschneidung ab 10 Pt.

Formatiert: Tiefgestellt, Unterschneidung ab 10 Pt.

Formatiert: Tiefgestellt, Unterschneidung ab 10 Pt.

Formatiert: Schriftart: Nicht Fett

2.21 Trace gas measurements

We employed the TRISTAR instrument (Tracer In Situ TDLAS for Atmospheric Research, and TDLAS is Tunable Diode Laser Absorption Spectrometry), which is an IR-quantum cascade laser absorption spectrometer for airborne measurements of trace gases (CO, CH_4, HCHO) on board HALO with a compact and robust design, consisting of an optical set-up and the instrument electronics. TRISTAR was described in more detail in previous publications (Tadic et al., 2017, Schiller et al., 2008 and references therein). The electronic part, including laser controller, data acquisition, etc., is integrated into the upper part of half a 19" rack. Mounted on the top of the rack is the optical set-up consisting of a liquid nitrogen cryostat, which houses three infrared quantum cascade lasers for CO, CH_4, and HCHO and two cryogenic photovoltaic mercury-cadmium-telluride detectors, a double corner cube multi pass cell according to White (1976), and several mirrors to reflect and collimate the beam. The optical unit is fixed on shock mounts for protection against vibrations. The trace gases are detected sequentially via pneumatically driven pop-up mirrors.

A detailed description of the electronic set-up is given in Schiller et al. (2008). With a 66 ms saw-tooth current ramp the laser emission is scanned across a rotational-vibrational absorption line of the target species. In addition, the frequency of the laser is modulated via its injection current with a sinusoidal shaped 20 kHz frequency. At the detector the signal is demodulated at 40 kHz by a lock-in amplifier. For CO and CH_4 two measurement modes are used: ambient air and in-flight calibration. The in-flight calibrations are realized with a secondary standard from pressurized bottles (6 l bottle, Auer GmbH, Germany), calibrated against certified reference gases. CO is calibrated against a reference gas (121.44±1.46 ppbv), which is calibrated against a secondary standard (155.8±0.45 ppbv). The latter was measured against a dilution gas (10ppm±1%) from EMPA (Swiss Federal Laboratories for Materials Science and Technology) referring to a NIST standard. CH_4 is calibrated against a working standard based on the scale of NOAA-2004 by Dlugokencky et al. (2005) and has an uncertainty of +-0.3 ppbv relating to the CMDL83-standard (Dlugokencky et al., 2005). Furthermore the in situ CO and CH_4 data are drift corrected by interpolation between regular in-flight calibrations (Tadic et al., 2017).

Under the assumption of a Gaussian error propagation the total uncertainty consists of the statistical error (noise and drift correction) and the systematical error (calibration to reference gases). The total campaign average uncertainties are 5.1% and 0.275% for CO and CH_4, respectively. During OMO the CO accuracy degraded, because of problems with the CO laser in the second half of the mission. A detailed overview of the total uncertainties for all the flights is presented in the supplement Table S1.

2.32 FLEXPART back trajectories

The origin of air masses was derived with the Lagrangian particle dispersion model FLEXPART Version 9.2 beta (Stohl et al., 1998). The model is driven by ECMWF (European Centre for Medium-Range Forecasts) operational data with a horizontal resolution of 1°x1° and a vertical resolution of 137 levels between 1013.25 hPa and 0.01 hPa. The temporal resolution is 3 h,

Kommentiert [TL17]: We calculated back trajectories and the initializations are along the flight tracks. The subtitle for section 2.3 is now "FLEXPART back trajectories".

with analyses at 00, 06, 12, 18 UTC and forecasts for 03, 09, 15, 21 UTC. FLEXPART accounts for turbulence using the mean wind plus turbulent fluctuations and also mesoscale wind fluctuations (Stohl et al., 2010). TAdditionally, the planetary boundary height is parameterized following the concept of Vogelezang and Holtslag (1996) using the critical Richardson number (Stohl et al., 2010). Vertical transport is calculated by using the Langevin equation (Thomson, 1987), which takes into account the turbulent vertical wind and its standard deviation. It includes also a decrease of air density with height. Additional moist convection is parameterized according to Emanuel and Zivkovic-Rothman (1999). Their parametrization builds on temperature and humidity fields to provide mass flux information (Stohl et al., 2005). Trajectories are started every 10 min along the flight tracks for air parcels, neglecting loss processes due to deposition or chemical reactions. The trajectories are calculated 10 days back in time for 10000 parcels that are initialized per release point (size: 1°x1°x500 m and 1 hour). The model output is a dispersion field, which consists of several parameters, i.e. geographical position, planetary boundary layer (PBL) height, and temperature, for each parcel per 3 h interval. The amount of data can be condensed via cluster analyses according to Stohl et al. (2002). These cluster trajectories are called centroid trajectories. They are comparable to traditional trajectories, but include contributions of turbulence and convection via the centroid of all particles per time step.

2.43 EMAC model data

The ECHAM/MESSy Atmospheric Chemistry (EMAC) model consists of the general circulation model ECHAM5 (fifth generation of the European Center HAMburg, Roeckener et al, 2006) and the Modular Earth Submodel System (MESSy, Jöckel et al. 2005, 2010), which extends the model into a fully coupled chemistry climate model. The horizontal resolution applied is 2.8°x2.8°, the vertical resolution is determined by 90 layers on a hybrid pressure grid between the surface and 0.01 hPa. The EMAC model was not run in an offline CTM mode, as the radiation calculations were based on simulated GHGs concentrations. Nevertheless, tThe model was weakly nudged towards ECMWF ERA Interim data (Jeuken et al., 1996) and therefore reproduced very similar dynamics to the ECMWF model (although not binary identical). The simulation is an extension of simulation RC1SD-base-10 (Joeöckel et al. 2016) so to cover the full OMO campaign. Few changes to the original simulation have been applied (i.e. increased South Asia SO_2 emissions and reduced lightning NO_x), as described in Lelieveld et al. (2018). Although the simulation is the continuation of a well evaluated experiment, the simulation was running from 1st of March 1st, 2015 so to give time to the SO_2 and NO_x to balance to the new emissions (i.e. 4 months spin up time). Only the data from July and August 2015, which covers the field campaign is actually used. The EMAC model is an hydrostatic model and the convective transport is parameterized (Ouwersloot et al. 2015, Tost et al. 2006). Indication of the vertical transport time in EMAC can be found in Krol et al. (2018), where also a comparison with model of similar complexity is shown. The emissions are based on the Representative Concentration Pathways (RCP) 8.5 for anthropogenic activity (Van Vuuren et al., 2011) and Global Fire Emissions Database (GFED) v3.1 for biomass burning emission of 2015 (Van der Werf et al., 2010).

Formatiert: Tiefgestellt

Formatiert: Tiefgestellt

Kommentiert [TL18]: We thank the reviewer for pointing out the lack of information regarding the model simulation. Here additional details are given, also added to manuscript.

For methane additional sources of both wetlands in the Amazon and North American shale gas drilling were added to simulate the methane trend since 2007 (Zimmermann et al., 2018).

We used two different model output. One is the output from the SD4 submodel, which was developed by Jöckel et al. (2010) for simulations along moving platforms, like ships or aircrafts. The data collection takes place in four dimensions (space and time) and the data are interpolated online, thus no information is lost due to interpolation after the simulation. The data along the flight track have a time resolution of 12 min (i.e. the model time-step), which are compared to the in situ data for CO and CH_4, averaged over 12 min. The second model output is given as three-dimensional daily mean data for different parameters, like CO, CH_4 and the wind field. With these data the position of the Asian monsoon anticyclone can be identified on different pressure levels, as well as its vertical extension, via vertical profiles. Additionally, the identification of emission sources at the surface is possible.

2.~~5~~4 Satellite data

Cloud top pressure information is used as a proxy for convection. We compared the location of the convective clouds with the location of the uplift of the back trajectories simulated by FLEXPART. The cloud top pressure data are~~is~~ collected from the MODIS instrument on board of AQUA, via measured radiances in the spectral absorption bands at 15 µm CO_2 (Menzel et al., 2008). In general, the atmosphere becomes more opaque with increasing wavelength due to the absorption of CO_2 between 13.3-15 µm. Thus, the measured radiances in these spectral bands are sensitive to different pressure levels. The cloud top pressure is determined by the ratio of two pairs of adjacent wavelengths in the infrared. For AQUA MODIS the ratios of 14.24/13.94 µm, 13.94/13.64 µm and 13.64/13.34 µm are used for high, midlevel, and low-level clouds, respectively. The data are derived from the level 3 MODIS Atmosphere Daily Global Product data (MYD08D3, Platnick, 2015), which are available from the NASA webpage (https://ladsweb.modaps.eosdis.nasa.gov/). The resolution of the data is 1°x1° for daily means.

Kommentiert [TL19]: Yes it is used as a proxy for the location of convection to compare the region with the calculated updraft of the back trajectories. This information is added in the actual section 2.5.

3 Results and Discussion

3.1 CH_4 and CO profiles

~~The OMO mission comprised 111 flight hours during 17 flights in the region between the Indian Ocean and the Mediterranean Sea (Figure 1).~~ Vertical profiles were flown over Oberpfaffenhofen (Germany), Paphos (Cyprus), Etna (Italy), Egypt, Bahrain and Gan (Maldives) (marked in Figure 1). As observed, the CO and CH_4 profiles measured during OMO indicate different altitude distributions depending on the geographical location and partly also on the meteorological situation, especially for Paphos and Egypt. Profiles over Egypt were ~~only~~ measured~~, while~~ when the AMA extended over this region. P~~In contrast~~profiles over Paphos were sampled during periods with and without the AMA being positioned over Cyprus. Here profiles over Paphos, Etna and Oberpaffenhofen are used to derive a northern hemisphere (NH) background, while profiles over Egypt

Kommentiert [TL20]: In the classification of the profiles for Northern hemisphere and AMA-influenced profiles the geographical location but also the meteorological situations are accounted. The profiles over Egypt were only sampled during the second double anticyclone mode with the westerly extending over Egypt. Profiles over Paphos spread over a longer period with representing the background atmosphere and partly also AMA-influenced air masses, which leads within the standard deviation to an average of a background profile. The figures 18-21 are only examples for the specific mode and they are in a height of 204hPa. Not necessarily representative for the atmosphere below or representative for different meteorological situations.

and Bahrain are used to derive altitude dependent information under monsoon influence (AMA profiles), and profiles over Gan are used to derive a southern hemispheric (SH) background (Figure 2). Average profiles were calculated in 500 m bins, starting above 4 km to avoid boundary layer effects. Inspection of the CH_4 AMA profile indicates a significant enhancement in the upper troposphere between 9 and 12.5 km corresponding to pressure levels between 300 and 170 hPa. ~~Randel and~~ Park et al. (200~~7~~6) used CO observations from satellites and wind fields to identify~~ied~~ monsoon influenced air masses inside the AMA at a similar pressure range (200-100 hPa). The average CH_4 mixing ratio of the AMA profile between 9 and 12.5 km is (1919.0±17.2) ppbv, while the average CH_4 mixing ratio for the northern hemisphere (NH) background is 1863.4±14.0 ppbv, comparable to CH_4 mixing ratios below 9 km measured for the AMA profile (1876.5±8.7) ppbv. The average CH_4 mixing ratio for the SH background is 1778.3±19.5 ppbv, significantly lower than either the NH background or the AMA profiles. While the NH background shows only a small increase of CH_4 above 11 km, the SH background profile steadily increases with height. Gan is located at the equator and thus influenced by the southern hemisphere during boreal summer when the ITCZ is shifted to the north (Waliser and Gautier, 1993). Since most of the methane sources are in the northern hemisphere north of the ITCZ, the profile over Gan thus to some extend represents the southern hemisphere (SH) background. The observed CH_4 increase with height can be explained by the global circulation. In the boundary layer CH_4 mixing ratios are influenced by turbulent mixing close to emission sources or by horizontal advection in remote places (Saito et al., 2013). At the surface the air at Gan is influenced by wind from southern directions with low CH_4 mixing ratios originating from the southern Indian Ocean. High altitude ~~At high altitudes the~~ advection leads to interhemispheric transport (Saito et al., 2013) thus to ~~a transport~~transfer of higher CH_4 mixing ratios from the NH into the SH, which have been convectivle~~e~~y uplifted from the boundary layer~~. upper branch of the Hadley circulation leads to air transport from the ITCZ to the SH. These air masses are influenced by local pollution from the NH air mixed into the SH background in the ITCZ~~. The observed difference in CH_4 background between the NH and the SH is 85.1 ppbv, which agrees with an interhemispheric gradient of 86-90 ppbv for the period 2007 to 2010 given in Bergamaschi et al. (2013).

The measured mean CO profiles for AMA (74.2±10.9 ppbv), NH background (68.8±7.3 ppbv) and SH background (63.2±4.3 ppbv) are rather similar and agree within the standard deviations. Nevertheless, in the upper troposphere the AMA profile indicates a slight increase of CO mixing ratios relative to the background. Enhanced CO and CH_4 mixing ratios in the upper troposphere over the eastern Mediterranean in summer 2001, associated with air masses influenced by the monsoon, were also observed during the MINOS aircraft campaign (Lelieveld et al, 2002, Scheeren et al., 2003). This is ~~in~~ consistent with the observed upper tropospheric increase of CO and CH_4 in the NH background profiles, which are found during ascends and descends over Paphos but not over Oberpfaffenhofen. In general, our observation of enhanced CO mixing ratios under monsoon influence are consistent with Park et al. (2008), who showed that satellite-based averaged CO profiles exhibit

Kommentiert [TL21]: Yes, there are other in situ profiles. Lelieveld et al. (2002) measured profiles over the Mediterranean in summer 2001 during MINOS. They have observed enhaved CH4 and CO values in the UT, especially during stronger influence from the AMA in the UT with CH4 mixing ratios up to ca. 1890 ppbv. Bergamaschi et al. (2013) presented CH4 profiles over the pacific in dependence of the latitude observed in 2009. The CH4 mixing ratios decrease from the norhtern hemisphere to the southern hemisphere. The highest values are reported for the lower troposphere in the northern hemisphere (around 1882 ppbv). In the UT CH4 increases towards the tropics to around 1800 ppbv.

Kommentiert [TL22]: The reference was wrong and the right one is Park et al. (2007).

Kommentiert [TL23]: This has been changed.

Formatiert: Tiefgestellt, Unterschneidung ab 10 Pt.

Kommentiert [TL24]: The paragraph is rewritten including supporting material and references.

Kommentiert [TL25]: This has been changed.

increased CO mixing ratios in the upper troposphere inside the AMA (around 100 ppbv in 10-15 km) in comparison to air outside the AMA (65-90 ppbv in 10-15 km).

To differentiate between air masses in and outside the AMA various approaches have been used in the literature. Often potential vorticity (PV) is used for this purpose (e.g. Randel and Park, 2006, Garny and Randel, 2013 or Ploeger et al., 2015). Ploeger et al. (2015) calculated PV from reanalysis data to determine a transport barrier isolating the AMA. In the restricted area of interest low PV values are found inside the anticyclone while higher PV values represent the background. A more direct approach is the use of a CO threshold (Park et al., 2008). Based on satellite data, Park et al. (2008) found that CO mixing ratios < 60 ppbv represent background air while CO mixing ratios > 60 ppbv represent air inside the AMA at 16.5 km. In our study the monsoon influence in the upper troposphere is most obvious in the CH_4 profile, while CO is less suitable due to its larger atmospheric variability associated with its shorter lifetime (Junge, 1974) and the instrumental problems experienced for CO during the second half of the campaign. Therefore, a methane threshold was derived to signify monsoon influenced air masses from the NH background profile. To avoid boundary layer effects and the above mentioned slight increase in the NH background profile above 11 km due to a small contribution of monsoon influenced air above the eastern Mediterranean, only data between 4 km and 10 km were used, yielding an average CH_4 mixing ratio for the background of 1859.4±10.2 ppbv, which is slightly lower than the above mentioned mixing ratio covering the whole altitude range. The CH_4 threshold is then defined as this average plus twice the standard deviation:

$$Threshold = \text{average} + 2\,\sigma = 1859.4\ \text{ppbv} + 2 * 10.2\ \text{ppbv} = 1879.8\ \text{ppbv}, \quad (1)$$

In situ CH_4 mixing ratios that exceed this threshold are assumed to be influenced by the South Asian monsoon and are therefore ~~being~~ representative of the AMA, in the following denoted as being AMA-influenced. While in the NH background profile, methane mixing ratios in the upper troposphere are generally smaller than this threshold CH_4 mixing ratios in the AMA profile significantly exceed this threshold above 9 km (Figure 2). ~~The f~~Further evaluation depends on the CH_4 threshold and thus the results are sensitive to it. Nevertheless, also other compounds measured during OMO showed the isolation of the anticyclone in the UT (Lelieveld et al., 2018) which ~~confirmes~~confirms the usefulness of CH_4. With a change in the absolute value the region which is supposed to be AMA-influenced will be either larger or smaller, thus the edge of the anticyclone would be differently defined but the whole dynamical process is not significantly changing.

3.2 Case study flight 19

To illustrate the connection between enhanced CH_4 mixing ratios, monsoon convection, and South Asian pollution sources at the surface we performed a case study on flight 19 data (August 13, 2015). The flight took place over the Arabian Peninsula. After take-off from Paphos HALO headed towards Oman before returning back to Paphos. Enhanced mixing ratios for CO and CH_4 were measured between 10-11UTC (Figure 3). Over Oman at a pressure level of 175 hPa mixing ratios for CO and

Kommentiert [TL26]: Park et al., 2008 reported CO MR in the UT (10-15km) of around 100ppbv in the AMA and 65-90ppbv outside. We measured in 10-14km around 74.0±15.2 ppbv and outside of 71.2±10.0 ppbv. Park et al., 2008 defined the AMA by a CO threshold opposite to our CH_4 approach and in our profiles inside and outside events are included, only separated by their location, which leads to a smaller difference in the CO mixing ratios for background and AMA-influence in the UT.

Kommentiert [TL27]: This problem only degraded the data quality of CO measurements.

Formatiert: Tiefgestellt, Unterschneidung ab 10 Pt.

Formatiert: Tiefgestellt, Unterschneidung ab 10 Pt.

Kommentiert [TL28]: The threshold is a simple tool to distinguish between background air masses and air masses influenced by the monsoon. It is based on in situ measurements and it is subjectively chosen, however its application to the in situ data showed a reasonable differentiation. The threshold itself was not be applied to the EMAC data along the flight tracks and in the histograms (Figures 16 and 17) as the model underestimated the in situ measurements. The in situ CO and the EMAC data are distinguished into AMA-influence and background according to the time, when the in situ CH4 was above or below the CH4 threshold. Nevertheless the CH4 threshold is represented in the EMAC horizontal trace gas distributions as a contour line for a better orientation of the AMA position. Consequently the analyses depend on the threshold. Nevertheless a change in the absolute value would increase or decrease the region which we assumed to be influenced by the monsoon.

CH_4 increased from background levels of (74.3±10.6) ppbv and (1846.7±16.1) ppbv to (99.5±14.3) ppbv and (1905.2±13.9) ppbv, respectively. According to the classification defined in the previous chapter CH_4 mixing ratios reached values well above the threshold indicating that air masses influenced by the monsoon were probed. Elevated mixing ratios were still observed after a flight level change (200 hPa). Accordingly, both flight levels were within the altitude range of the AMA confinement of 200-100 hPa reported by Randel and Park ~~et al.~~ (2006). Within the AMA the average increase relative to background for CO is around 25 ppbv and for CH_4 around 58 ppbv. The increase in CH_4 is rather sharp, indicating a rather well defined edge of the AMA, as has been reported in previous studies (e.g. Park et al., 2008).

For the MINOS campaign over the eastern Mediterranean, Scheeren et al. (2003) distinguished between air masses that originated over South Asia and those over North America/North Atlantic, corresponding to our classification a AMA air masses and NH background, respectively. Note that Scheeren's South Asia air mass would be incorporated in our background, due to its location over the eastern Mediterranean. Scheeren et al. (2003) reported in situ trace gas measurements for the 6-13 km altitude range. Mean CO mixing ratios were (74±12) ppbv for North American/North Atlantic origin and (102±4) ppbv for air masses with a South Asian origin, resulting in a difference of 28 ppbv. The relative difference in CH_4 observed by Scheeren is 63 ppbv (North America/North Atlantic: (1819±26) ppbv, South Asia: (1882±21) ppbv). The enhancements observed during MINOS are similar to those observed during OMO flight 19, although absolute mixing ratios in particular for CH_4 are higher, since global CH_4 concentrations have been increasing since summer 2001 (Zimmermann et al., 2018).

Using FLEXPART, 10-day centroid back trajectories along the flight track were calculated. An analysis indicates that in general enhanced CH_4 mixing ratios are associated with an air mass origin inside the AMA, while lower CH_4 mixing ratios are associated with background air (Figure 4). In particular the back trajectories starting at release points with the highest CH_4 mixing ratios (Figure 7, 8) have been confined in the AMA for several days with their origin over Northern India and Bangladesh. Between five to ten days before observations the back-trajectories are found in the boundary layer or the lower troposphere, before they are uplifted into the upper troposphere by deep convection (> 200 hPa) (Figure 5). This finding is in good agreement with Bergman et al. (2013), who calculated trajectory transit times of 2-22 days from the surface to the 200 hPa level in the region of the Tibetan Plateau and India/SE Asia. After the convective injection into the upper troposphere the air masses in this case study are advected at the southern edge of the AMA, following the tropical easterly jet towards the measurement region over the Arabian Peninsula. The transport distance of an air parcel in the upper troposphere depends on its origin and takes 1-6 days in the present study depending on the area of convective transport (Northern India, Bangladesh, Bay of Bengal). Scheeren et al. (2003) during MINOS found a longer transport time for polluted air masses ranging from 7 to 10 days from the South Asian source region towards the eastern Mediterranean, which also represents a longer transport pathway. During ESMVal the long range transport in the upper troposphere from the eastern part of the AMA towards the

Kommentiert [TL29]: Zimmermann et al. (2018) calculated a CH_4 mixing ratio of 1781 ppbv for the upper troposphere between 2000 and 2006. The CH_4 values in Scheeren at al. (2003) are 1819±26 ppbv for North America/North Atlantic origin and 1882±21 oobv for South Asia origin. The value in Zimmermann et al. (2018) is a global average over seven years in contrast to the values of Scheeren et al. (2203), which represent only one summer month of northern hemispheric origin, thus not accounting for the lower southern hemispheric CH_4 mixing ratios. Zimmermann et al. (2018) increased the CH_4 mixing ratio due to additional CH_4 emissions starting in 2007 up to 1815 ppbv for 2015. In this study the CH_4 mixing ratio is in average 1866.4±43.0 ppbv.

Arabian Peninsula along the southern fringe of the AMA took 2-4 days and the majority of the trajectories were circulating around the AMA within 10 days prior to the observation (Gottschaldt et al., 2017).

By comparing the back trajectories with satellite images of daily mean cloud top ~~height~~ pressure it was possible to identify regions with strong convection that were intercepted by the trajectories during their uplifting phase (illustrated in Figure 6). Matches were generally found over the Bay of Bengal, the Indo-Gangetic Plain, Bangladesh, the north eastern region of India, and Myanmar~~, although shallower convection also occurred over central India d~~During the days when the back trajectories passed over central India, convection occurred also in this area, but the cloud top ~~height~~ pressure was at a lower altitude than the height of the trajectories. Thus the influence from central India seems to be negligible for this particular flight. Convective cloud top information for estimating the influence of convection on the transport pathways of trajectories were already applied in previous studies, like Scheeren et al. (2003) and Gottschaldt et al. (2017). They found the strongest convection occurring in the same area as mentioned above.

To compare observations with model simulations, Figure 3 shows time series for CO and CH_4. For flight 19, EMAC model simulation results for CO and CH_4 agree well with the observations (CO: (2.1±8.7) ppbv, CH_4: (11.9±21.7) ppbv), reproducing observed trends in mixing ratios for both species, although the model has a rather course resolution of 2.8°x2.8°. In general, the model tends to underestimate the enhanced CH_4 mixing ratios in particular for AMA-influenced regions and overestimates CO. A comparison for all flights during the OMO mission yields a model overestimation of (4.6±11.8) ppbv for CO and an underestimation of (7.0±32.8) ppbv for CH_4 (see section 3.4.). A comparison between in situ CO and EMAC simulations for the ESMVal flight showed good agreement with a negative bias of the simulated CO, which was in regions of strong CO gradients about 10 ppbv, otherwise smaller (Gottschaldt et al., 2017). Since the trace gases mixing ratios and trends are in general well reproduced by the EMAC model, it will be extensively used for further interpretation of the measurements in the remainder of the manuscript.

The position of the AMA can be determined from horizontal transects of EMAC daily means of trace gas distributions and meteorological data on a pressure level of 204 hPa (Figure 7, 8). Here the anticyclone is identified by the wind field and corresponding CO and CH_4 fields. Enhanced trace gas mixing ratios are found to be confined within the anticyclone due to the strong isolation caused by the anticyclonic~~high pressure~~ circulation (Park et al., 2008). On August 13, 2015, the AMA extended from the eastern part of the Arabian Peninsula to the eastern part of China and from the northern part of the Bay of Bengal to the Gobi Desert. Its centre was located over the Tibetan Plateau, which is consistent with the climatological mean position of the AMA as documented by Nützel et al. (2016). The simulated mixing ratios inside the anticyclone increase from around 90 ppbv (CO) and 1860 ppbv (CH_4) at the fringes of the anticyclone to values inside the AMA above 150 ppbv and 1920 ppbv for CO and CH_4, respectively. Mixing ratios in background air over the Mediterranean are around 65 ppbv for CO and 1840 ppbv for CH_4 and thus below those simulated inside the AMA. Enhanced mixing ratios in the AMA were reported also in previous studies, e.g. increased CH_4 mixing ratios in satellite data over the summer monsoon region by Park et al. (2004)

Kommentiert [TL30]: This has been changed.

Kommentiert [TL31]: The sentence is rewritten.

Kommentiert [TL32]: This has been changed.

and Xiong et al. (2009), or enhanced CO values from satellite measurements in the monsoon region by Li et al. (2005). The latter study reported CO mixing ratios of up to 133 ppbv at a pressure level of 147 hPa over the monsoon region, which fits with our slightly higher simulated CO values at a lower pressure level, if we assume that CO mixing ratios decrease with height (Park et al., 2008).

Since the 200 hPa level is representative for the dominant flight altitude, the in situ observations along the flight track can also be compared to the simulated 2D fields. Further, we assume that the 200 hPa level is where most of the convective outflow takes place, and therefore pollution levels are expected to be highest (Park et al., 2009). Figure 7 and 8 show that OMO flight 19 only scratches the western edge of the AMA. Measured CH_4 mixing ratios are higher inside the AMA than the simulated ones. This is in line with the above mentioned CH_4 underestimation by the model. In the model simulations the anticyclone shows a more distinct signal in CH_4 compared to CO, since the edge in CH_4 is well-defined, with mixing ratios dropping off significantly outside the anticyclone. In contrast, the CO pattern is more diffuse. The simulated CO pattern, especially the enhanced values over Oman, fits well to the observed CO mixing ratios along the flight track~~, which can be partly due to the effect that the model overestimates CO while CH_4 values are generally underestimated by the model~~. The EMAC model underestimates CH_4 and CO in the upper troposphere. As shown by Krol et al. (2018), EMAC seems to have a weaker transport of surface tracers than other models. There are two potential reasons for that, but it is difficult to distinguish them. First, a too slow vertical velocity, thus the convective updraft is too ineffective, or second, the numerical diffusion implied by the coarse resolution restricts the updraft too strong. Nevertheless we would like to notice that for the comparison of CO with the model, the results are in line with other literature studies at such resolution (e.g. Baret et al., 2016).

Additional vertical transects along 23.7°N latitude and 56.2°E longitude on August 13, 2015 complete the picture of the AMA with respect to its extension. In a vertical CH_4 transect along 23.7°N (Figure 9) it is obvious that the flight touches only the western edge of the anticyclone in the upper troposphere and that the majority of the flight took place outside the anticyclone. According to the model simulation, convective uplift of CH_4 takes place between 75°E and 95°E, which corresponds to India and the Bay of Bengal. Moreover, the upward transport of polluted air masses is only simulated in a rather restricted area, analogous to a chimney, as reported by Bergman et al. (2013). This area was also the preferred location for convection 10 days prior to the flight as reported above. Rauthe-Schöch et al. (2016) reported a similar longitudinal position for convection between 80°E and 100°E in summer 2008 for CARIBIC flights over India. In the vertical transect along 56.2°E (Figure 10) CH_4 mixing ratios show an increase at the surface from the equator towards higher northern latitudes. In the upper troposphere the AMA is located approximately between 15°N and 30°N, which fits well with the location of the AMA in summer 2008 identified by enhanced CH_4 mixing ratios observed on a CARIBIC flight between 10-40°N (Baker et al., ~~(~~2012). In vertical transects at longitudes between 75-95°E (not shown) the convection can be determined to occur between 20°N to 35°N, which reflects the area Indo-Gangetic Plain, Tibetan Plateau, Bangladesh, and the north eastern part of India. In the vertical transects for CO (Figure 11, 12) the same patterns are found, although less pronounced compared to CH_4. In the CO latitudinal transect

Kommentiert [TL33]: We added contour lines for the CH_4 threshold (1879.8 ppbv) and the CH_4 background (1859.4 ppbv) value in Figure 7 and 8 according to the suggestion of reviewer 1. The flight track crosses the edge of the AMA with higher mixing ratios inside the AMA, which can be seen in the measured and the modeled data. The difference between the in situ and simulated values show that on a regional scale the model is not able to reproduce the reality with respect to the absolute values.

Formatiert: Tiefgestellt

Kommentiert [TL34]: Indeed, the referee is correct in mentioning a possible too low transport of methane and carbon monoxide as a reason for underestimation in the upper troposphere. As shown by Krol et al. (2018), EMAC seems to have a weaker transport of surface tracers than other models. Both reasons suggested by the referee are possible, and it is difficult (if not impossible) to really distinguish the real reason for the underestimation of the transport. Nevertheless we would like to notice that for the comparison of CO with the model, the results are in line with other literature studies at such resolution (e.g. Baret et al., 2016). Horizontal wind components are added to the cross sections in figures 9-12, in detail: eastward wind component in cross sections along a longitude and northward wind component in cross sections along a latitude.

along 23.7°N (Figure 11) the enhanced mixing ratios range from around 90 ppbv inside the anticyclone to over 400 ppbv at the surface, while CH_4 mixing ratios scale from around 1850 ppbv inside the anticyclone to surface values above 2250 ppbv (Figure 9).

3.3 Emission source region

Emission source regions are identified by combining the FLEXPART single particle information with EMAC daily means for CO and CH_4 mixing ratios in the planetary boundary layer. With FLEXPART the last boundary contact can be determined as a footprint of parcels, which started from release points with enhanced methane, i.e. CH_4 mixing ratios > threshold. The last boundary layer contact of a parcel is determined if its height position is within ± 5% of the PBL height (in m above ground level). These parcels are sorted depending on their geographical position and then summed-up in each grid cell (1°x1°), yielding a number of parcels per grid cell in the PBL. For flight 19 (August 13, 2015) the footprint of the last PBL contact approximately 10 days prior to the parcel release shows highest values over Bangladesh and the north eastern part of India (Figure 13). The last boundary layer contact is assumed to be a useful indicator for the area where parcels are uplifted by convection and subsequently injected into the AMA.

To identify emission sources, EMAC daily mean trace gas mixing ratios at a pressure level of 1008 hPa (assumed to be the surface) are presented. The CH_4 mixing ratios in Figure 14 exhibit the highest values in the Indo-Gangetic Plain and Bangladesh, spreading southward along the east coast of India and towards Myanmar. Peak values reach up to 2600 ppbv. Figure 15 shows that CO has the highest mixing ratios in the same region as CH_4, with peak values up to 400 ppbv. A comparison to Figure 13 indicates that high CO and CH_4 mixing ratios are co-located with the areas of convection, leading to an updraft of polluted air masses to the upper troposphere. In the footprint (Figure 13) the east coast of Africa, the Indian Ocean, and the Pacific indicate a minor influence, but they do not correspond to enhanced mixing ratios in EMAC daily mean CH_4 or CO. Thus, they are assumed not to contribute to the pollution of the air masses in the AMA. The EMAC daily mean data also indicate polluted areas along the east coast of China. This area is not reflected in the parcel footprint, which indicates that the south-eastern part of China is only a minor contributor to the pollution of the AMA on this particular flight. Note that some convection in the daily mean cloud top ~~height~~ pressure maps occurs approximately 10 days prior to the observation over eastern China, confirming that Chinese emissions could have a minor contribution on the composition of the AMA.

The above mentioned peak values at the surface for CO and CH_4 over Southern Asia can be related to different emission sources. The regions including the Indo-Gangetic Plain and Bangladesh are densely populated areas with an increasing population trend in combination with strong economic development (Rauthe-Schöch et al., 2016, Ohara et al., 2007). Potential CO sources are biomass, fossil, and domestic fuel combustion as well as oxidation of CH_4 and volatile organic compounds (Pandis and Seinfeld, 2006). CH_4 is emitted by rice cultivation, wetlands, domestic ruminants, biomass burning, fossil fuels, waste decomposition (Khalil, 2000), and flood plains, especially if they are polluted by urban waste and sewage (Baker et al.,

Kommentiert [TL35]: This has been changed.

2012). The latter has its maximum emission during the monsoon due to the influence of rain. At the same time rice has its primary growing period in the wet season and hence CH_4 emissions have a seasonal cycle and are strongest during the monsoon, contributing significantly to the CH_4 emissions (Baker et al., 2012). The simultaneous appearance of a CH_4 emission maximum and the strong convection leads to a more pronounced chemical signature in the AMA for CH_4 than for CO. The CO emission sources do not experience such a strong seasonal dependency. This emphasizes again the use of the CH_4 threshold to differentiate between AMA-influenced and background air masses.

Bangladesh and the north eastern part of India are also mentioned in the study of Pan et al. (2016) as the preferred uplifting regions, which agrees with the main areas of the footprint determined in this study. The marked source regions were also identified by Park et al. (2009), as they reported the origin of upper tropospheric CO to be mainly from India and Southeast Asia, and by Pan et al. (2016) who identified Northeast India, the southern flank of the Tibetan Plateau, Nepal, and north of the Bay of Bengal to be the most preferred spots for CO uplifting. Rauthe-Schöch et al. (2016) identified similar source regions using FLEXPART 10 day back trajectories for CARIBIC flight tracks over the South Asian monsoon region. They used geographical positions of back trajectory points below 5 km, thus not only the boundary layer as used here, and documented air originating from India, Indo-Gangetic Plain, Bay of Bengal, mainland of Southeast Asia, and the western part of the Arabian Sea. Consequently, their area of source regions covers a larger part in comparison to the source region identified for flight 19. Bergman et al. (2013) demonstrated that trajectories from eastern China have only a minor influence to the AMA at the 200 hPa level, which supports our footprint analysis as it does not show any boundary layer influence from the eastern coast of China.

3.4 The AMA during OMO

Similar analysis as for flight 19 is discussed in detail for the other OMO flights including time series, back trajectories, and model results in the supplement. Here we extend the analysis of OMO results by analysing CO and CH_4 mixing ratios between 300 and 140 hPa from all research flights. In Table 1 observations and model data are separated by the CH_4 threshold into monsoon-affected and background periods. Observed CO mixing ratios increased under monsoon influence by about 20.1 ppbv, while CH_4 mixing ratios were enhanced by about 72.1 ppbv. EMAC SD4 CO and CH_4 also indicate increased mixing ratios along the flight tracks within the AMA, but not as strong as for the observations (~ 14.7 ppbv for CO and 24.0 ppbv for CH_4).

The observed increase in CH_4 inside the AMA by ~ 70 ppbv is in good agreement with the reported increase of 30-80 ppbv (at 8-12.5 km) between pre-monsoon and monsoon season reported by Schuck et al. (2012). Xiong et al. (2009) reported a CH_4 increase of up to 100 ppbv from June to September (for 2003-2007) at 300 hPa. Both studies are based on data observed over India, thus much closer to the AMA centre, which might explain the difference in absolute values. Moreover, they mirror

seasonal variations by comparing pre-monsoon with monsoon conditions and thus are not necessarily representative for background conditions as determined during OMO.

In Figure 16 and 17 histograms for CH_4 and CO mixing ratios, respectively, are shown for observations and model data at altitudes between 300 and 140 hPa separated into values above (AMA) and below (background) the CH_4 threshold. The CO observations and model data have similar distributions for background as well as AMA conditions. Average CO mixing ratios for observations and model data for AMA and background conditions agree within their 1σ-standard deviations (Table 1). The CH_4 mixing ratio average from the model for background conditions also agrees with the observation within their combined standard deviations, while the difference of the AMA CH_4 averages between the model and the observations is more pronounced. Observed CH_4 averages for background and AMA can be clearly distinguished, which is mostly due to the CH_4 threshold itself, which subdivides the data into two regimes. The distribution of the in situ CH_4 background data consists of two modes. The one with the low mixing ratios is associated to the SH background, and consists of observations over the Indian Ocean from or towards Gan. In the southern hemisphere the CH_4 mixing ratios range from 1760 ppbv to 1820 ppbv. The second mode represents the NH background with mixing ratios in the range of 1820 to 1880 ppbv, comprised of observations over the Mediterranean and partly the Arabian Peninsula. In comparison, the simulated CH_4 background distribution lacks the SH mode. EMAC also underestimates the AMA CH_4 mixing ratios. Accordingly, the CH_4 enhancement of the model is smaller than in the observations. AMA-influenced air masses show a broad distribution of CH_4 mixing ratios with values ranging from 1880 ppbv to 1980 ppbv. During the OMO campaign the position of the anticyclone changed repeatedly and thus observations were made at varying distance between the aircraft and the centre of the anticyclone (see next chapter). As expected, this leads to variations in the observed CH_4 mixing ratios for air masses influenced by the AMA. Furthermore, changes in the location of deep convection, the strength of the updraft or differences in emission sources lead also to variability in the observed CH_4 mixing ratios (see section 3.5). While the observed background conditions for both NH and SH each cover a range of approximately 60 ppbv, the AMA mixing ratios vary by about 100 ppbv.

3.5 AMA modes

Over the course of the OMO campaign the occurrence, position and extent of the AMA varied. The AMA pattern can be subdivided into four meteorological situations, which can be identified in the EMAC daily means for CH_4 and the wind pattern on a pressure level of 204 hPa. The first mode (Figure 18) is composed of 2 distinct anticyclones, which slowly move eastward between July 21 and August 1, 2015. On July 21 a western anticyclone is positioned over the Eastern Mediterranean. Its centre subsequently shifts towards the east. The eastern anticyclone with its centre around 70°E shifts eastward towards the Tibetan Plateau. The second mode (Figure 19) which consists of a single anticyclone is found during the period from August 6, 2015 to August 10, 2015. This mode has its centre over the Kashmir region (~70-80°E), which corresponds to the climatic mean location of the AMA centre (Zhang et al., 2002) and is called the central mode. The third single anticyclone mode (Figure 20)

has its centre over the Tibetan Plateau (~82.5°-92.5°E) and was observed between August 11, 2015 and August 18, 2015 (Tibetan mode; ~~(~~Zhang et al., 2002). In the following (August 20, 2015 to August 27, 2015) the anticyclone of the Tibetan mode moves westward and splits-up into 2 anticyclones (Figure 21). Here the westward movement of the AMA leads to instabilities in the circulation (Popovic and Plumb, 2001) so that a second anticyclone can break-off the main feature (Hsu and Plumb, 2000). The western anticyclone now has its centre above the Middle East and the eastern part over the Tibetan Plateau. During OMO the time period between the reoccurrence of the 2 distinct anticyclones is around 20 days. A 10-20 day cycle of westward propagation of the anticyclone including splitting into two anticyclones has been reported by Krishnamurti and Ardanuy (1980) and shown to lead to a succession of rainy and dry periods in India during the monsoon season. Zhang et al. (2002) presented a bimodality of the AMA with a center position of the anticyclone over the Iranian or the Tibetan Plateau. During OMO we found both positions, which ~~can lead to the assumption of a~~in line with the bimodality assumption. In contrast, Nützel et al. (2016) reported ~~also~~ different center positions of the AMA in several models, but most of them ~~have~~did not simulate~~d~~ a preferred bimodality. Regarding the eastern anticyclones during the double anticyclones modes, the positions were in ~~–~~between the Iranian and Tibetan Plateau (first mode) and in the fourth mode over the Tibetan Plateau. Consequently, they ~~will~~do not support a preferred bimodality. In Zhang et al. (2002) and Nützel et al. (2016) the Iranian and the Tibetan mode are further distinguished by parameters, like diabatic heating, rain patterns or areas of convection, which are out of ~~the~~ scope ~~of~~in the present study. Here the focus is on the dynamics with respect to the trace gas distributions. The subdivision into four modes represents the dynamics of the AMA over the course of the campaign.

Kommentiert [TL36]: A short discussion about bimodality of the AMA is now added I section 3.5.

Different trace gas levels between these four modes can also be identified in the CH_4 and CO observations by subdividing the observations into AMA-influenced and background values at altitudes between 300 hPa and 140 hPa (Table 2). The lowest CH_4 mixing ratios in background air are observed during the central mode, since during this time HALO was flying mostly over the Indian Ocean at low latitudes. These flights were influenced by southern hemisphere air masses due to the ITCZ shift to the north during boreal summer. Especially over India, the position of the ITCZ is in general between 5°-30°N in summer (Lawrence and Lelieveld, 2010). For the three other AMA modes the CH_4 background values are comparable, representing northern hemispheric background conditions. Their mixing ratios reflect also the CH_4 mixing ratio derived for the NH background profile (1859.4 ppbv) in section 3.1.

CO mixing ratios in background air masses show hardly any difference between the northern and the southern hemisphere in the upper troposphere. This is consistent with airborne observations during the Indian winter monsoon (January 1999) over the northern part of the Indian Ocean during the INDOEX campaign (Gouw et al., 2001). While no significant CO gradient was observed in the upper troposphere, a pronounced north-south gradient of 3.9±1.9 ppbv deg^{-1} latitude was observed below 3 km (~~de~~ Gouw et al., 2001)

Differences in CH_4 and CO mixing ratios for AMA-influenced air masses during OMO can be explained by the relative distance between the position of HALO and the position of the centre of the AMA. With increasing distance from the centre

of the anticyclone, mixing ratios tend to decrease. The distribution of the trace gases in the upper troposphere depends on the dynamics of the monsoon, since position and strength of the convection change during the wet season (Randel and Park, 2006). For example, if convection takes place over the Bay of Bengal, less polluted air is uplifted. In contrast, if the convection is directly over densely populated regions, e.g. Bangladesh, which are more polluted, convection transports the pollutants to the upper troposphere. At the same time, the strength of the convection changes within the monsoon due to differences in thermal heating between the relative cold ocean compared to the hot land (Dethof et al., 1999).

During OMO, the CH_4 mixing ratios for AMA influenced air masses varied temporally from mode to mode. The different mixing ratios do not follow a simple systematic (Table 2), and cannot be fully explained by the relative distance towards the AMA centre. Although the distances to the respective anticyclone centres were shortest during the two anticyclones modes, the observed CH_4 mixing ratios were both lowest and highest. In these cases, only the western AMA was probed above the eastern Mediterranean or the Middle East, because the flight tracks were in the same region. In contrast, the CH_4 mixing ratios for the two single AMA modes represented levels in between the minimum and the maximum CH_4 mixing ratios. In fact, CH_4 mixing ratios influenced by the monsoon increased from the first mode towards the fourth. The increase in average CH_4 is even more pronounced if we only include flights 22 and 23 in the fourth mode, as the flight track of flight 24 over the Mediterranean was not at all impacted by the AMA. Thus, the average CH_4 mixing ratio for the last mode becomes 1927.1 ppbv, which indicates an even stronger CH_4 increase over the course of the OMO campaign. The CH_4 enhancement can be most likely explained with a combination of the position of the convection, the temporal development of the AMA, and the accumulation of emission in time. A strengthening of the convection and/or a shift of the convection towards areas with larger emission sources would lead to higher CH_4 mixing ratios in the upper troposphere. A temporal increase in emissions, as described for CH_4 in section 3.3, induces also an increase of CH_4 in the AMA as reported by Xiong et al. (2009). They observed an enhancement of CH_4 in the upper troposphere during the monsoon season, starting with pre-monsoon conditions around June, increasing toward the end of the monsoon season (September). Accordingly, the strong AMA circulation traps the polluted air masses and the degree of pollution increases during the monsoon season.

The CH_4 mixing ratios in the EMAC data at 204 hPa show similar distributions to the observations along the flight tracks, indicating that the simulations of the AMA position agrees with the observations. Note that the model may not resolve small scale features due to its coarse resolution, which will lead to deviations between simulated and observed trace gas distribution, in particular close to the fringe of the AMA. In Section 3.6 we will describe a case study were the model successfully captures the weakening of the transport barrier and subsequent outflow of air masses from the AMA.

3.6 Outflow event from the AMA

Besides the different modes mentioned above, an outflow event was detected during OMO. In the EMAC data on 204 hPa an air mass with enhanced CH_4 mixing ratios started to move from Bangladesh westwards on August 2, 2015. In the previous days, convection took place over Bangladesh and injected polluted air masses into the upper troposphere. The convection can also be identified in the cloud top height data showing high clouds over Bangladesh. The air mass was further transported at the southern edge of the AMA following the tropical jet towards the west.

On August 3/4, a disturbance in the subtropical jet caused an instability in the AMA circulation which led to a weakening of the wind field especially in the south western part of the AMA. The slow AMA circulation was associated with a weakened transport barrier, thus offering the possibility that air masses inside the AMA were split -off. As the observed air mass was already at the fringe of the AMA circulation and thus transported into the region of the weak wind field, it left the AMA on August 5. Afterwards the circulation of the AMA strengthened again. The air mass that left the AMA was probed by HALO over Oman on August 6 (Figure 22). In the following days the westward transport of the air mass continued over the Arabian Peninsula following a south westerly flow on August 8. During its advection the originally compact air mass was stretched and transported north eastwards. On August 10 (Figure 23) it was located above the Red Sea and next moved further northeastward, to be reintegrate into the AMA circulation at the north western edge of the AMA in close proximity to the subtropical jet.

We measured the expelled air mass outside the AMA on two consecutive flights in a quasi-Lagrangian experiment. On August 6 (flight 12/13, Figure 22) HALO probed the expulsion with enhanced CO and CH_4 over Oman. In the air mass CO and CH_4 mixing ratios increased to 117.3±22.2 ppbv and 1893.5±9.8 ppbv, respectively (background: CO=78.6±33.3 ppbv and CH_4=1827.4±26.8 ppbv), which can be seen in Figure 24. The second probing of this air mass took place at August 10 (flight 17/18, Figure 23) over the Red Sea yielding mixing ratios of 94.2±6.8 ppbv and 1903.7±19.2 ppbv. This corresponds to the increase at around 12-13 UTC in Figure 25. The CO and CH_4 mixing ratios observed on both flights agree well within their standard deviations, with the small (but insignificant) differences probably caused by different flight levels (flight 12/13: 11.9 km and flight 17/18: 12.4 km). Note that the standard deviation for CO during flight 12/13 is larger than for flight 17/18 due to technical problems with the CO. Comparing the EMAC simulations with the in situ data along the flight tracks (Figure 24 and 25), the trends for the outflow agree. The EMAC average mixing ratios for CO and CH_4 are 112.2±1.2 ppbv and CH_4=1891.7±1.2 ppbv for flight 12/13 and 90.8±3.1 ppbv and CH_4=1864.6±5.9 ppbv for flight 17/18, respectively. Thus also the values agree within their standard deviation beside CH_4 in flight 17/18, where the outflow is underestimated by the model.

To check if the expelled air masses probed in the two flights were connected in a Lagrangian sense, we use centroid back trajectories. In Figure 264 the 10-day back trajectories for the enhanced CH_4 values are shown for the flights 12/13 and 17/18. The trajectories have their origin in the lower troposphere (below ~550 hPa) over the Arabian Sea and the Indian subcontinent. In the area of Bangladesh, the trajectories are convectively uplifted to the upper troposphere. From there they follow the

Kommentiert [TL37]: According to the suggestion of the reviewer the CO and CH4 distributions along the flight track as a time line are added in Figures 24 and 25. The trace gas mixing ratios (observed and simulated) show clear enhancement due to the outflow event for both flights (flight 12/13 and flight 17/18).

Kommentiert [TL38]: The outflow regions are marked in grey in the Figures. Additionally, we add in the manuscript the average CO and CH4 mixing ratios calculated from EMAC for the outflow periods for both flights (flight 12/13: CO=112.2±1.2 ppbv and CH_4=1891.7±1.2 ppbv and flight 17/18: CO=90.8±3.1 ppbv and CH_4=1864.6±5.9 ppbv) for a better comparison with the measured data in the outflow.

tropical jet towards the west, towards Oman and the Red Sea. The trajectories fit well to the simulated movement of the air mass with the enhanced CH_4 values. Besides the similar geographical and altitude position of the trajectories of both flights, the positions also agree in time, which means that the back trajectories of flight 17/18, released on August 10, needed four days between their release points and the crossing with the release points of flight 12/13. This travel duration is exactly the time between the two flights. Therefore, in Figure 275 the trajectories are colour-coded with time, starting from August 10 (day zero) counting backward in time. The trajectories are uplifted in the same period and exceed the 300 hPa level around -9 days. Subsequently, the trajectories of both flights travel together westwards in the same latitudinal band. On August 6 (-4 days), when the trajectories of flight 12/13 are released, they reach Oman and accordingly the release points of flight 12/13. Thus, the trajectories for both flights coincide in time and space. Therefore, they complete the picture of the outflow observed in the simulations and confirm the in situ measurement analysis.

4 Summary and Conclusion

The AMA is a ~~dynamical~~ circulation system in the upper troposphere and lower stratosphere, which appears over Asia during boreal summer. The anticyclone is coupled to deep convection (Hoskins and Rodwell, 1995), which pumps up polluted air masses. The relatively strong anticyclonic circulation traps the pollutants inside the AMA and constitutes a clear chemical signature. The emissions have pre~~their~~ dominant sources in South Asia, and are growing owing to population increase and economic development. It is not fully understood how the pollutants influence the chemical composition in the AMA, nor in the upper troposphere on a global scale. We especially lack information about the transport pathways of the boundary layer air masses into the AMA and how they escape the anticyclone. In the present work, we address the~~se~~ transport pathways, including the convective transport from the boundary layer into the UT, the circulation in the AMA, the transport at and across the edges of the AMA ~~and across the edges, which can lead to~~associated with outflow events and further transport in the UT partly in connection with the jet streams. The aircraft campaign OMO took place in July/August 2015 in the upper troposphere over the Mediterranean, the Arabian Peninsula, and the Arabian Sea to investigate the AMA and regions west and south of the AMA. On board HALO the trace gases CO and CH_4 were measured with the IR-absorption spectrometer TRISTAR. Both trace gases exhibit enhancements in the mixing ratios when influenced by the monsoon. To support our analysis, FLEXPART back trajectories and EMAC model simulations were used. In this study we focused on the dynamics with respect to trace constituents and their transport pathways into and in the AMA and their origin. In view of the flight tracks in the west of the AMA, the focus is on eastward transport pathways. To investigate the long range transport of relatively long-lived species, CO and CH_4 are suitable.

The AMA extends vertically from the upper troposphere ~~up~~ into the stratosphere. It could be clearly distinguished in the observed CH_4 AMA profile at altitudes of 9-12.5 km, while the NH and SH background profiles show no or ~~only a~~ minor

Kommentiert [TL39]: A detailed description of the transport processes is added.

influence. In the observed CO profiles and the simulated CH_4 and CO profiles the signature is not as clear as in the observed CH_4 profiles. With the help of the observed CH_4 background profile, we calculated a CH_4 threshold of 1879.8 ppbv to distinguish between background and AMA-influenced air masses. Over the course of OMO the mixing ratios of CO grew by about 20.1 ppbv due to the influence of the monsoon. The increase in the CH_4 mixing ratios was about 72.1 ppbv between background and AMA influenced air. Furthermore, CH_4 had ~~smaller~~ less background variability than CO, and the CH_4 emissions exhibit a seasonality with a maximum during the monsoon season. Consequently, CH_4 is an ideal monsoon tracer. In a case study of flight 19 the increase in the trace gas mixing ratios of CO and CH_4 can be unambiguously associated with the AMA. Back trajectories indicate transport pathways from the source regions in South Asia towards the measurement region for release points with enhanced CH_4 values. Source regions include the Indo-Gangetic Plain, Northeast India, Bangladesh, and the Bay of Bengal. These regions are densely populated with agricultural, urban and industrial emissions. Due to convection mainly over the same region the polluted air was uplifted and then transported with the easterly jet towards the measurement region. The transport time was approximately 10 days. The mode of the anticyclone changed during OMO according to Zhang et al. (2002): starting with a double anticyclone mode, transforming to a central mode, shifting to a Tibetan mode and then splitting again into two anticyclones. The position of the anticyclone is visible in the EMAC simulations, but can also be identified in the observations. Moreover, the observed CH_4 mixing ratios influenced by the AMA indicate strengthening in the convection or in the emissions or a combination of both as well as an accumulation in time over the course of OMO by a continuous increase. Additionally, the transport of an air mass with enhanced trace gas mixing ratios out of the AMA towards the west was observed.

In conclusion, the AMA has a distinct fingerprint in the upper troposphere, which was most prominent in observed CH_4, with enhanced mixing ratios inside the AMA circulation owing to the strong~~est~~ CH_4 emissions during the monsoon season. The AMA influences the region between the Eastern Mediterranean and East Asia through its extent, position and by outflow events. ~~Further, the long-range transport~~We demonstrated the pathways of trace gas from the source regions into and within the AMA. The outflow of polluted air masses from the AMA, by overcoming the transport barrier during weakening circulation, represents how emissions can be further distributed in the upper troposphere and therefore may influence the upper troposphere at~~on~~ a global scale. Consequently, surface emissions alter the chemical composition of the upper troposphere, leading to changes in the atmospheric chemistry, ~~and probably to changes~~which can influence ~~in~~ radiative heating ~~or~~ and cooling rates of different trace gases in the upper troposphere. Further investigations will be needed concerning the composition and trace gas chemistry and aerosols in the AMA. In the present study the focus was on long ~~-~~range transport, ~~but~~ while with shorter lived chemical constituents~~,~~ further understanding of the chemical composition can be gained, as in Bourtsoukidis et al. (2017). It will be helpful to extend the measurements further to the east, e.g. over India and the Bay of Bengal region.

Acknowledgements

We would like to thank all the participants of the OMO mission, the German Aerospace Center (DLR), and EDT Offshore Ltd in Cyprus for the great cooperation during the mission. We also thank Angelika Heil for help with the ECMWF data for the FLEXPART calculations.

References

Baker, A. K., Schuck, T. J., Brenninkmeijer, C. A., Rauthe-Schöch, A., Slemr, F., Velthoven, P. F., and Lelieveld, J.: Estimating the contribution of monsoon-related biogenic production to methane emissions from South Asia using CARIBIC observations, Geophys Res Lett, 39, 2012.

Barret, B., Sauvage, B., Bennouna, Y., and Le Flochmoen, E.: Upper-tropospheric CO and O3 budget during the Asian summer monsoon, Atmos. Chem. Phys, 16, 9129-9147, 2016.

Bergamaschi, P., Houweling, S., Segers, A., Krol, M., Frankenberg, C., Scheepmaker, R., Dlugokencky, E., Wofsy, S., Kort, E., and Sweeney, C.: Atmospheric CH_4 in the first decade of the 21st century: Inverse modeling analysis using SCIAMACHY satellite retrievals and NOAA surface measurements, Journal of Geophysical Research: Atmospheres, 118, 7350-7369, 2013.

Bergman, J. W., Fierli, F., Jensen, E. J., Honomichl, S., and Pan, L. L.: Boundary layer sources for the Asian anticyclone: Regional contributions to a vertical conduit, Journal of Geophysical Research: Atmospheres, 118, 2560-2575, 2013.

Bloom, A. A., Bowman, K. W., Lee, M., Turner, A. J., Schroeder, R., Worden, J. R., Weidner, R., McDonald, K. C., and Jacob, D. J.: A global wetland methane emissions and uncertainty dataset for atmospheric chemical transport models (WetCHARTs version 1.0), Geosci Model Dev, 10, 2141-2156, 2017.

Bourtsoukidis, E., Helleis, F., Tomsche, L., Fischer, H., Hofmann, R., Lelieveld, J., and Williams, J.: An aircraft gas chromatograph–mass spectrometer System for Organic Fast Identification Analysis (SOFIA): design, performance and a case study of Asian monsoon pollution outflow, Atmos. Meas. Tech., 10, 5089-5105, 10.5194/amt-10-5089-2017, 2017.

Dethof, A., O'neill, A., Slingo, J., and Smit, H.: A mechanism for moistening the lower stratosphere involving the Asian summer monsoon, Q J Roy Meteor Soc, 125, 1079-1106, 1999.

Dlugokencky, E. J., Myers, R. C., Lang, P. M., Masarie, K. A., Crotwell, A. M., Thoning, K. W., Hall, B. D., Elkins, J. W., and Steele, L. P.: Conversion of NOAA atmospheric dry air CH_4 mole fractions to a gravimetrically prepared standard scale, J Geophys Res-Atmos, 110, Artn D18306

10.1029/2005jd006035, 2005.

Emanuel, K. A., and Zivkovic-Rothman, M.: Development and evaluation of a convection scheme for use in climate models, J Atmos Sci, 56, 1766-1782, Doi 10.1175/1520-0469(1999)056<1766:Daeoac>2.0.Co;2, 1999.

Garny, H., and Randel, W.: Dynamic variability of the Asian monsoon anticyclone observed in potential vorticity and correlations with tracer distributions, Journal of Geophysical Research: Atmospheres, 118, 2013.

Gottschaldt, K.-D., Schlager, H., Baumann, R., Bozem, H., Eyring, V., Hoor, P., Jöckel, P., Jurkat, T., Voigt, C., and Zahn, A.: Trace gas composition in the Asian summer monsoon anticyclone: a case study based on aircraft observations and model simulations, Atmos Chem Phys, 17, 6091-6111, 2017.

Gouw, J., Warneke, C., Scheeren, H., Veen, C., Bolder, M., Scheele, M., Williams, J., Wong, S., Lange, L., and Fischer, H.: Overview of the trace gas measurements on board the Citation aircraft during the intensive field phase of INDOEX, Journal of Geophysical Research: Atmospheres, 106, 28453-28467, 2001.

Hoskins, B. J., and Rodwell, M. J.: A model of the Asian summer monsoon. Part I: The global scale, J Atmos Sci, 52, 1329-1340, 1995.

Hsu, C. J., and Plumb, R. A.: Nonaxisymmetric thermally driven circulations and upper-tropospheric monsoon dynamics, J Atmos Sci, 57, 1255-1276, 2000.

Jeuken, A., Siegmund, P., Heijboer, L., Feichter, J., and Bengtsson, L.: On the potential of assimilating meteorological analyses in a global climate model for the purpose of model validation, Journal of Geophysical Research: Atmospheres, 101, 16939-16950, 1996.

Jöckel, P., Sander, R., Kerkweg, A., Tost, H., and Lelieveld, J.: Technical note: The Modular Earth Submodel System (MESSy) - a new approach towards Earth System Modeling, Atmos Chem Phys, 5, 433-444, 2005.

Jöckel, P., Kerkweg, A., Pozzer, A., Sander, R., Tost, H., Riede, H., Baumgaertner, A., Gromov, S., and Kern, B.: Development cycle 2 of the modular earth submodel system (MESSy2), Geosci Model Dev, 3, 717, 2010.

Jöckel, P., Tost, H., Pozzer, A., Kunze, M., Kirner, O., Brenninkmeijer, C. A., Brinkop, S., Cai, D. S., Dyroff, C., and Eckstein, J.: Earth System Chemistry integrated Modelling (ESCiMo) with the Modular Earth Submodel System (MESSy) version 2.51, Geosci Model Dev, 9, 2016.

Junge, C. E.: Residence time and variability of tropospheric trace gases, Tellus, 26, 477-488, 1974.

Khalil, M. A. K.: Atmospheric methane: an introduction, in: Atmospheric Methane, Springer, 1-8, 2000.

Krishnamurti, T., and Ardanuy, P.: The 10 to 20-day westward propagating mode and "Breaks in the Monsoons", Tellus, 32, 15-26, 1980.

Krol, M., de Bruine, M., Killaars, L., Ouwersloot, H., Pozzer, A., Yin, Y., Chevallier, F., Bousquet, P., Patra, P., and Belikov, D.: Age of air as a diagnostic for transport timescales in global models, Geosci. Model Dev., 11, 3109–3130, in, 2018.

Lawrence, M., and Lelieveld, J.: Atmospheric pollutant outflow from southern Asia: a review, Atmos Chem Phys, 10, 11017, 2010.

Lelieveld, J., Berresheim, H., Borrmann, S., Crutzen, P., Dentener, F., Fischer, H., Feichter, J., Flatau, P., Heland, J., and Holzinger, R.: Global air pollution crossroads over the Mediterranean, Science, 298, 794-799, 2002.

Lelieveld, J., Gromov, S., Pozzer, A., and Taraborrelli, D.: Global tropospheric hydroxyl distribution, budget and reactivity, Atmos. Chem. Phys, 16, 12477-12493, 2016.

Lelieveld, J., Bourtsoukidis, E., Brühl, C., Fischer, H., Fuchs, H., Harder, H., Hofzumahaus, A., Holland, F., Marno, D., and Neumaier, M.: The South Asian monsoon—Pollution pump and purifier, Science, eaar2501, 2018.

Li, Q., Jiang, J. H., Wu, D. L., Read, W. G., Livesey, N. J., Waters, J. W., Zhang, Y., Wang, B., Filipiak, M. J., and Davis, C. P.: Convective outflow of South Asian pollution: A global CTM simulation compared with EOS MLS observations, Geophys Res Lett, 32, 2005.

Menzel, W. P., Frey, R. A., Zhang, H., Wylie, D. P., Moeller, C. C., Holz, R. E., Maddux, B., Baum, B. A., Strabala, K. I., and Gumley, L. E.: MODIS global cloud-top pressure and amount estimation: Algorithm description and results, Journal of Applied Meteorology and Climatology, 47, 1175-1198, 2008.

Nützel, M., Dameris, M., and Garny, H.: Movement, drivers and bimodality of the South Asian High, Atmos Chem Phys, 16, 14755-14774, 2016.

Ohara, T., Akimoto, H., Kurokawa, J.-I., Horii, N., Yamaji, K., Yan, X., and Hayasaka, T.: An Asian emission inventory of anthropogenic emission sources for the period 1980–2020, Atmos Chem Phys, 7, 4419-4444, 2007.

Ojha, N., Pozzer, A., Rauthe-Schöch, A., Baker, A. K., Yoon, J., Brenninkmeijer, C. A., and Lelieveld, J.: Ozone and carbon monoxide over India during the summer monsoon: regional emissions and transport, Atmos. Chem. Phys, 16, 3013-3032, 2016.

Ouwersloot, H., Pozzer, A., Steil, B., Tost, H., and Lelieveld, J.: Revision of the convective transport module CVTRANS 2.4 in the EMAC atmospheric chemistry–climate model, Geosci Model Dev, 8, 2435-2445, 2015.

Pan, L. L., Honomichl, S. B., Kinnison, D. E., Abalos, M., Randel, W. J., Bergman, J. W., and Bian, J.: Transport of chemical tracers from the boundary layer to stratosphere associated with the dynamics of the Asian summer monsoon, J Geophys Res-Atmos, 121, 14159-14174, 10.1002/2016jd025616, 2016.

Pandis, S. N., and Seinfeld, J. H.: Atmospheric chemistry and physics: From air pollution to climate change, Wiley, 2006.

Park, M., Randel, W. J., Kinnison, D. E., Garcia, R. R., and Choi, W.: Seasonal variation of methane, water vapor, and nitrogen oxides near the tropopause: Satellite observations and model simulations, Journal of Geophysical Research: Atmospheres, 109, 2004.

Park, M., Randel, W. J., Gettelman, A., Massie, S. T., and Jiang, J. H.: Transport above the Asian summer monsoon anticyclone inferred from Aura Microwave Limb Sounder tracers, Journal of Geophysical Research: Atmospheres, 112, 2007.

Park, M., Randel, W. J., Emmons, L. K., Bernath, P. F., Walker, K. A., and Boone, C. D.: Chemical isolation in the Asian monsoon anticyclone observed in Atmospheric Chemistry Experiment (ACE-FTS) data, Atmos Chem Phys, 8, 757-764, 2008.

Park, M., Randel, W. J., Emmons, L. K., and Livesey, N. J.: Transport pathways of carbon monoxide in the Asian summer monsoon diagnosed from Model of Ozone and Related Tracers (MOZART), Journal of Geophysical Research: Atmospheres, 114, 2009.

Platnick, S.: MODIS Atmosphere L3 Daily Product. NASA MODIS Adaptive Processing System, Goddard Space Flight Center, USA.[Available at https://dx. doi/10.5067/MODIS/MOD08_D3. 006.], 2015.

Ploeger, F., Gottschling, C., Griessbach, S., Grooß, J.-U., Guenther, G., Konopka, P., Müller, R., Riese, M., Stroh, F., and Tao, M.: A potential vorticity-based determination of the transport barrier in the Asian summer monsoon anticyclone, Atmos Chem Phys, 15, 13145-13159, 2015.

Popovic, J. M., and Plumb, R. A.: Eddy shedding from the upper-tropospheric Asian monsoon anticyclone, J Atmos Sci, 58, 93-104, 2001.

Randel, W. J., and Park, M.: Deep convective influence on the Asian summer monsoon anticyclone and associated tracer variability observed with Atmospheric Infrared Sounder (AIRS), J Geophys Res-Atmos, 111, Artn D1231410.1029/2005jd006490, 2006.

Rauthe-Schöch, A., Baker, A. K., Schuck, T. J., Brenninkmeijer, C. A., Zahn, A., Hermann, M., Stratmann, G., Ziereis, H., van Velthoven, P. F., and Lelieveld, J.: Trapping, chemistry, and export of trace gases in the South Asian summer monsoon observed during CARIBIC flights in 2008, Atmos Chem Phys, 16, 3609-3629, 2016.

Roeckner, E., Brokopf, R., Esch, M., Giorgetta, M., Hagemann, S., Kornblueh, L., Manzini, E., Schlese, U., and Schulzweida, U.: Sensitivity of simulated climate to horizontal and vertical resolution in the ECHAM5 atmosphere model, J Climate, 19, 3771-3791, 2006.

Saito, R., Patra, P. K., Sweeney, C., Machida, T., Krol, M., Houweling, S., Bousquet, P., Agusti-Panareda, A., Belikov, D., and Bergmann, D.: TransCom model simulations of methane: Comparison of vertical profiles with aircraft measurements, Journal of Geophysical Research: Atmospheres, 118, 3891-3904, 2013.

Scheeren, H., Lelieveld, J., Roelofs, G., Williams, J., Fischer, H., Reus, M. d., De Gouw, J., Warneke, C., Holzinger, R., and Schlager, H.: The impact of monsoon outflow from India and Southeast Asia in the upper troposphere over the eastern Mediterranean, Atmos Chem Phys, 3, 1589-1608, 2003.

Schiller, C. L., Bozem, H., Gurk, C., Parchatka, U., Konigstedt, R., Harris, G. W., Lelieveld, J., and Fischer, H.: Applications of quantum cascade lasers for sensitive trace gas measurements of CO, CH4, N2O and HCHO, Appl Phys B-Lasers O, 92, 419-430, 10.1007/s00340-008-3125-0, 2008.

Schuck, T., Ishijima, K., Patra, P., Baker, A., Machida, T., Matsueda, H., Sawa, Y., Umezawa, T., Brenninkmeijer, C., and Lelieveld, J.: Distribution of methane in the tropical upper troposphere measured by CARIBIC and CONTRAIL aircraft, Journal of Geophysical Research: Atmospheres, 117, 2012.

Stohl, A., Hittenberger, M., and Wotawa, G.: Validation of the Lagrangian particle dispersion model FLEXPART against large-scale tracer experiment data, Atmos Environ, 32, 4245-4264, Doi 10.1016/S1352-2310(98)00184-8, 1998.

Stohl, A., Eckhardt, S., Forster, C., James, P., Spichtinger, N., and Seibert, P.: A replacement for simple back trajectory calculations in the interpretation of atmospheric trace substance measurements, Atmos Environ, 36, 4635-4648, Pii S1352-2310(02)00416-8, Doi 10.1016/S1352-2310(02)00416-8, 2002.

Stohl, A., Forster, C., Frank, A., Seibert, P., and Wotawa, G.: The Lagrangian particle dispersion model FLEXPART version 6.2, Atmos Chem Phys, 5, 2461-2474, 2005.

Stohl, A., Sodemann, H., Eckhardt, S., Frank, A., Seibert, P., and Wotawa, G.: The Lagrangian particle dispersion model FLEXPART version 8.2. Norwegian Institute of Air Research, Kjeller, Norway, in, 2010.

Tadic, I., Parchatka, U., Konigstedt, R., and Fischer, H.: In-flight stability of quantum cascade laser-based infrared absorption spectroscopy measurements of atmospheric carbon monoxide, Appl Phys B-Lasers O, 123, ARTN 146 10.1007/s00340-017-6721-z, 2017.

Thomson, D.: Criteria for the selection of stochastic models of particle trajectories in turbulent flows, J Fluid Mech, 180, 529-556, 1987.

Tost, H., Jöckel, P., and Lelieveld, J.: Influence of different convection parameterisations in a GCM, Atmos Chem Phys, 6, 5475-5493, 2006.

Van der Werf, G. R., Randerson, J. T., Giglio, L., Collatz, G., Mu, M., Kasibhatla, P. S., Morton, D. C., DeFries, R., Jin, Y. v., and van Leeuwen, T. T.: Global fire emissions and the contribution of deforestation, savanna, forest, agricultural, and peat fires (1997–2009), Atmos Chem Phys, 10, 11707-11735, 2010.

Van Vuuren, D. P., Edmonds, J., Kainuma, M., Riahi, K., Thomson, A., Hibbard, K., Hurtt, G. C., Kram, T., Krey, V., and Lamarque, J.-F.: The representative concentration pathways: an overview, Climatic Change, 109, 5, 2011.

Vogelezang, D. H. P., and Holtslag, A. A. M.: Evaluation and model impacts of alternative boundary-layer height formulations, Bound-Lay Meteorol, 81, 245-269, Doi 10.1007/Bf02430331, 1996.

Waliser, D. E., and Gautier, C.: A satellite-derived climatology of the ITCZ, J Climate, 6, 2162-2174, 1993.

White, J. U.: Very Long Optical Paths in Air, J Opt Soc Am, 66, 411-416, Doi 10.1364/Josa.66.000411, 1976.

Xiao, Y., Jacob, D. J., and Turquety, S.: Atmospheric acetylene and its relationship with CO as an indicator of air mass age, Journal of Geophysical Research: Atmospheres, 112, 2007.

Xiong, X., Houweling, S., Wei, J., Maddy, E., Sun, F., and Barnet, C.: Methane plume over south Asia during the monsoon season: satellite observation and model simulation, Atmos Chem Phys, 9, 783-794, 2009.

Zhang, Q., Wu, G., and Qian, Y.: The bimodality of the 100 hPa South Asia High and its relationship to the climate anomaly over East Asia in summer, Journal of the Meteorological Society of Japan. Ser. II, 80, 733-744, 2002.

Zimmermann, P. H., Brenninkmeijer, C. A. M., Pozzer, A., Jöckel, P., Zahn, A., Houweling, S., and Lelieveld, J.: Model simulations of atmospheric methane and their evaluation using AGAGE/NOAA surface- and IAGOS-CARIBIC aircraft observations, 1997-2014, Atmos. Chem. Phys. Discuss., 2018, 1-45, 10.5194/acp-2017-1212, 2018.

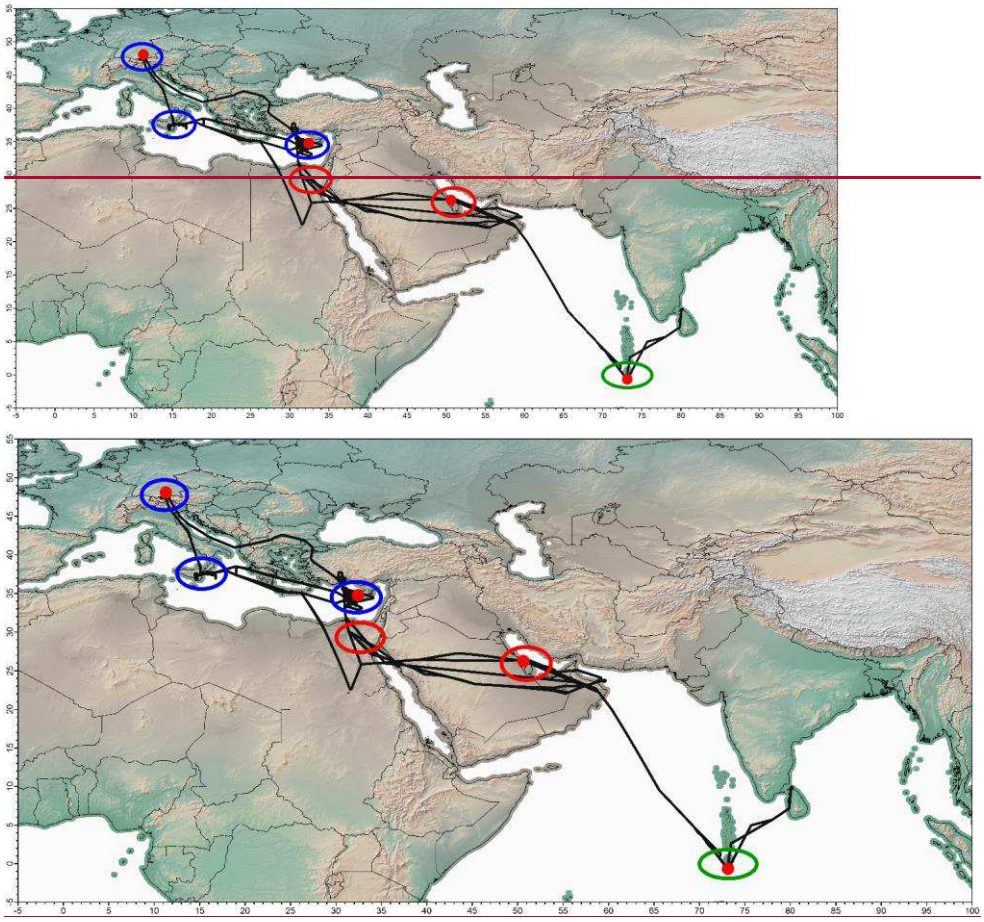

Figure 1: Overview of the flight tracks during OMO with all four airports (red dots): Oberpfaffenhofen (Germany), Paphos (Cyprus), Bahrain and Gan (Maldives). Additionally, the regions of the profiles for northern hemispheric background (blue), AMA (red), and southern hemispheric background (green) are marked.

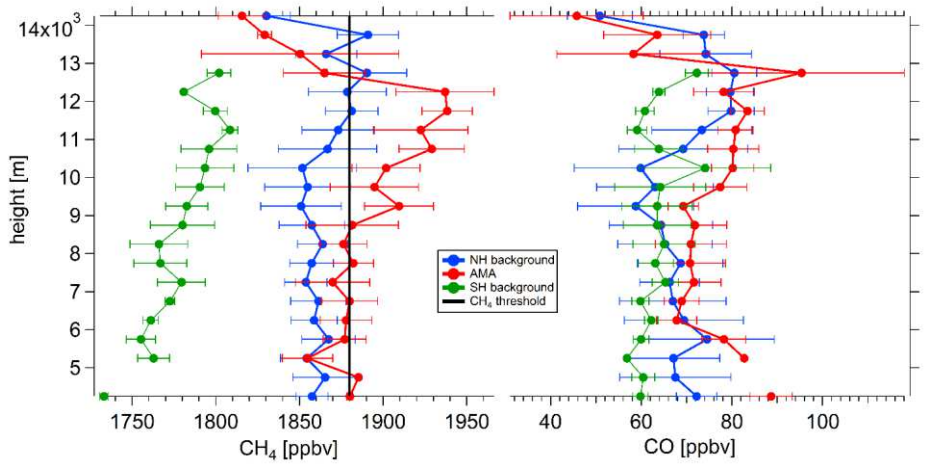

Figure 2: Average profiles for northern hemispheric (NH) background, AMA and southern hemisphere (SH) background for CH_4 (left) and CO (right); profile locations are presented in Figure 1. The CH_4 threshold (1879.8 ppbv) is indicated by the black line.

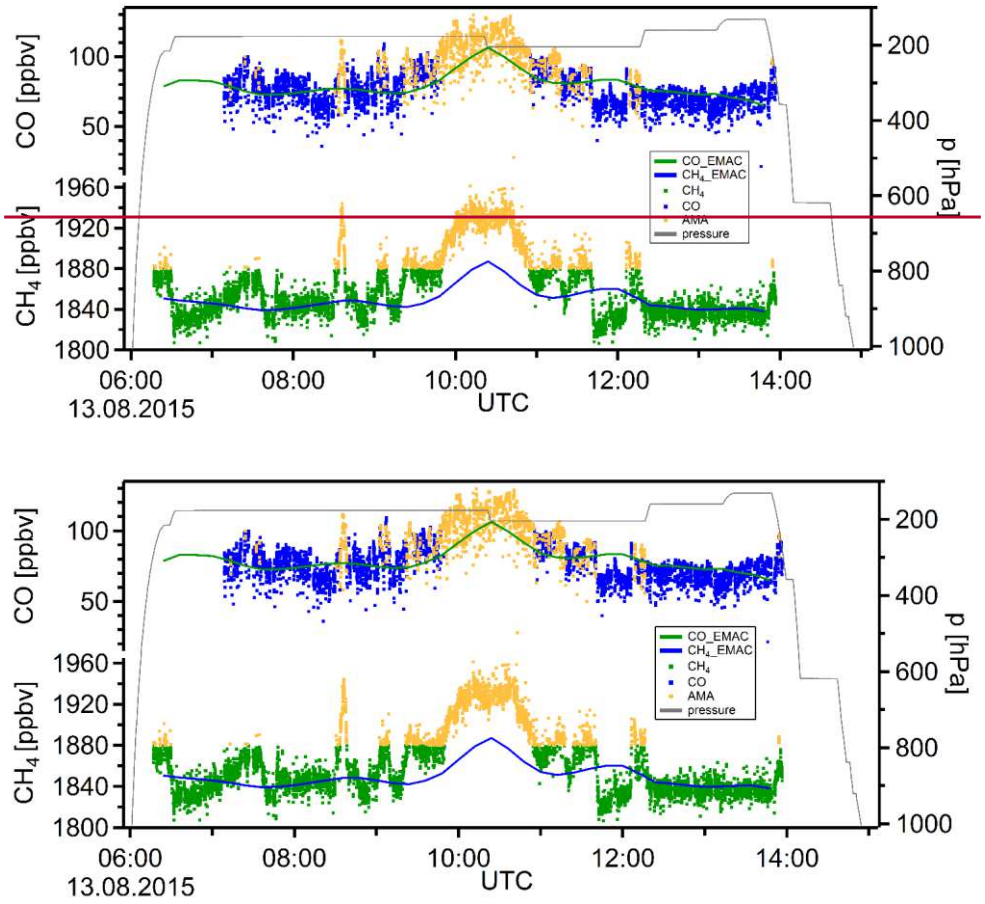

Figure 3: Flight 19 (August 13, 2015) in situ CH_4 and CO data and EMAC results along the flight track, as well as the flight altitude. The AMA is colour coded by CH_4>1879.8 ppbv.

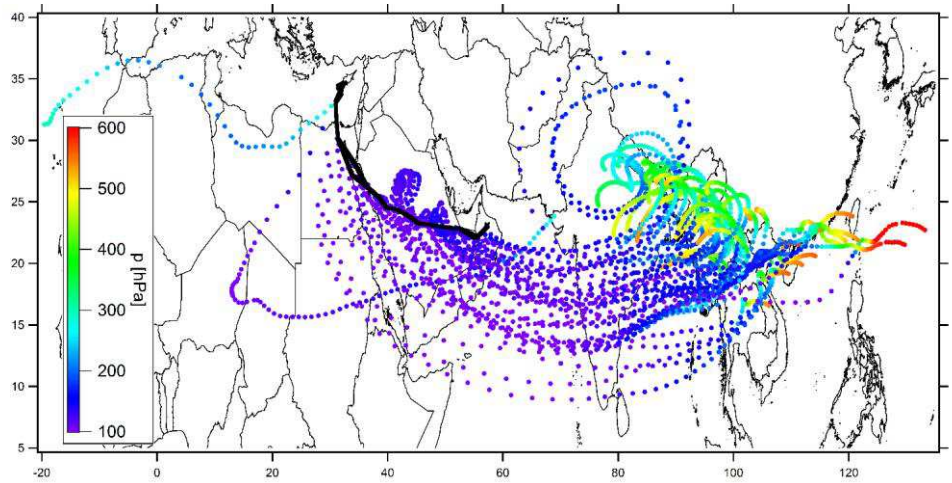

Figure 4: Centroid trajectories for flight 19 (August 13, 2015) with colour coded altitude.

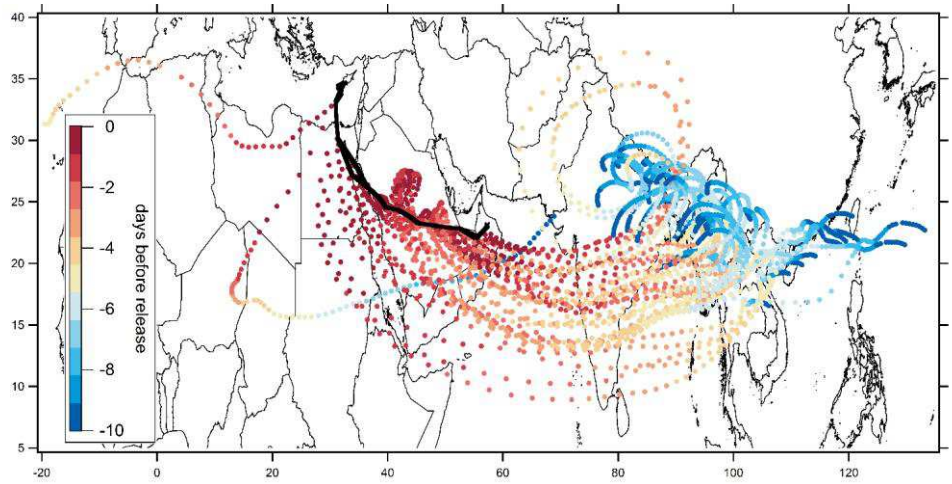

Figure 5: Centroid trajectories for flight 19 (August 13, 2015) with colour coded transport time.

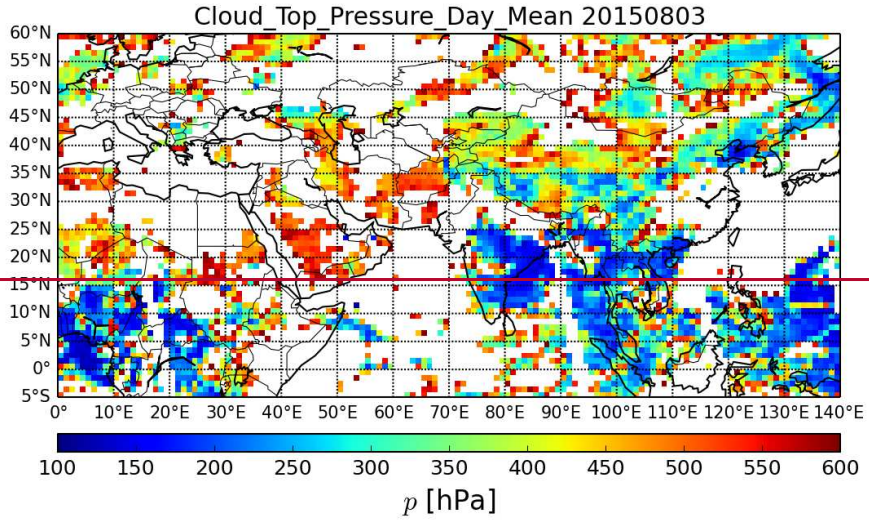
Cloud_Top_Pressure_Day_Mean 20150803
60°N
55°N
50°N
45°N
40°N
35°N
30°N
25°N
20°N
15°N
10°N
5°N
0°
5°S
0°
10°E
20°E
30°E
40°E
50°E
60°E
70°E
80°E
90°E
100°E
110°E
120°E
130°E
140°E
100
150
200
250
300
350
400
450
500
550
600
p [hPa]

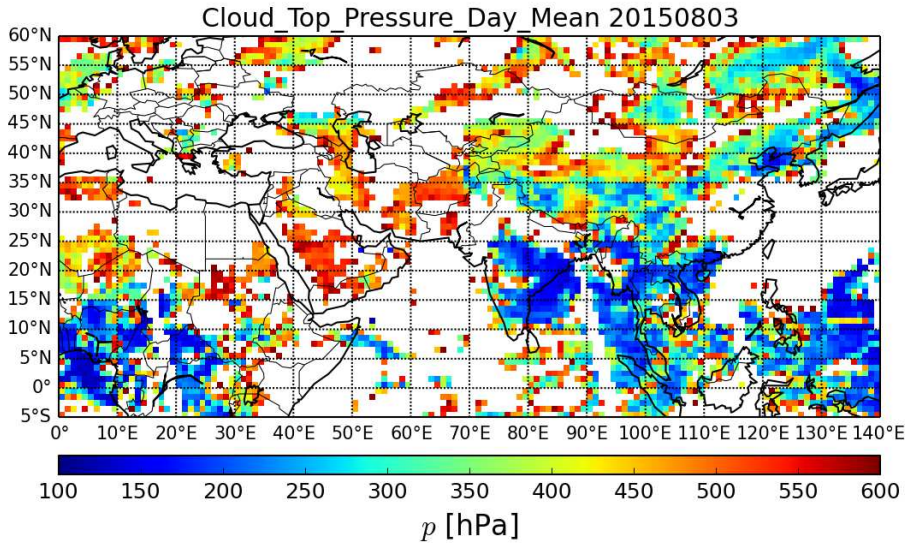

Figure 6: Satellite-derived cloud top pressure 10 days prior (August 03, 2015) to flight 19.

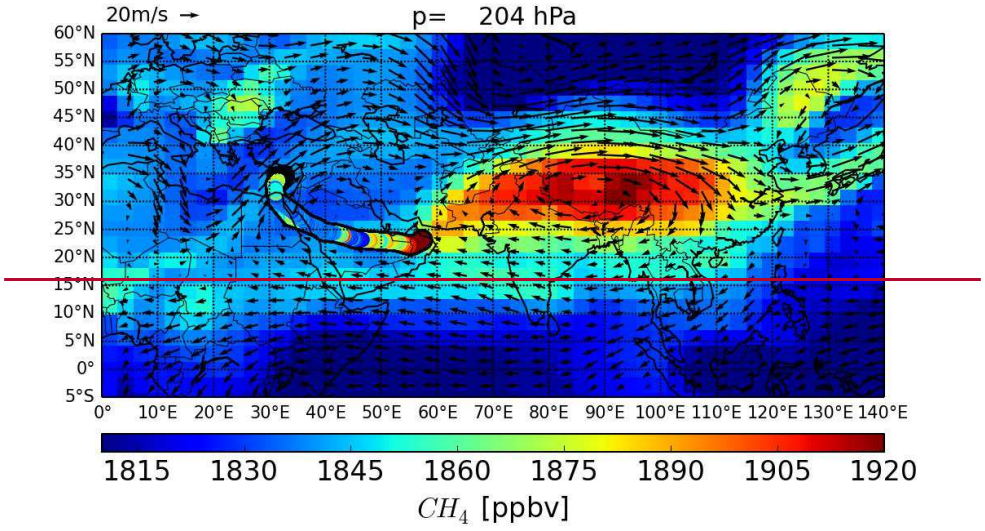
20m/s
p= 204 hPa
60°N
55°N
50°N
45°N
40°N
35°N
30°N
25°N
20°N
15°N
10°N
5°N
0°
5°S
0° 10°E 20°E 30°E 40°E 50°E 60°E 70°E 80°E 90°E 100°E 110°E 120°E 130°E 140°E
1815 1830 1845 1860 1875 1890 1905 1920
CH_4 [ppbv]

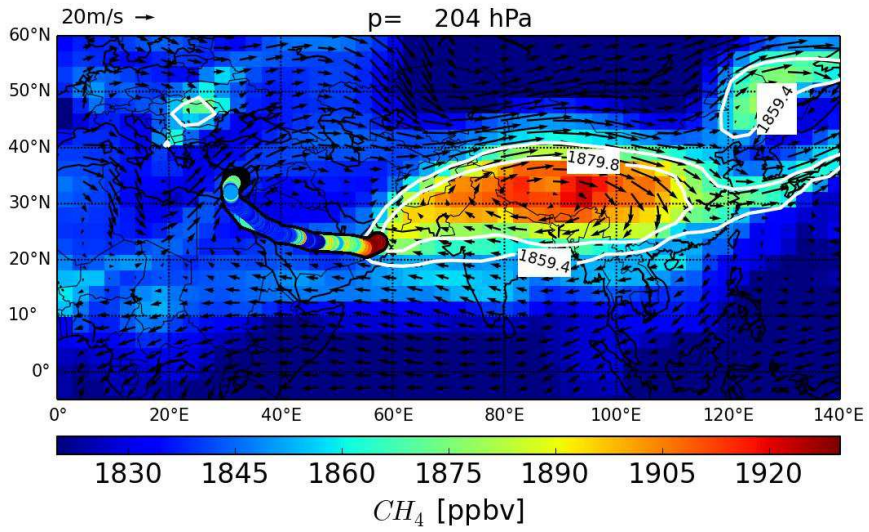

Figure 7: EMAC modelled CH_4 and wind field; daily means at 204 hPa, and in situ CH_4 (above 300 hPa) along the flight track for flight 19 (August 13, 2015). White contours represent CH_4 threshold and background values according to section 3.1.

Kommentiert [TL40]: In Figures 7,8, 18-21 and also in Figures 22 and 23 now contour lines are added for the CH4 threshold (1879.8 ppbv) and the CH4 background (1859.4 ppbv) value according to the calculation of the CH4 threshold in section 3.1. In the horizontal CO distribution also the CH4 threshold is added. Now the position of the AMA is easier to identify with respect to the flight tracks.

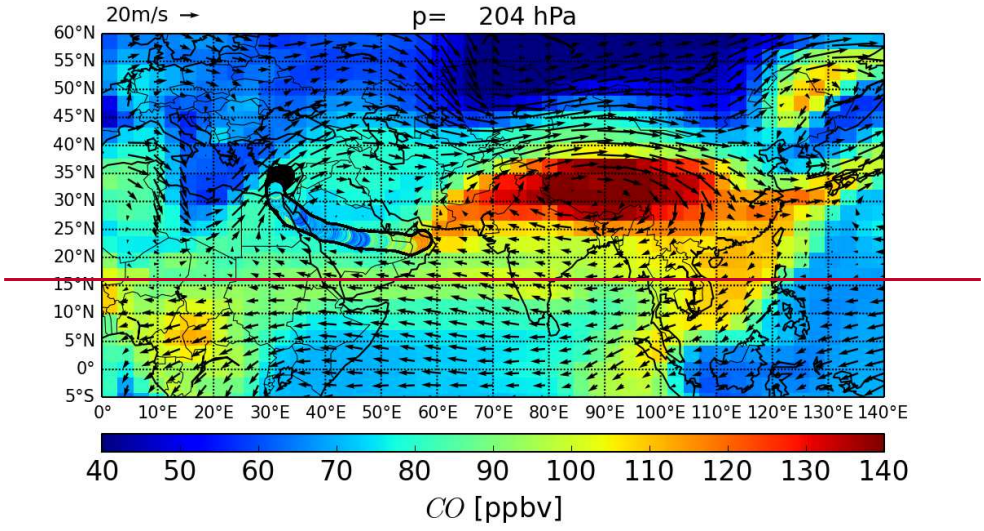
20m/s
p= 204 hPa
60°N
55°N
50°N
45°N
40°N
35°N
30°N
25°N
20°N
15°N
10°N
5°N
0°
5°S
0° 10°E 20°E 30°E 40°E 50°E 60°E 70°E 80°E 90°E 100°E 110°E 120°E 130°E 140°E
40 50 60 70 80 90 100 110 120 130 140
CO [ppbv]

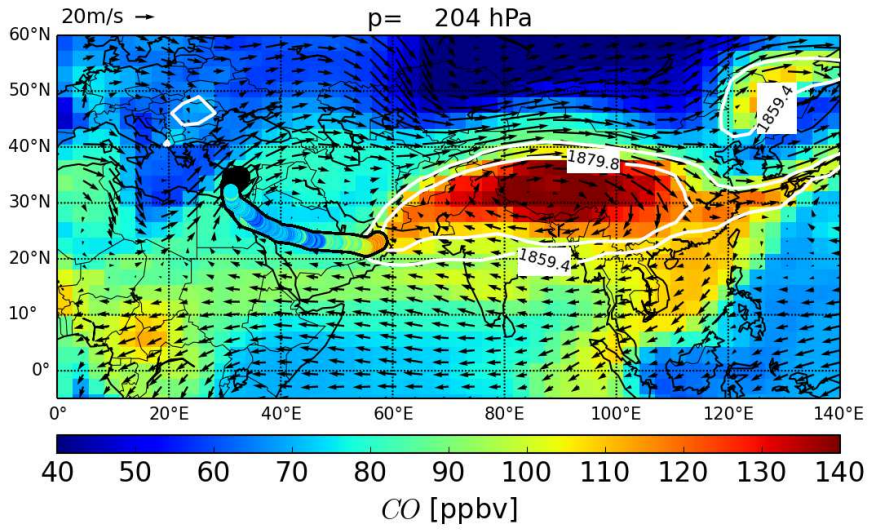

Figure 8: **EMAC modelled CO and wind field; daily mean at 204 hPa, and in situ CO (above 300 hPa) along the flight track for flight 19 (August 13, 2015).** White contours represent CH_4 threshold and background values according to section 3.1.

Kommentiert [TL41]: In Figures 7,8, 18-21 and also in Figures 22 and 23 now contour lines are added for the CH4 threshold (1879.8 ppbv) and the CH4 background (1859.4 ppbv) value according to the calculation of the CH4 threshold in section 3.1. In the horizontal CO distribution also the CH4 threshold is added. Now the position of the AMA is easier to identify with respect to the flight tracks.

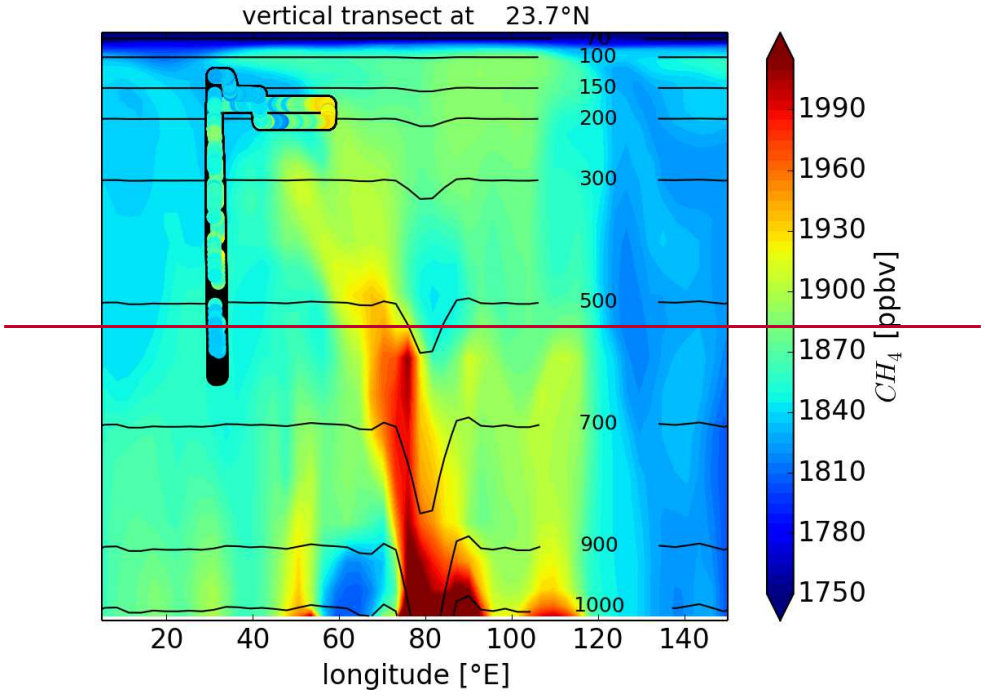
vertical transect at 23.7°N
70
100
150
200
300
500
700
900
1000
20
40
60
80
100
120
140
longitude [°E]
1990
1960
1930
1900
1870
1840
1810
1780
1750
CH_4 [ppbv]

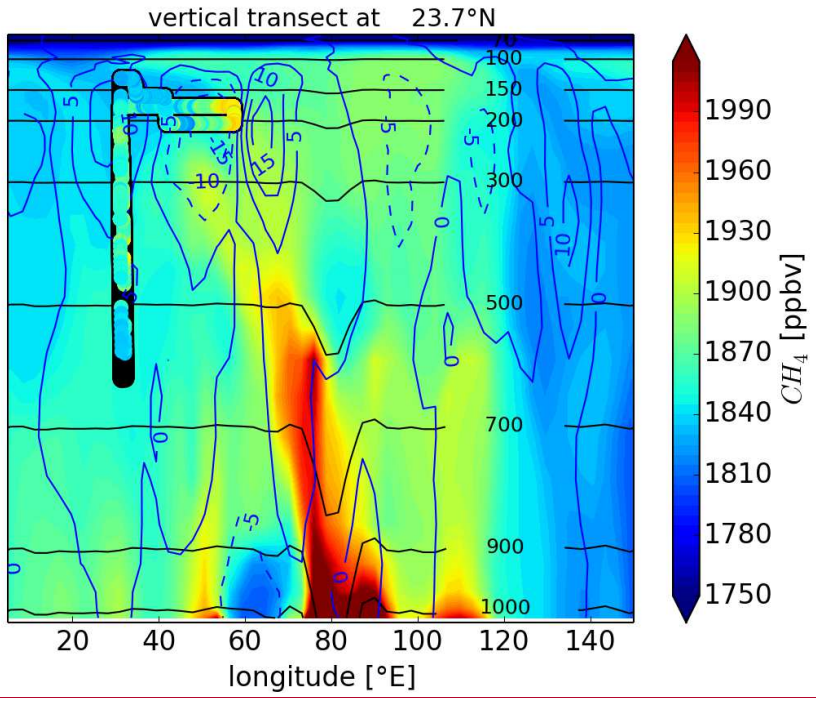

Figure 9: EMAC modelled CH_4; daily mean transect along 23.7°N, and measured CH_4 along the aircraft track for flight 19. Additional EMAC pressure (black lines in hPa) and EMAC northward wind component (blue lines in m/s; southward wind dashed lines).

Kommentiert [TL42]: Horizontal wind components are added to the cross sections in figures 9-12, in detail: eastward wind component in cross sections along a longitude and northward wind component in cross sections along a latitude.

5

40

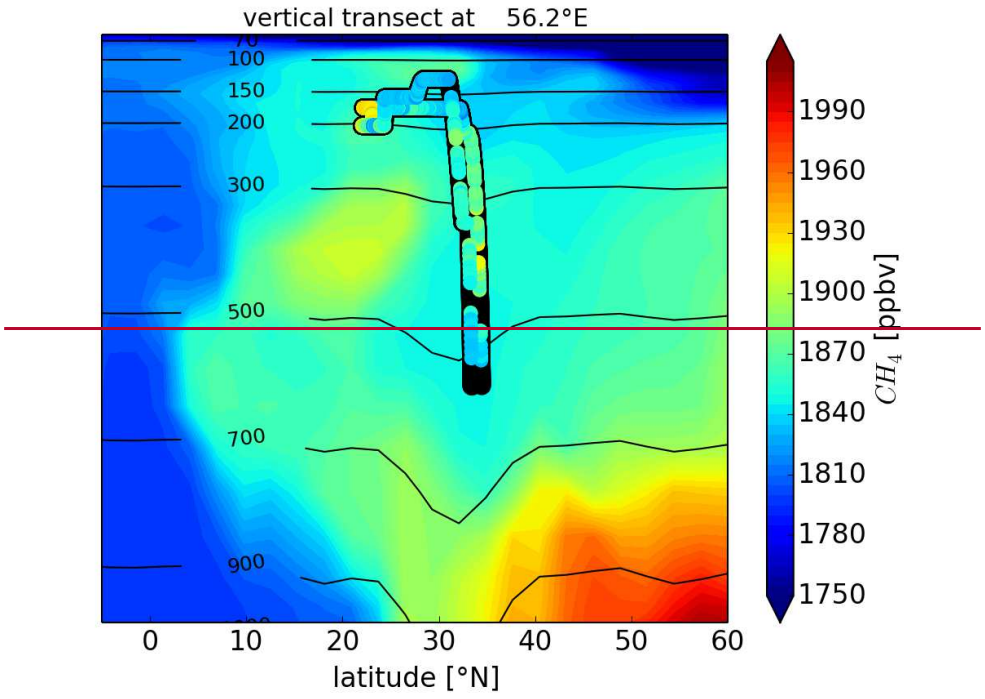
vertical transect at 56.2°E
100
150
200
300
500
700
900
0
10
20
30
40
50
60
latitude [°N]
1990
1960
1930
1900
1870
1840
1810
1780
1750
CH_4 [ppbv]

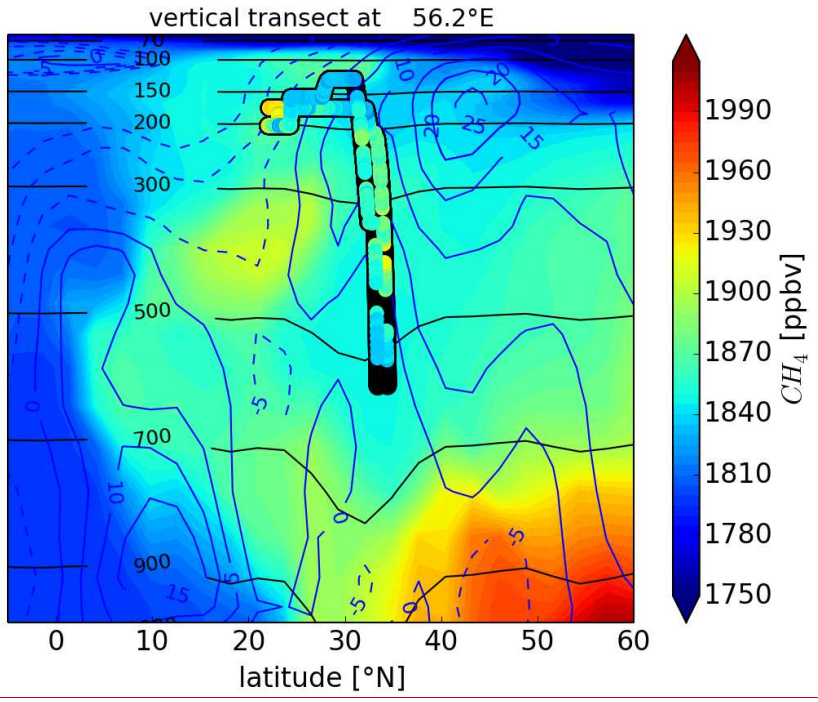

Figure 10: EMAC calculated CH_4; daily mean transect along 56.2°E, and measured CH_4 along the aircraft track for flight 19. Additional EMAC pressure (black lines in hPa) and EMAC eastward wind component (blue lines in m/s; westward wind dashed lines).

Kommentiert [TL43]: Horizontal wind components are added to the cross sections in figures 9-12, in detail: eastward wind component in cross sections along a longitude and northward wind component in cross sections along a latitude.

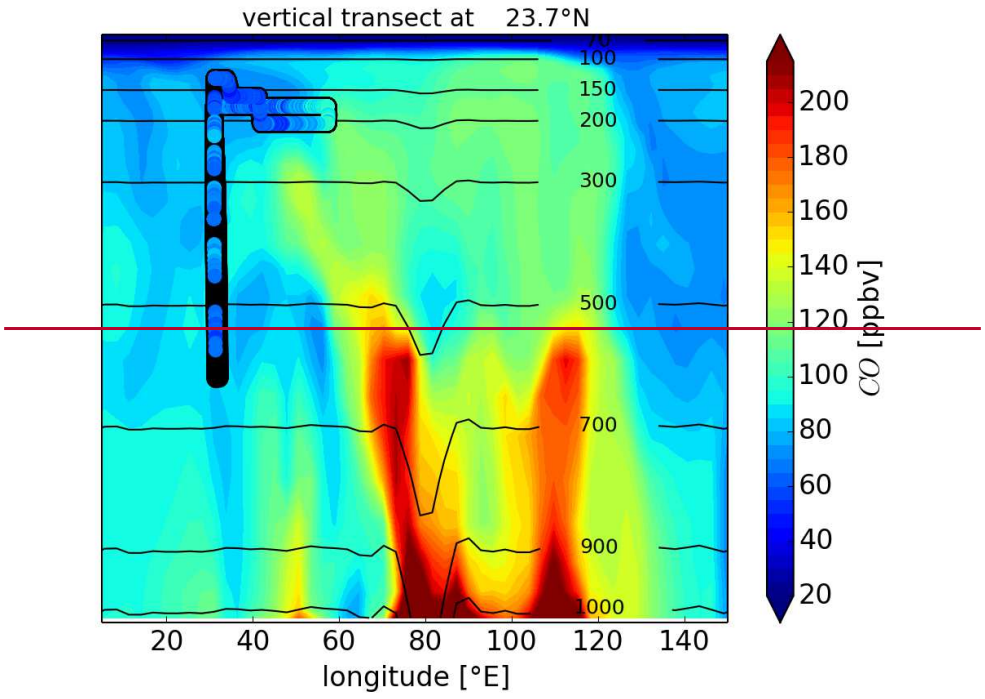
vertical transect at 23.7°N
70
100
150
200
300
500
700
900
1000
20
40
60
80
100
120
140
longitude [°E]
200
180
160
140
120
100
80
60
40
20
CO [ppbv]

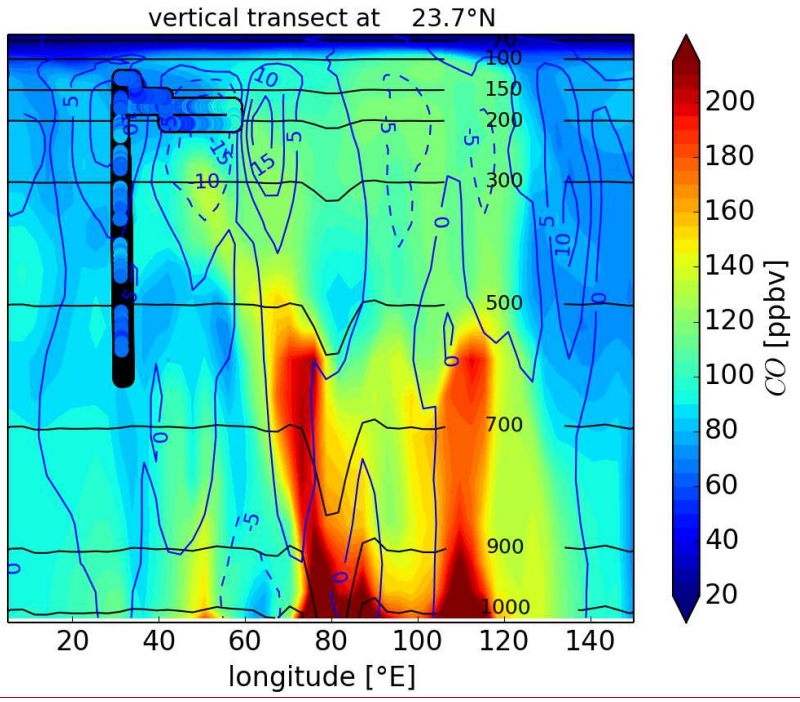

Figure 11: EMAC modelled CO; daily mean transect along 23.7°N, and CO measured along the aircraft track for flight 19. Additional EMAC pressure (black lines in hPa) and EMAC northward wind component (blue lines in m/s; southward wind dashed lines).

Kommentiert [TL44]: Horizontal wind components are added to the cross sections in figures 9-12, in detail: eastward wind component in cross sections along a longitude and northward wind component in cross sections along a latitude.

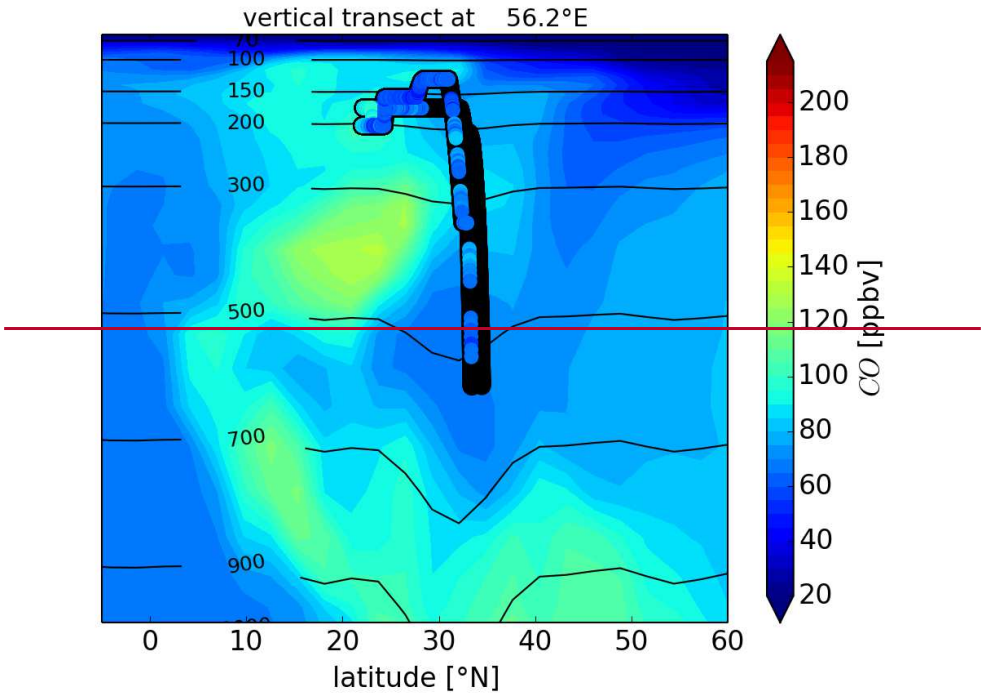
vertical transect at 56.2°E
100
150
200
300
500
700
900
0
10
20
30
40
50
60
latitude [°N]
200
180
160
140
120
100
80
60
40
20
CO [ppbv]

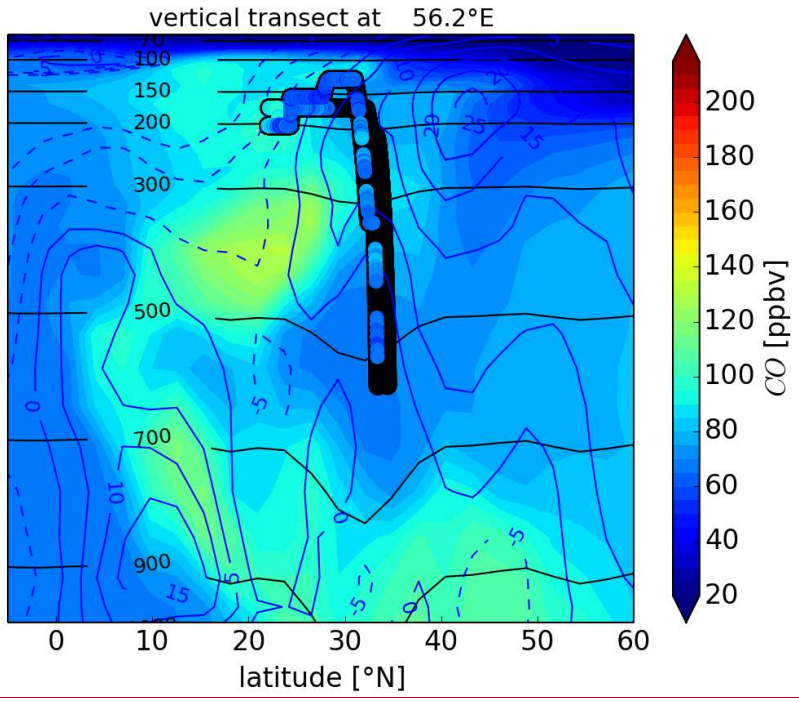

Figure 12: EMAC modelled CO; daily mean transect along 56.2°E, and CO measured along the aircraft track for flight 19. Additional EMAC pressure (black lines in hPa) and EMAC eastward wind component (blue lines in m/s; westward wind dashed lines).

Kommentiert [TL45]: Horizontal wind components are added to the cross sections in figures 9-12, in detail: eastward wind component in cross sections along a longitude and northward wind component in cross sections along a latitude.

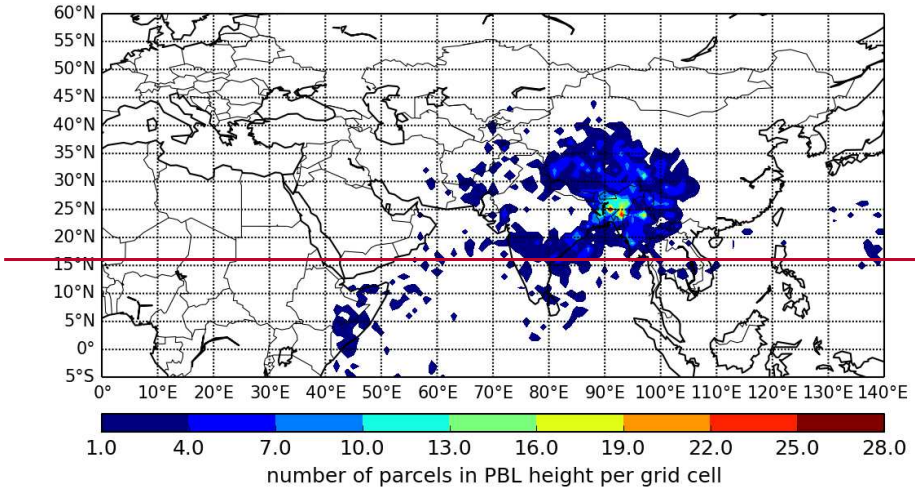
60°N
55°N
50°N
45°N
40°N
35°N
30°N
25°N
20°N
15°N
10°N
5°N
0°
5°S
0° 10°E 20°E 30°E 40°E 50°E 60°E 70°E 80°E 90°E 100°E 110°E 120°E 130°E 140°E
1.0 4.0 7.0 10.0 13.0 16.0 19.0 22.0 25.0 28.0
number of parcels in PBL height per grid cell

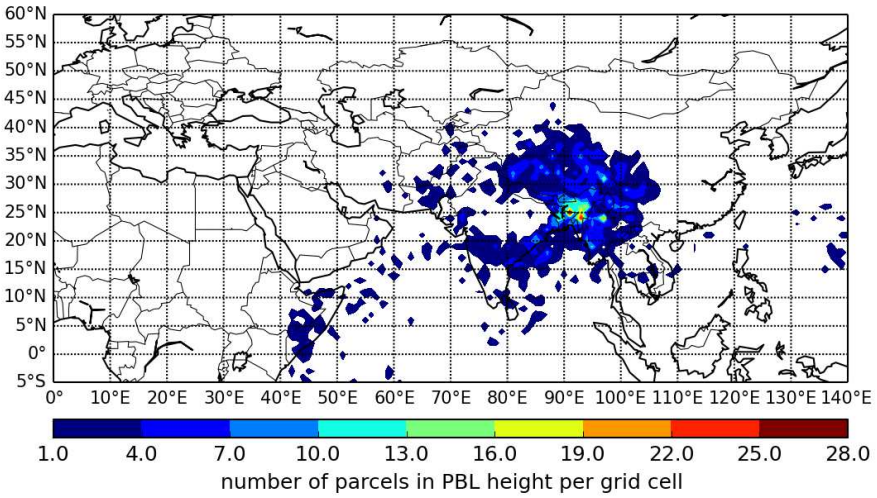

Figure 13: Last boundary layer contact of parcels before they were transported to the track of flight 19 (10 days prior to flight).

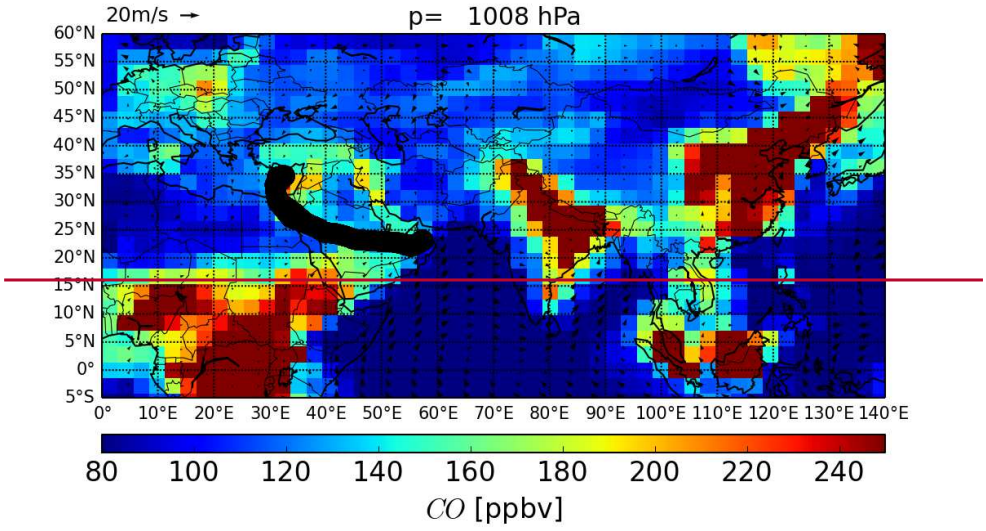
20m/s
p= 1008 hPa
60°N
55°N
50°N
45°N
40°N
35°N
30°N
25°N
20°N
15°N
10°N
5°N
0°
5°S
0° 10°E 20°E 30°E 40°E 50°E 60°E 70°E 80°E 90°E 100°E 110°E 120°E 130°E 140°E
80 100 120 140 160 180 200 220 240
CO [ppbv]

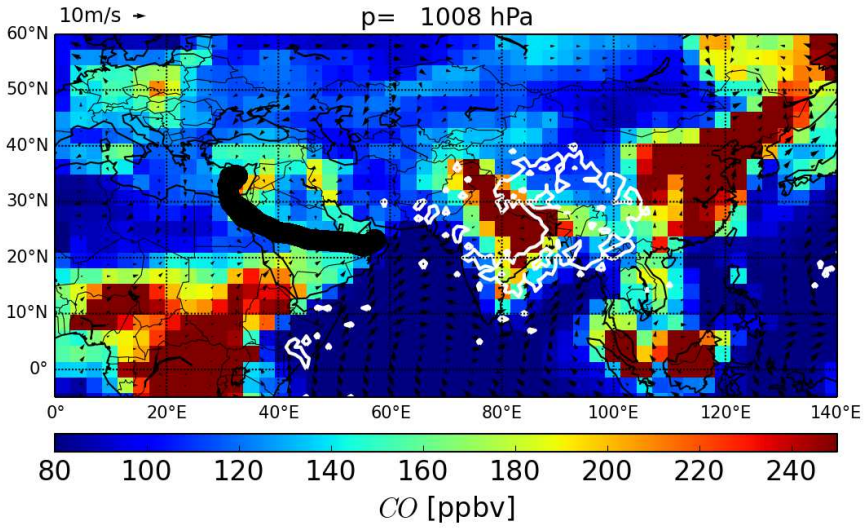

Figure 14: EMAC calculated CO; daily mean at the surface (1008 hPa, August 03, 2015) as an indicator for surface emissions (10 days prior to measurement) and the flight track of flight 19 (black). Additionally, the footprint of the last boundary layer contact as white contour line from Figure 13.

Kommentiert [TL46]: Footprint is now added as white contour lines for the number of particles per grid cell = 2 to the surface emission charts for CH4 and CO (Figures14 and 15).
.

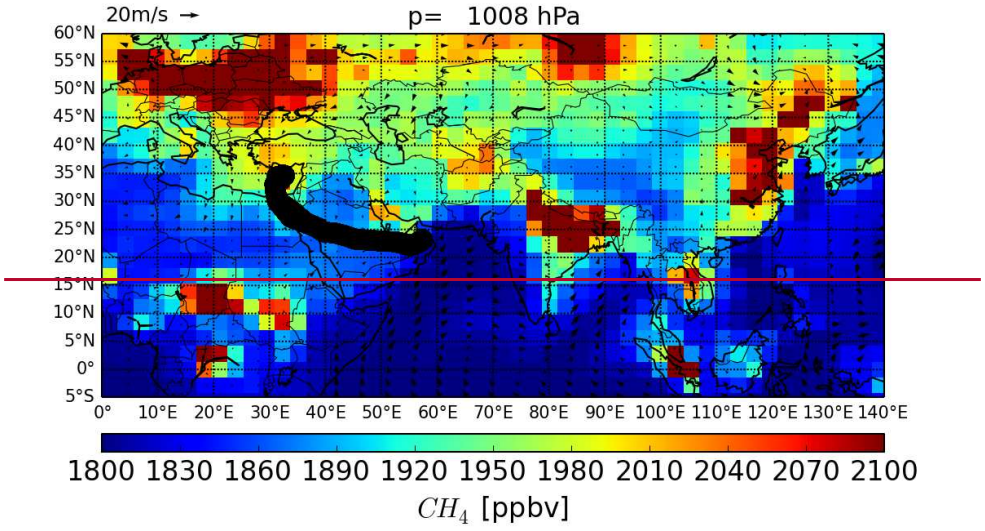
20m/s
p= 1008 hPa
60°N
55°N
50°N
45°N
40°N
35°N
30°N
25°N
20°N
15°N
10°N
5°N
0°
5°S
0° 10°E 20°E 30°E 40°E 50°E 60°E 70°E 80°E 90°E 100°E 110°E 120°E 130°E 140°E
1800 1830 1860 1890 1920 1950 1980 2010 2040 2070 2100
CH_4 [ppbv]

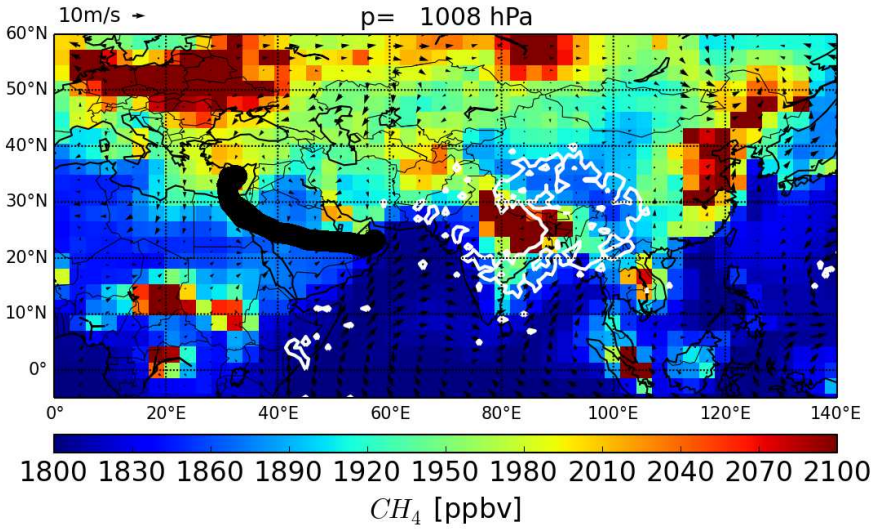

Figure 15: EMAC calculated CH_4; daily mean at the surface (1008 hPa, August 03, 2015) as an indicator for surface emissions (10 days prior to measurements), and the track of flight 19 (black). Additionally, the footprint of the last boundary layer contact as white contour line from Figure 13.

Kommentiert [TL47]: Footprint is now added as white contour lines for the number of particles per grid cell = 2 to the surface emission charts for CH4 and CO (Figures14 and 15).
.

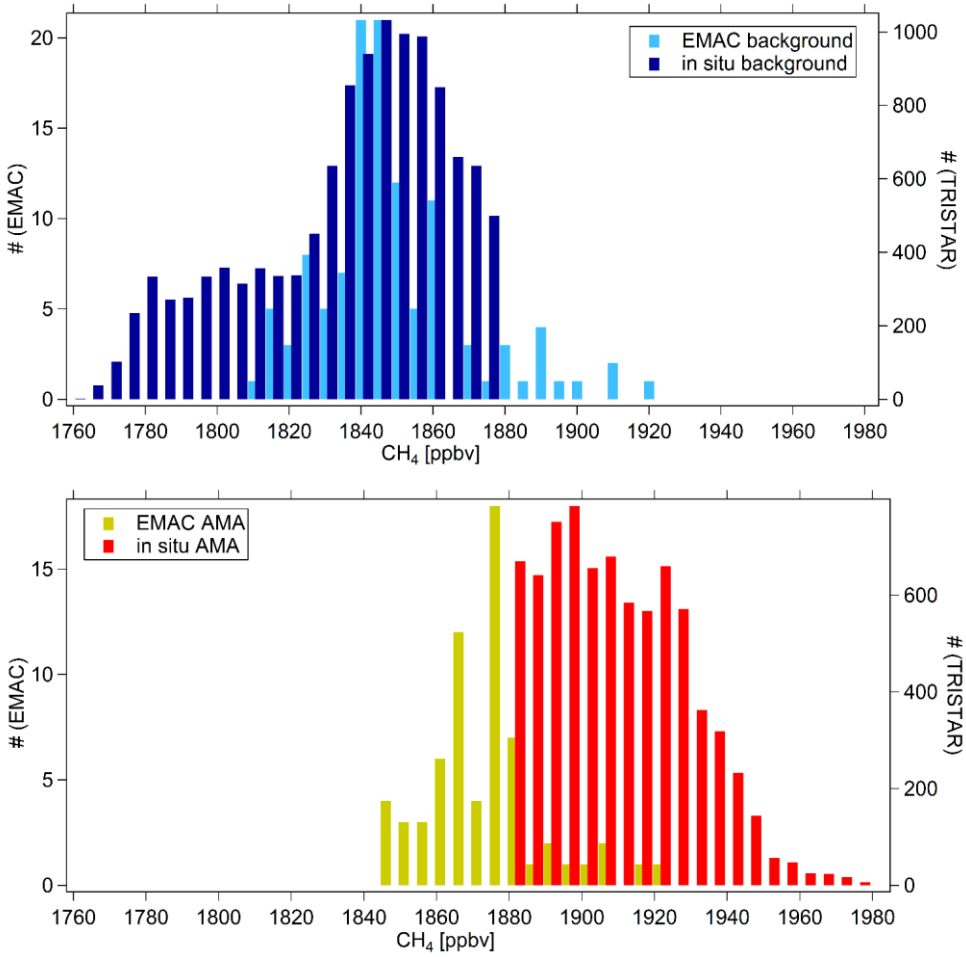

Figure 16: Histogram for in situ measured and EMAC modelled CH_4 within the altitude range 300-140 hPa, both for background and AMA air.

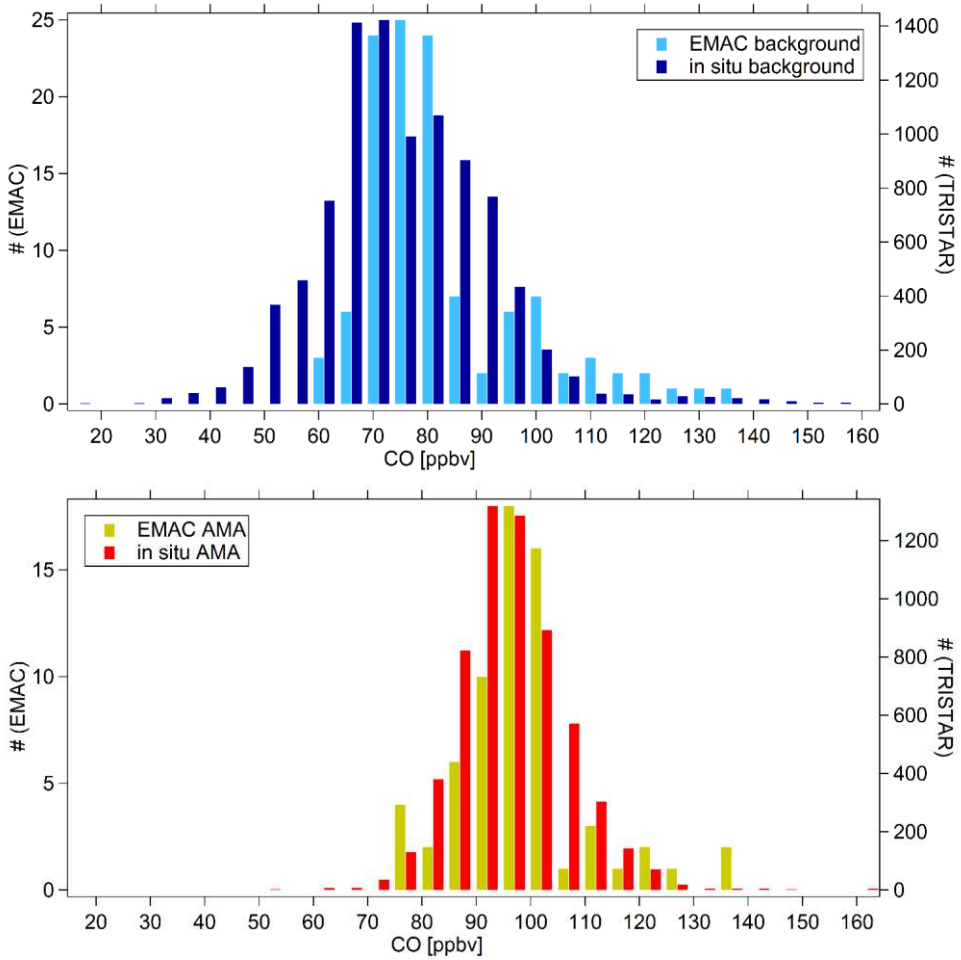

Figure 17: Histogram for in situ measured and EMAC modelled CO within the altitude range 300-140 hPa, both for background and AMA air.

Table 1: CH_4 and CO averages and standard deviations for in situ measured and EMAC data, both for background and monsoon influenced air masses according to the CH_4 threshold for altitudes between 300-140 hPa.

p=[300-140] hPa		CH_4 [ppbv]		CO [ppbv]	
		avg	std	avg	std
monsoon	in situ	1910.0	19.2	96.9	10.0
	EMAC	1874.4	15.3	99.0	11.9
background	in situ	1837.9	27.6	76.8	15.7
	EMAC	1850.5	21.2	84.3	15.1

Formatiert: Beschriftung3

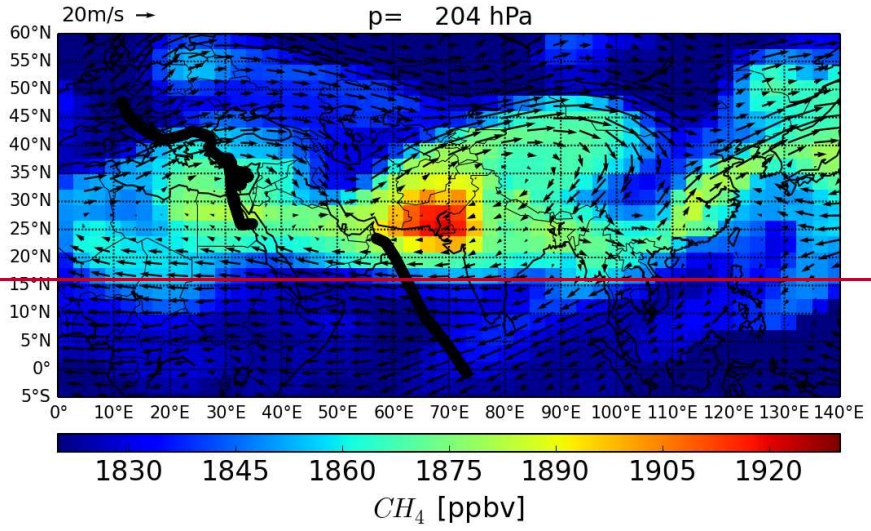
20m/s
p= 204 hPa
60°N
55°N
50°N
45°N
40°N
35°N
30°N
25°N
20°N
15°N
10°N
5°N
0°
5°S
0° 10°E 20°E 30°E 40°E 50°E 60°E 70°E 80°E 90°E 100°E 110°E 120°E 130°E 140°E
1830 1845 1860 1875 1890 1905 1920
CH_4 [ppbv]

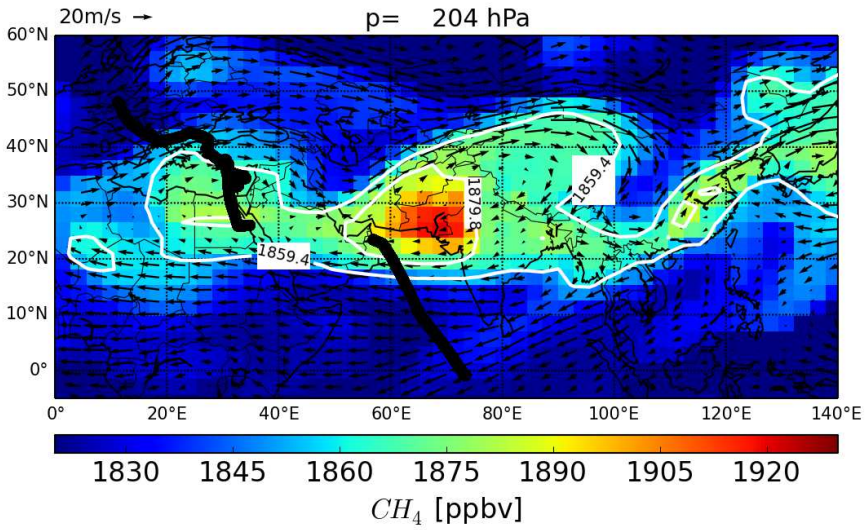

Figure 18: Double anticyclone mode illustrated with wind field and CH_4 EMAC daily means at 204 hPa (July 25, 2015) and the associated flight tracks. White contours represent CH_4 threshold and background values according to section 3.1.

Kommentiert [TL48]: In Figures 7,8, 18-21 and also in Figures 22 and 23 now contour lines are added for the CH4 threshold (1879.8 ppbv) and the CH4 background (1859.4 ppbv) value according to the calculation of the CH4 threshold in section 3.1. In the horizontal CO distribution also the CH4 threshold is added. Now the position of the AMA is easier to identify with respect to the flight tracks.

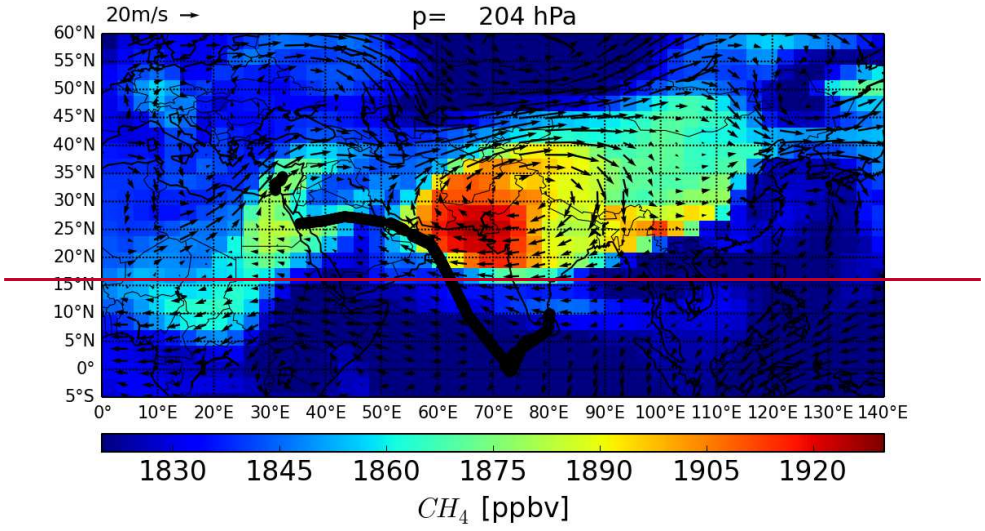
20m/s
p= 204 hPa
60°N
55°N
50°N
45°N
40°N
35°N
30°N
25°N
20°N
15°N
10°N
5°N
0°
5°S
0° 10°E 20°E 30°E 40°E 50°E 60°E 70°E 80°E 90°E 100°E 110°E 120°E 130°E 140°E
1830 1845 1860 1875 1890 1905 1920
CH_4 [ppbv]

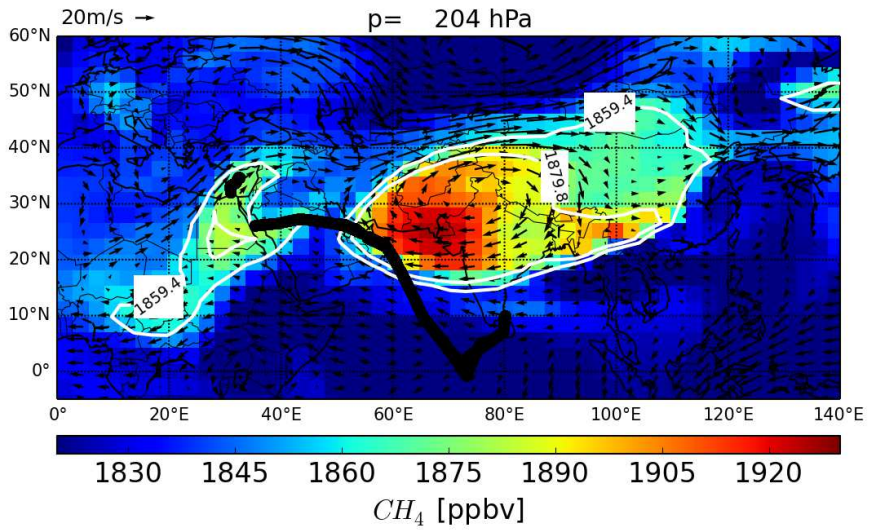

Figure 19: **Central anticyclone mode illustrated with wind field and CH_4 EMAC daily means at 204 hPa (August 09, 2015) and the associated flight tracks.** White contours represent CH_4 threshold and background values according to section 3.1.

Kommentiert [TL49]: In Figures 7,8, 18-21 and also in Figures 22 and 23 now contour lines are added for the CH4 threshold (1879.8 ppbv) and the CH4 background (1859.4 ppbv) value according to the calculation of the CH4 threshold in section 3.1. In the horizontal CO distribution also the CH4 threshold is added. Now the position of the AMA is easier to identify with respect to the flight tracks.

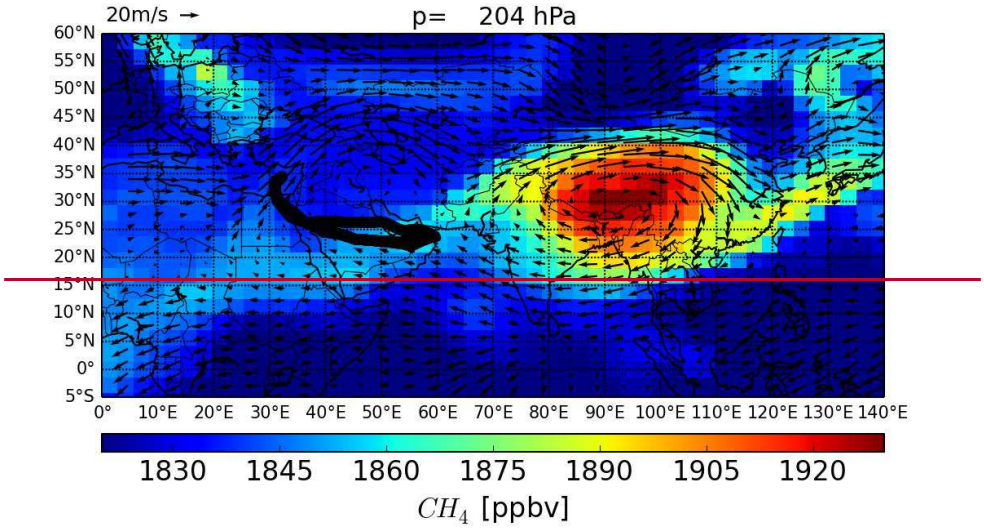
20m/s
p= 204 hPa
60°N
55°N
50°N
45°N
40°N
35°N
30°N
25°N
20°N
15°N
10°N
5°N
0°
5°S
0° 10°E 20°E 30°E 40°E 50°E 60°E 70°E 80°E 90°E 100°E 110°E 120°E 130°E 140°E
1830 1845 1860 1875 1890 1905 1920
CH_4 [ppbv]

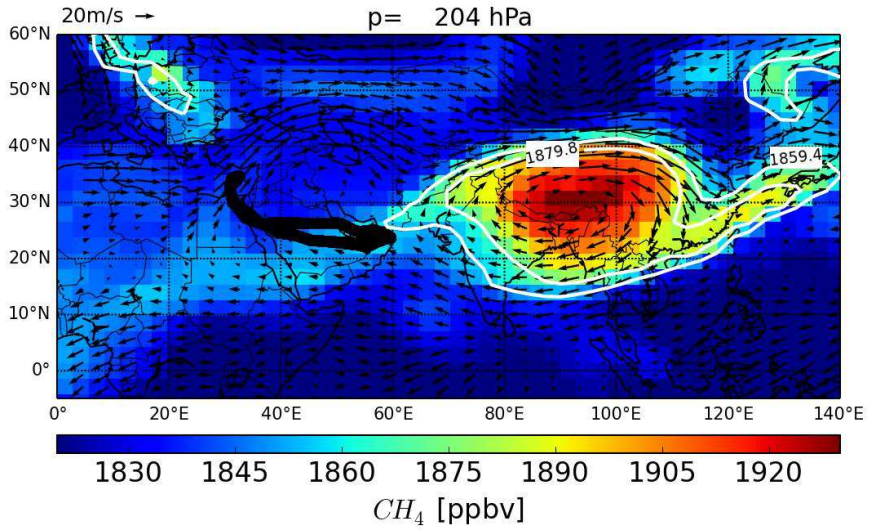

Figure 20: Tibetan anticyclone mode illustrated with wind field and CH_4 EMAC daily means at 204 hPa (August 15, 2015) and the associated flight tracks. White contours represent CH_4 threshold and background values according to section 3.1.

Kommentiert [TL50]: In Figures 7,8, 18-21 and also in Figures 22 and 23 now contour lines are added for the CH4 threshold (1879.8 ppbv) and the CH4 background (1859.4 ppbv) value according to the calculation of the CH4 threshold in section 3.1. In the horizontal CO distribution also the CH4 threshold is added. Now the position of the AMA is easier to identify with respect to the flight tracks.

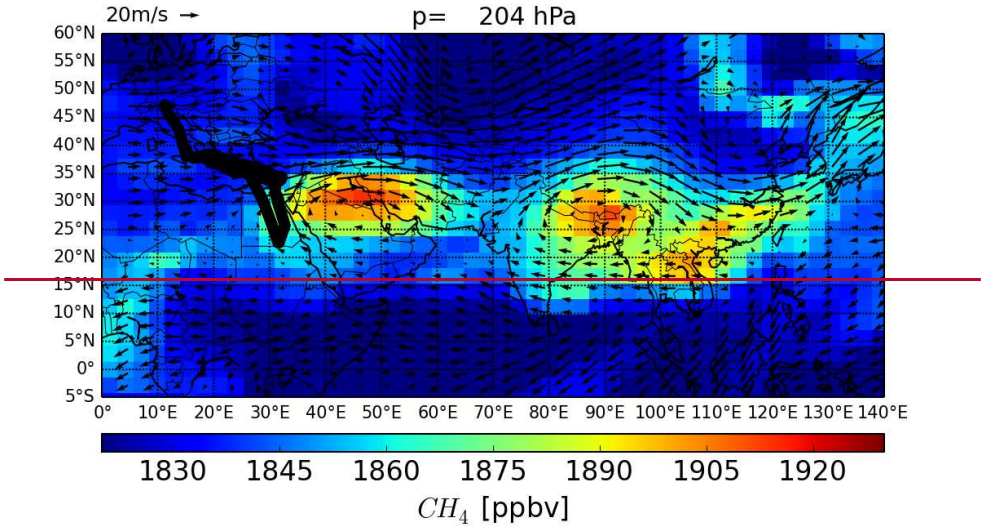
20m/s
p= 204 hPa
60°N
55°N
50°N
45°N
40°N
35°N
30°N
25°N
20°N
15°N
10°N
5°N
0°
5°S
0° 10°E 20°E 30°E 40°E 50°E 60°E 70°E 80°E 90°E 100°E 110°E 120°E 130°E 140°E
1830 1845 1860 1875 1890 1905 1920
CH_4 [ppbv]

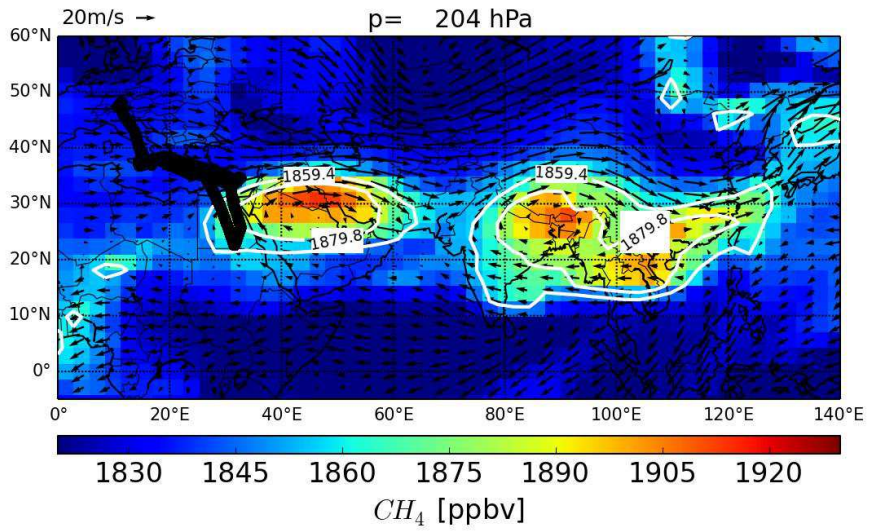

Figure 21: Double anticyclone mode illustrated with wind field and CH_4 EMAC daily means at 204 hPa (August 25, 2015) and the associated flight tracks. White contours represent CH_4 threshold and background values according to section 3.1.

Kommentiert [TL51]: In Figures 7,8, 18-21 and also in Figures 22 and 23 now contour lines are added for the CH4 threshold (1879.8 ppbv) and the CH4 background (1859.4 ppbv) value according to the calculation of the CH4 threshold in section 3.1. In the horizontal CO distribution also the CH4 threshold is added. Now the position of the AMA is easier to identify with respect to the flight tracks.

Table 2: In situ CO and CH_4 for the four different anticyclone situations. Differentiation between AMA and background for each flight between 300-140 hPa.

meteorological situation	flight no.	date	position relative to AMA	in situ at 300-140 hPa							
				CO [ppbv]				CH_4 [ppbv]			
				background	sigma	monsoon	sigma	background	sigma	monsoon	sigma
double anticyclone	#8	21.07.2015	partly in the western AMA	67.8	8.7	89.8	7.4	1847.1	12.3	1898.6	7.8
	#9	25.07.2015	in the western AMA	83.1	9.4	94.5	6.1	1870.0	11.4	1913.7	16.7
	#10	28.07.2015	in the western AMA	76.1	16.4	91.4	5.1	1856.4	24.8	1896.4	12.4
	#11	01.08.2015	partly in residuals of the AMA	92.8	6.8	108.6	4.5	1823.5	21.0	1889.0	4.8
				80.0	10.3	96.1	5.8	1849.3	17.4	1899.4	10.4
central mode	#12/13	06.08.2015	in outflow region	78.6	33.3	117.3	22.2	1827.4	26.8	1893.5	9.8
	#14	08.08.2015	in background south of the AMA	76.3	8.0	-		1788.2	9.2	-	-
	#15/16	09.08.2015	at the south western edge	77.5	12.0	-		1812.6	34.3	-	-
	#17/18	10.08.2015	at the south eastern edge and in outflow region	76.5	7.9	98.3	7.8	1832.0	19.5	1909.3	15.0
				77.2	15.3	107.8	15.0	1815.1	22.5	1901.4	12.4
Tibetan mode	#19	13.08.2015	at the western edge of the AMA	74.7	10.4	99.4	13.8	1848.0	16.3	1907.3	20.8
	#20	15.08.2015	at the western edge of the AMA	-	-	-		1855.2	11.6	1905.2	13.9
	#21	18.08.2015	in and outside the AMA	87.9	16.3	104.8	9.8	1853.0	12.9	1917.1	20.6
				81.3	13.4	102.1	11.8	1852.1	13.6	1909.9	18.4
double anticyclone	#22	23.08.2015	at the western edge of the western AMA	-	-	-		1857.0	8.2	1927.9	22.6
	#23	25.08.2015	at the western edge of the western AMA	65.7	12.4	93.8	7.6	1855.9	8.5	1926.4	21.0
	#24	27.08.2015	outside the AMA	-	-	-		1853.7	14.6	1889.1	8.8
				65.7	12.4	93.8	7.6	1855.5	10.4	1914.4	17.5

Kommentiert [TL52]: In table 2 a column is added, to describe the relative position of the flight tracks to the position of the AMA.

Formatierte Tabelle

Formatiert: Tiefgestellt, Unterschneidung ab 9 Pt.

Formatiert: Nicht Hochgestellt/ Tiefgestellt

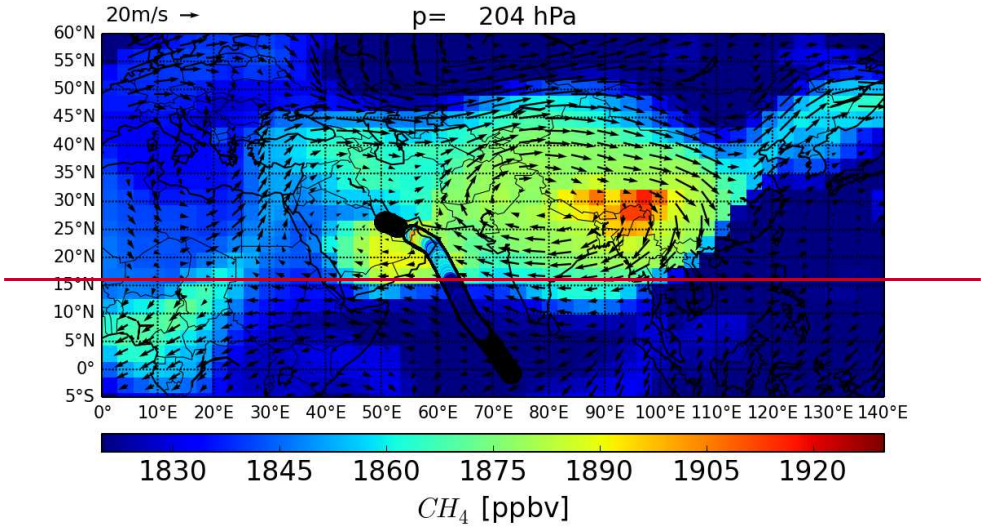
20m/s
p= 204 hPa
60°N
55°N
50°N
45°N
40°N
35°N
30°N
25°N
20°N
15°N
10°N
5°N
0°
5°S
0° 10°E 20°E 30°E 40°E 50°E 60°E 70°E 80°E 90°E 100°E 110°E 120°E 130°E 140°E
1830 1845 1860 1875 1890 1905 1920
CH_4 [ppbv]

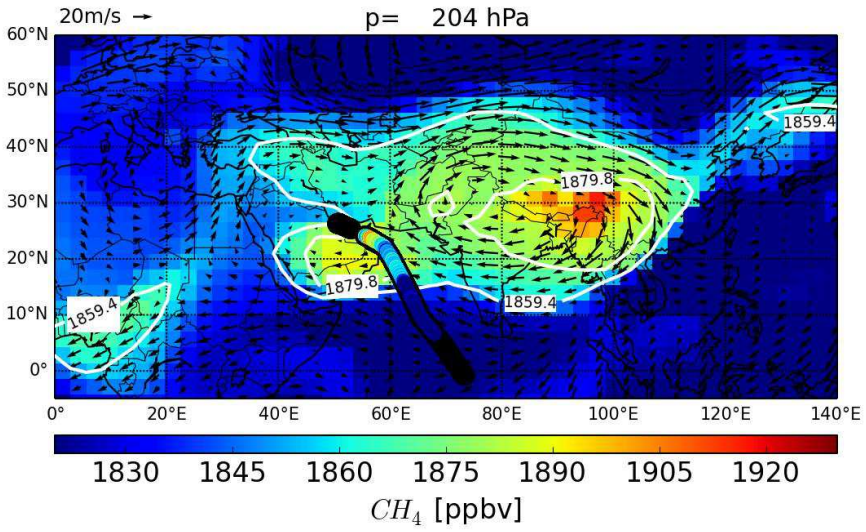

Figure 22: EMAC calculated CH_4 and wind field; daily means at 204 hPa, and in situ CH_4 (above 300 hPa) along the aircraft track for flight 12/13 (August 06, 2015). White contours represent CH_4 threshold and background values according to section 3.1.

Kommentiert [TL53]: In Figures 7,8, 18-21 and also in Figures 22 and 23 now contour lines are added for the CH4 threshold (1879.8 ppbv) and the CH4 background (1859.4 ppbv) value according to the calculation of the CH4 threshold in section 3.1. In the horizontal CO distribution also the CH4 threshold is added. Now the position of the AMA is easier to identify with respect to the flight tracks.

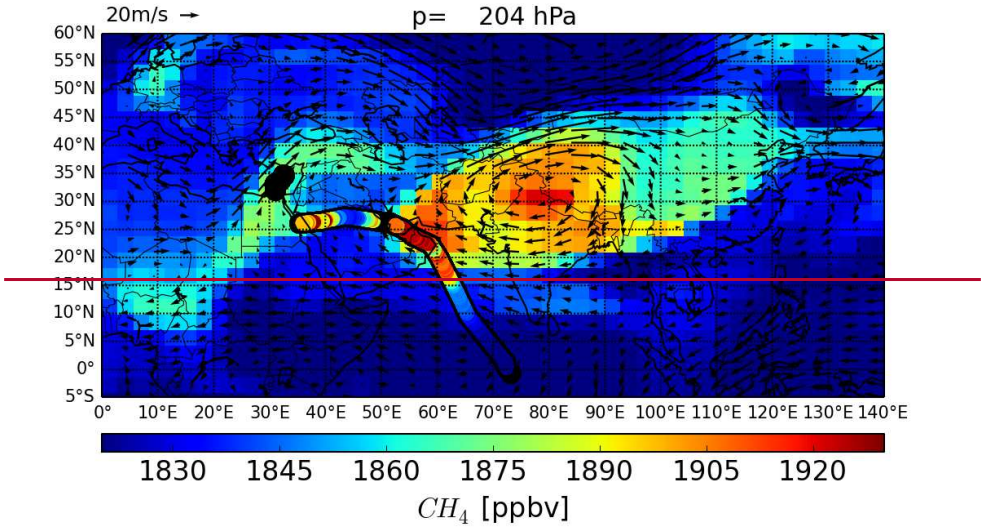
20m/s
p= 204 hPa
60°N
55°N
50°N
45°N
40°N
35°N
30°N
25°N
20°N
15°N
10°N
5°N
0°
5°S
0° 10°E 20°E 30°E 40°E 50°E 60°E 70°E 80°E 90°E 100°E 110°E 120°E 130°E 140°E
1830 1845 1860 1875 1890 1905 1920
CH_4 [ppbv]

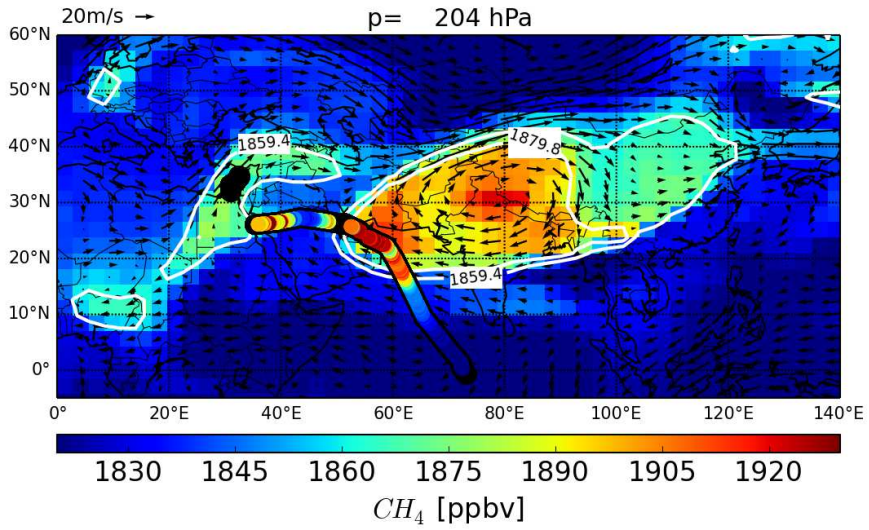

Figure 23: EMAC calculated CH_4 and wind field; daily means at 204 hPa, and in situ measured CH_4 (above 300 hPa) along the aircraft track for flight 17/18 (August 10, 2015). White contours represent CH_4 threshold and background values according to section 3.1.

Kommentiert [TL54]: In Figures 7,8, 18-21 and also in Figures 22 and 23 now contour lines are added for the CH4 threshold (1879.8 ppbv) and the CH4 background (1859.4 ppbv) value according to the calculation of the CH4 threshold in section 3.1. In the horizontal CO distribution also the CH4 threshold is added. Now the position of the AMA is easier to identify with respect to the flight tracks.

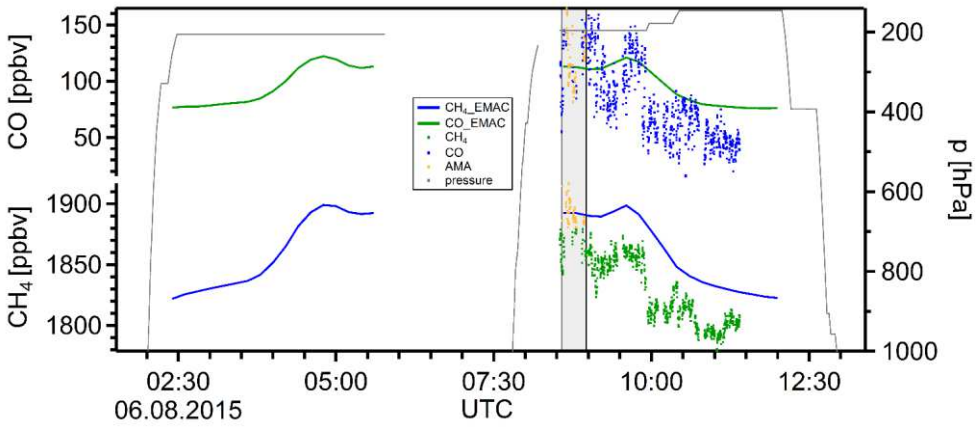

Figure 24: Flight 12/13 (August 6, 2015) in situ CH_4 and CO data and EMAC results along the flight track, as well as the flight altitude. The AMA is colour coded by CH_4>1879.8 ppbv.

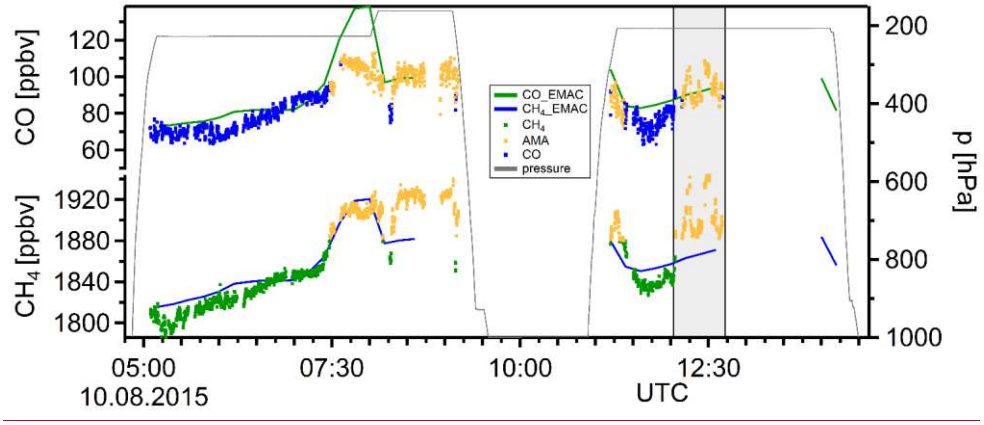

Figure 25: Flight 17/18 (August 10, 2015) in situ CH_4 and CO data and EMAC results along the flight track, as well as the flight altitude. The AMA is colour coded by CH_4>1879.8 ppbv.

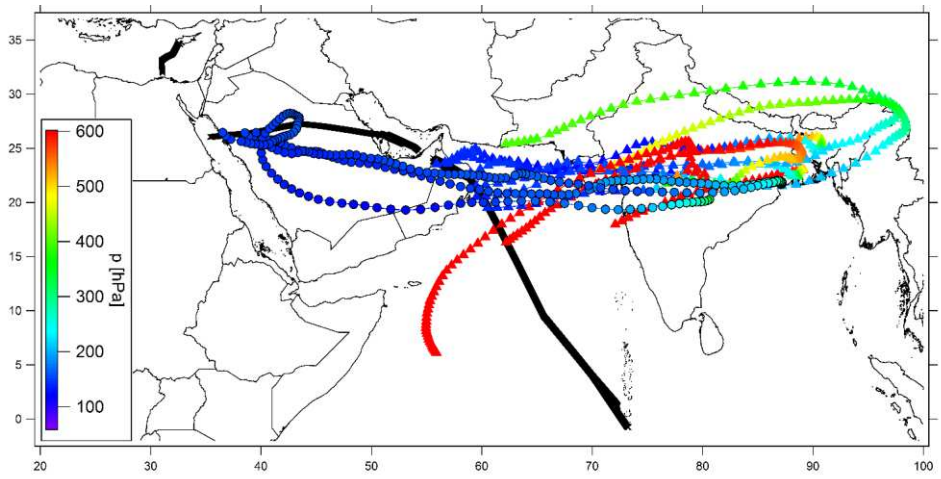

Figure 264: Centroid back trajectories for enhanced CH_4 mixing ratios during flight 12/13 (triangles) and flight 17/18 (circles) with colour coded height.

Formatiert: Tiefgestellt, Unterschneidung ab 9 Pt.

Formatiert: Beschriftung3

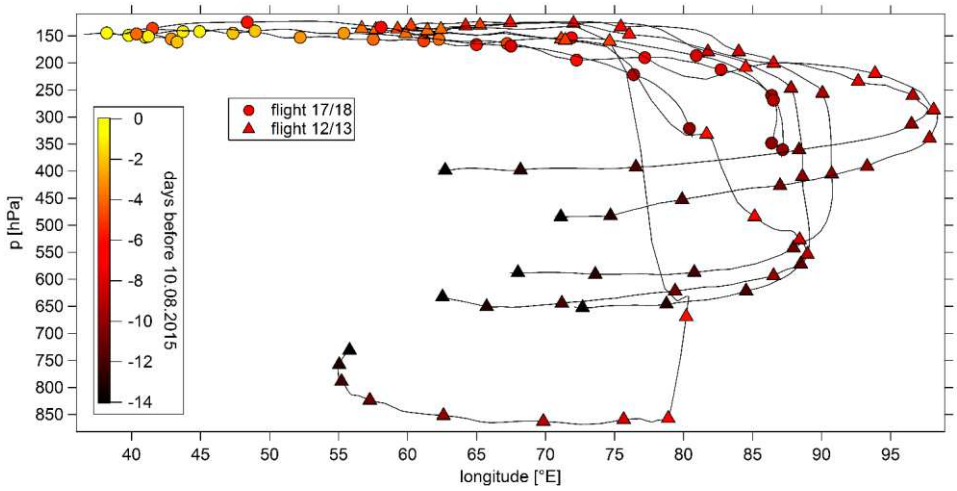

Figure 275: Centroid back trajectories for enhanced CH_4 mixing ratios during flight 12/13 (triangles) and flight 17/18 (circles) with colour coded days before the release on August 10, 2015.

Supplementary Information for "Upper tropospheric CH_4 and CO affected by the Indian summer monsoon during OMO"

by
Laura Tomsche, Andrea Pozzer, Narendra Ojha, Uwe Parchatka, Jos Lelieveld, Horst Fischer

Table S1: Uncertainty for CO and CH_4 for all flights during OMO.

flight no.	date	CO uncertainty [%]	CH_4 uncertainty [%]
8	7.21.2015	3.52	0.33
9	7.25.2015	3.47	0.34
10	7.28.2015	3.23	0.33
11	8.1.2015	3.41	0.23
12/13	8.6.2015	19.42	0.26
14	8.8.2015	4.64	0.24
15/16	8.9.2015	4.08	0.19
17/18	9.10.2015	3.78	0.21
19	8.13.2015	7.89	0.34
20	8.15.2015		0.19
21	8.18.2015	5.26	0.21
22	8.23.2015		0.20
23	8.25.2015	3.61	0.31
24	8.27.2015		0.23

Detailed overview of all OMO flights for p>300 hPa:

a) CO and CH_4 in situ and EMAC data along the flight track. The AMA is color coded due to c[CH_4]>=1879.8 ppb (yellow). Further the deviation between EMAC and in situ data are shown for CO and CH_4. Additionally, the flight altitude is in grey.

b) 204 hPa EMAC data for CO and wind field and in situ CO along the flight track. White contours represent CH_4 threshold and background values according to section 3.1.

c) 204 hPa EMAC data for CH_4 and wind field and in situ CH_4 along the flight track. White contours represent CH_4 threshold and background values according to section 3.1.

d) 10-day back centroid trajectories for 10 min releases along the flight track (black); color coded is the altitude in hPa.

Kommentiert [TL1]: In Table 2 we add a column for the relative position to the AMA, which is quite descriptive. As most of the flight tracks are in and outside the AMA a more detailed geographical location with respect to the AMA can be realized better in a graphical way. Thus we added for each flight in the supplement the CH_4 threshold (1879.8ppbv) for the AMA-influence and the background value (1859.4ppbv) as contour lines in the EMAC CH_4 and CO distributions as already done in the manuscript, e.g. Figure 7 and 8 for flight 19. In these plots the position of the flight track with respect to the AMA is more obvious.

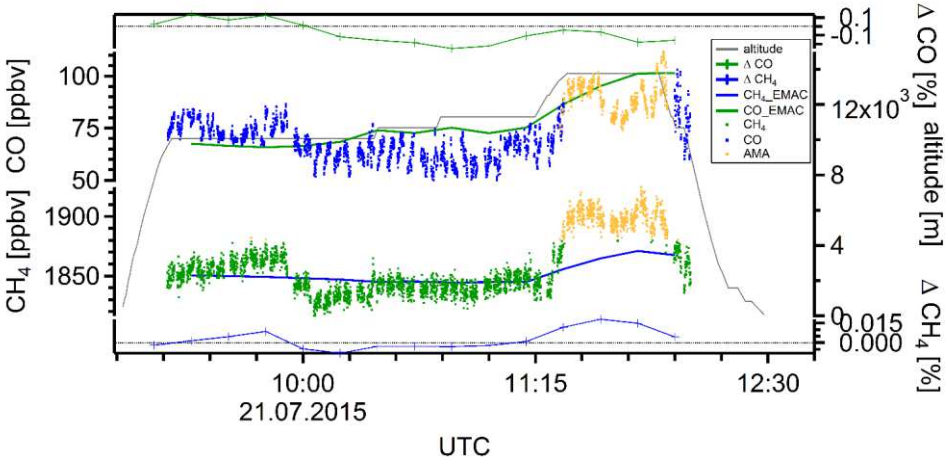
CH4 [ppbv] CO [ppbv]
100
75
50
1900
1850
altitude
Δ CO
Δ CH4
CH4_EMAC
CO_EMAC
CH4
CO
AMA
0.1
-0.1
12x10^3
8
4
0
0.015
0.000
Δ CO [%] altitude [m] Δ CH4 [%]
10:00
21.07.2015
11:15
12:30
UTC

a)

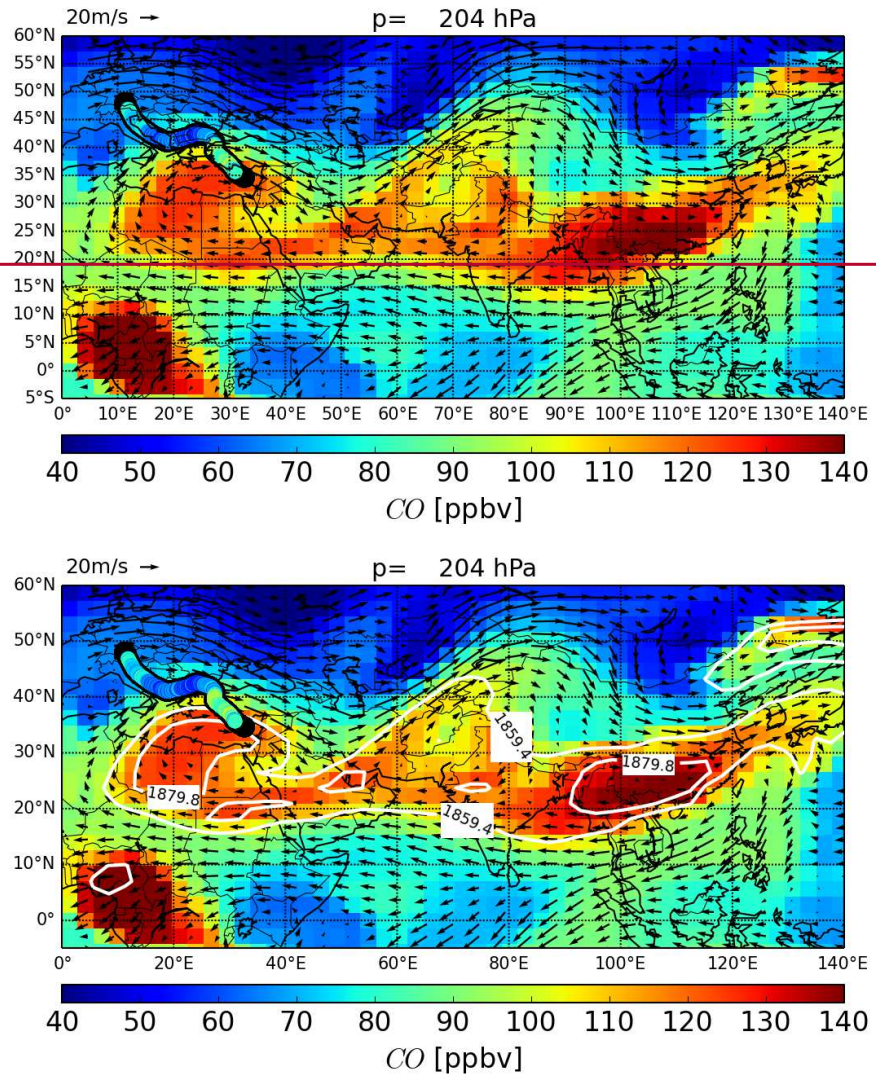
20m/s
p= 204 hPa
60°N
55°N
50°N
45°N
40°N
35°N
30°N
25°N
20°N
15°N
10°N
5°N
0°
5°S
0° 10°E 20°E 30°E 40°E 50°E 60°E 70°E 80°E 90°E 100°E 110°E 120°E 130°E 140°E
40 50 60 70 80 90 100 110 120 130 140
CO [ppbv]
20m/s
p= 204 hPa
60°N
50°N
40°N
30°N
20°N
10°N
0°
1879.8
1859.4
1879.8
1859.4
0° 20°E 40°E 60°E 80°E 100°E 120°E 140°E
40 50 60 70 80 90 100 110 120 130 140
CO [ppbv]

b)

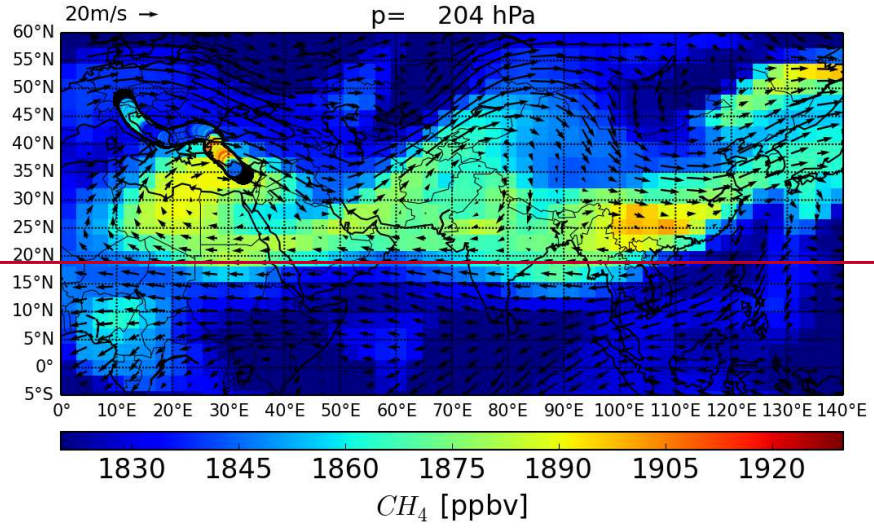
20m/s
p= 204 hPa
60°N
55°N
50°N
45°N
40°N
35°N
30°N
25°N
20°N
15°N
10°N
5°N
0°
5°S
0° 10°E 20°E 30°E 40°E 50°E 60°E 70°E 80°E 90°E 100°E 110°E 120°E 130°E 140°E
1830 1845 1860 1875 1890 1905 1920
CH_4 [ppbv]

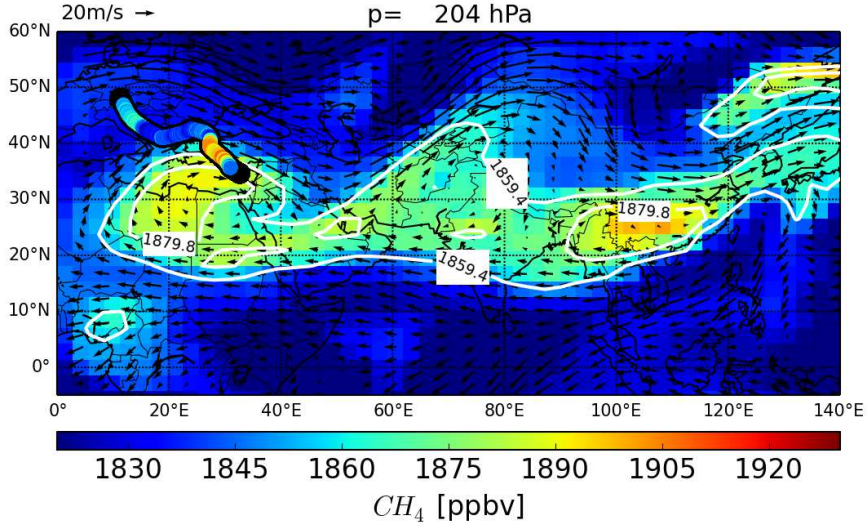
20m/s
p= 204 hPa
60°N
50°N
40°N
30°N
20°N
10°N
0°
0° 20°E 40°E 60°E 80°E 100°E 120°E 140°E
1859.4
1879.8
1879.8
1859.4
1830 1845 1860 1875 1890 1905 1920
CH_4 [ppbv]

c)

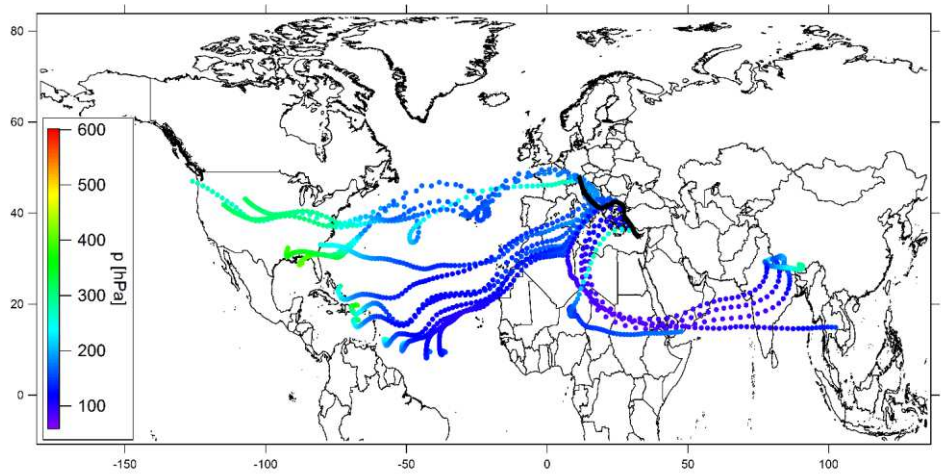

d)

Figure S2: Flight 08 (07.21.2015): transfer flight from Oberpfaffenhofen to Paphos.

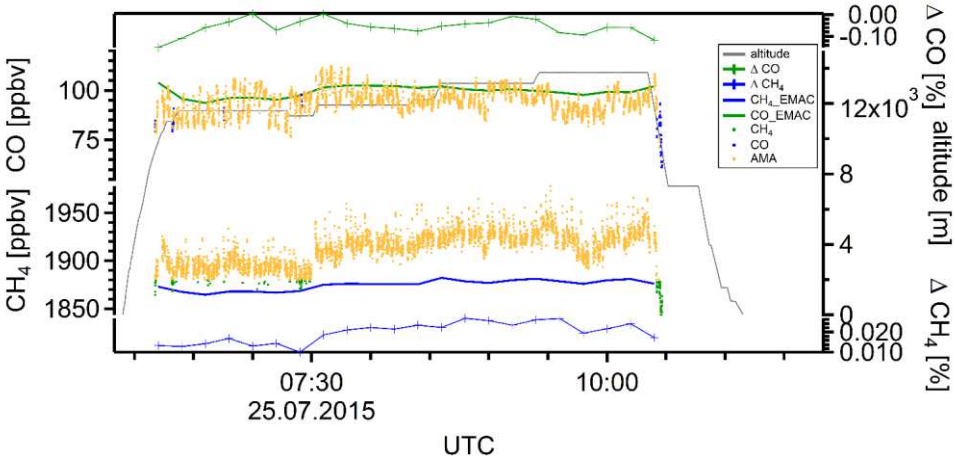

a)

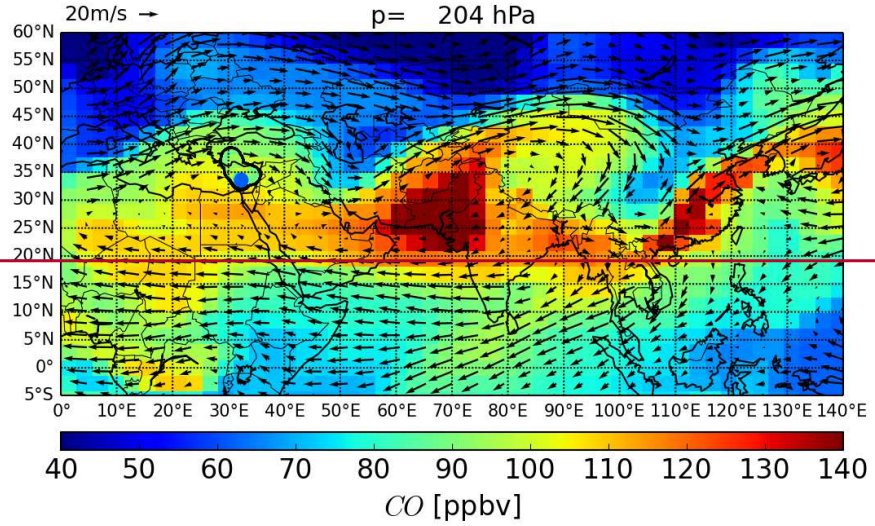
20m/s
p= 204 hPa
60°N
55°N
50°N
45°N
40°N
35°N
30°N
25°N
20°N
15°N
10°N
5°N
0°
5°S
0° 10°E 20°E 30°E 40°E 50°E 60°E 70°E 80°E 90°E 100°E 110°E 120°E 130°E 140°E
40 50 60 70 80 90 100 110 120 130 140
CO [ppbv]

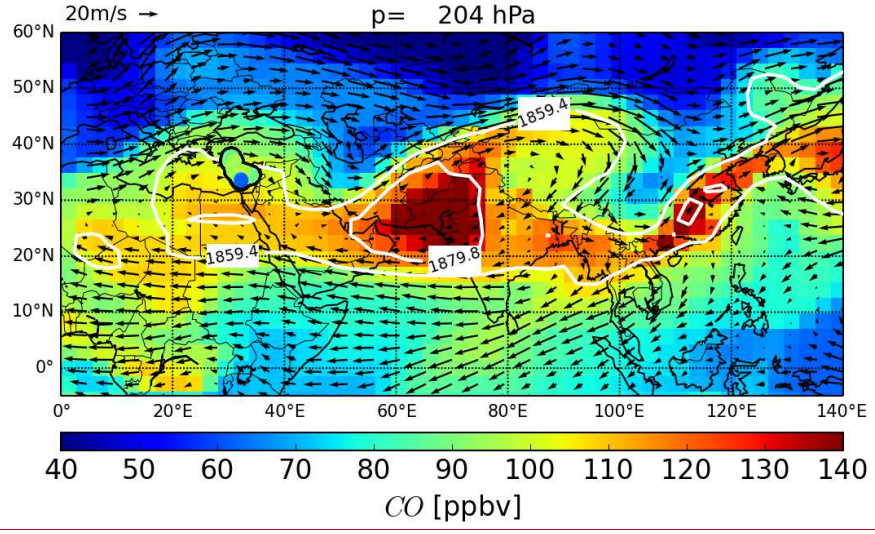
20m/s
p= 204 hPa
60°N
50°N
40°N
30°N
20°N
10°N
0°
1859.4
1859.4
1879.8
0° 20°E 40°E 60°E 80°E 100°E 120°E 140°E
40 50 60 70 80 90 100 110 120 130 140
CO [ppbv]

b)

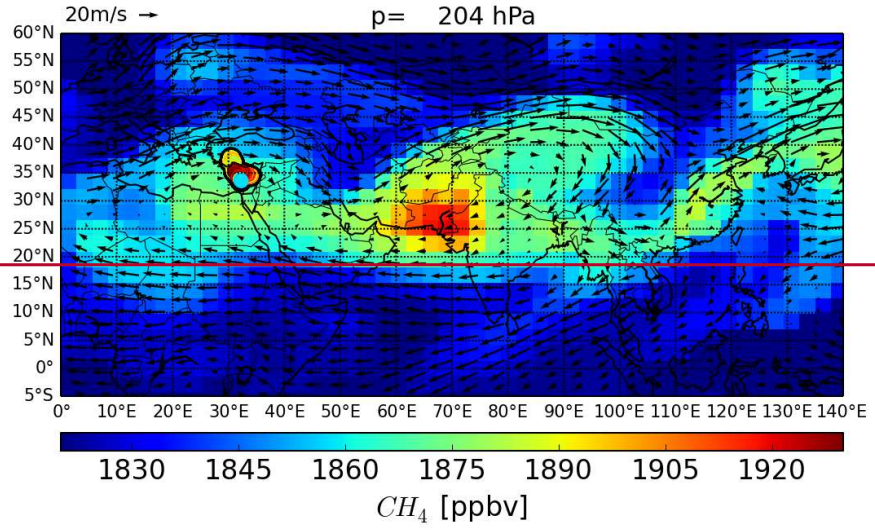
20m/s
p= 204 hPa
60°N
55°N
50°N
45°N
40°N
35°N
30°N
25°N
20°N
15°N
10°N
5°N
0°
5°S
0° 10°E 20°E 30°E 40°E 50°E 60°E 70°E 80°E 90°E 100°E 110°E 120°E 130°E 140°E
1830 1845 1860 1875 1890 1905 1920
CH_4 [ppbv]

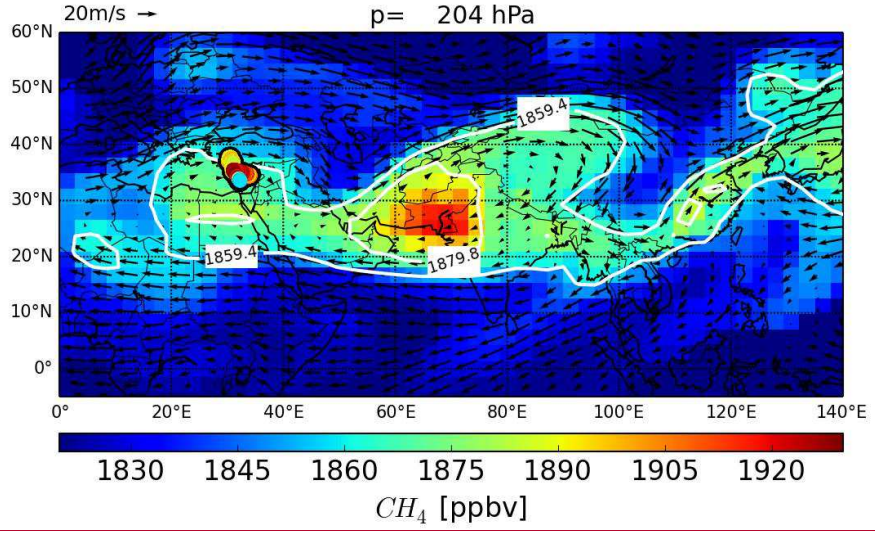
20m/s
p= 204 hPa
60°N
50°N
40°N
30°N
20°N
10°N
0°
1859.4
1859.4
1879.8
0° 20°E 40°E 60°E 80°E 100°E 120°E 140°E
1830 1845 1860 1875 1890 1905 1920
CH_4 [ppbv]

c)

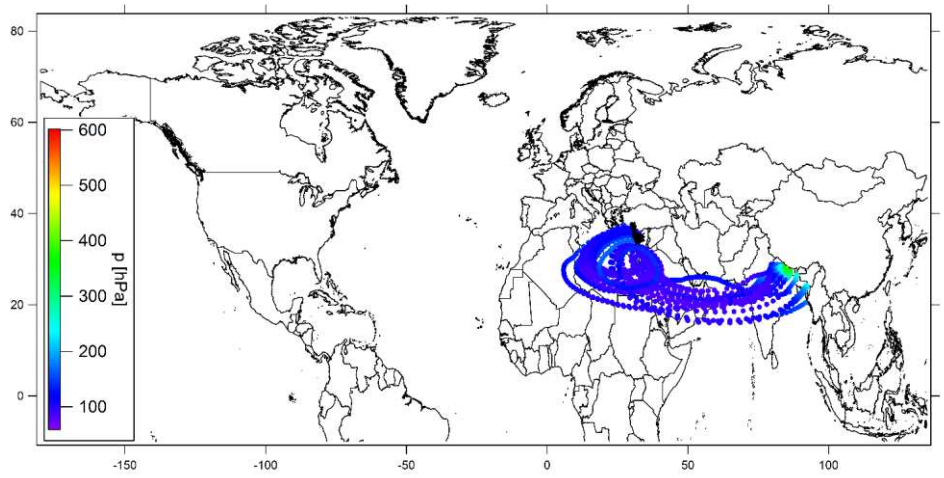

d)

Figure S2: Flight 09 (07.25.2015): measurement flight from Paphos to Paphos over Cyprus.

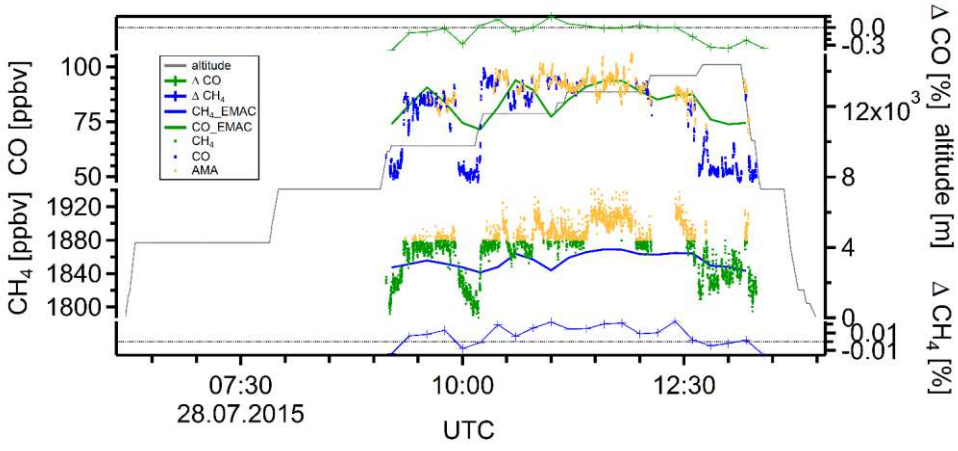

a)

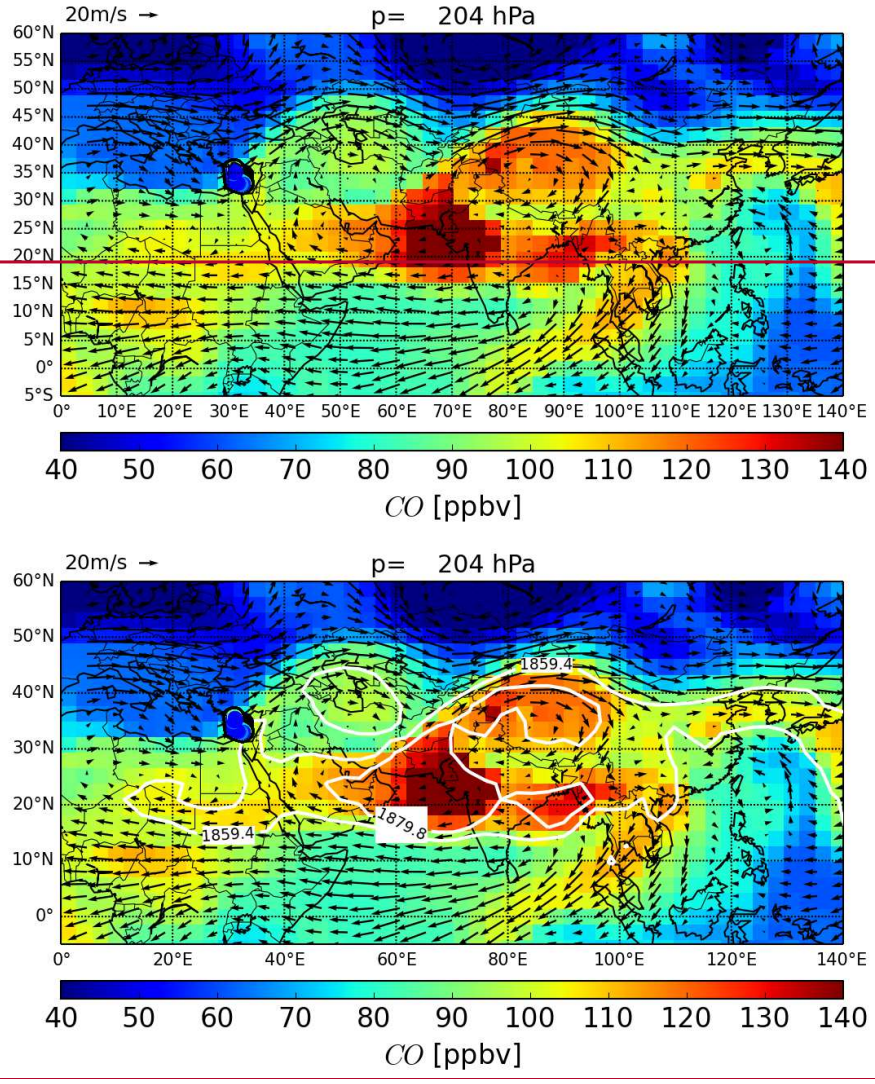
20m/s
p= 204 hPa
60°N
55°N
50°N
45°N
40°N
35°N
30°N
25°N
20°N
15°N
10°N
5°N
0°
5°S
0° 10°E 20°E 30°E 40°E 50°E 60°E 70°E 80°E 90°E 100°E 110°E 120°E 130°E 140°E
40 50 60 70 80 90 100 110 120 130 140
CO [ppbv]
20m/s
p= 204 hPa
60°N
50°N
40°N
30°N
20°N
10°N
0°
1859.4
1879.8
1859.4
0° 20°E 40°E 60°E 80°E 100°E 120°E 140°E
40 50 60 70 80 90 100 110 120 130 140
CO [ppbv]

b)

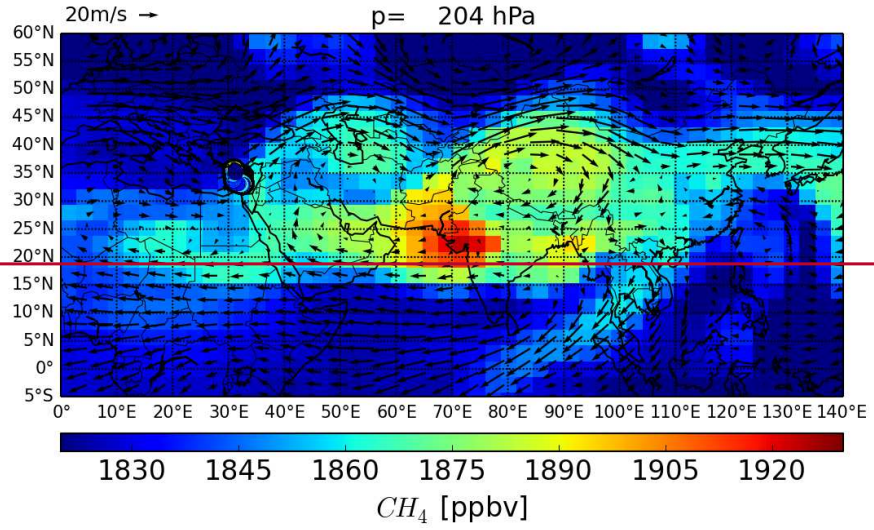
20m/s
p= 204 hPa
60°N
55°N
50°N
45°N
40°N
35°N
30°N
25°N
20°N
15°N
10°N
5°N
0°
5°S
0° 10°E 20°E 30°E 40°E 50°E 60°E 70°E 80°E 90°E 100°E 110°E 120°E 130°E 140°E
1830 1845 1860 1875 1890 1905 1920
CH_4 [ppbv]

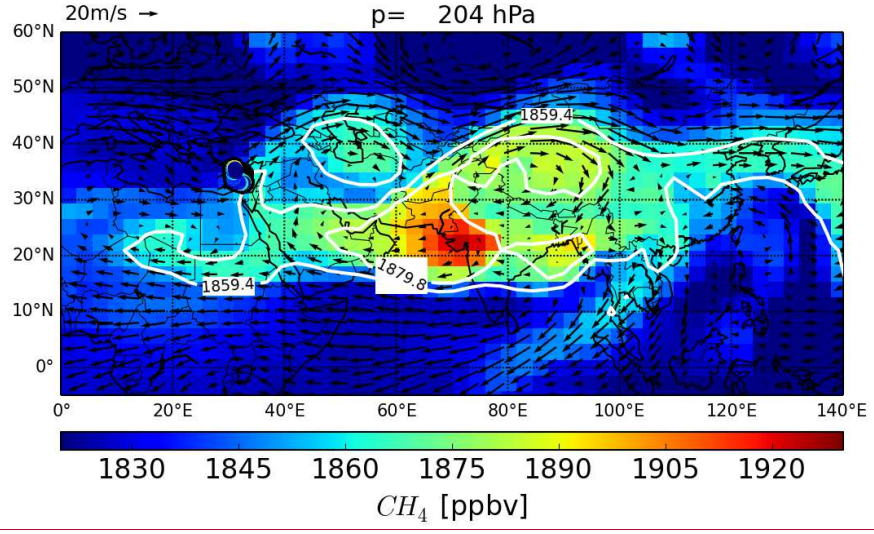
20m/s
p= 204 hPa
60°N
50°N
40°N
30°N
20°N
10°N
0°
1859.4
1879.8
1859.4
0° 20°E 40°E 60°E 80°E 100°E 120°E 140°E
1830 1845 1860 1875 1890 1905 1920
CH_4 [ppbv]

c)

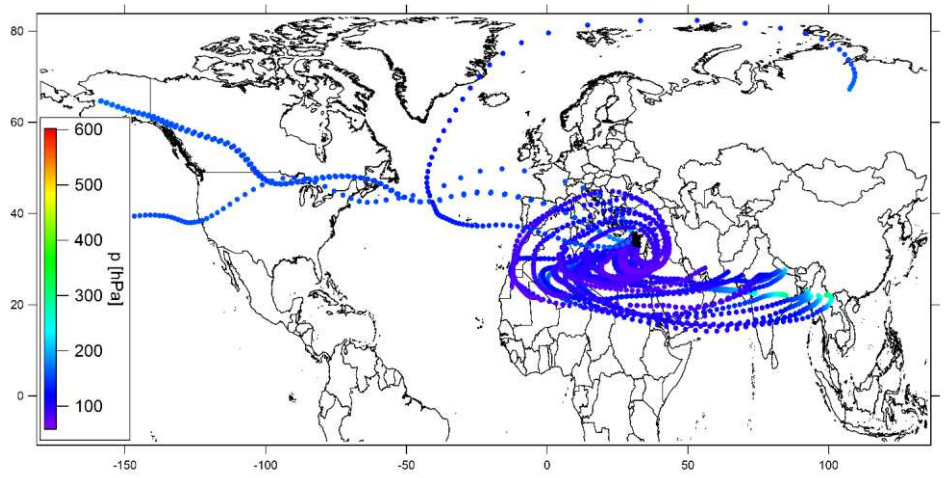

d)

Figure S3: Flight 10 (07.28.2015): measurement flight from Paphos to Paphos over Cyprus.

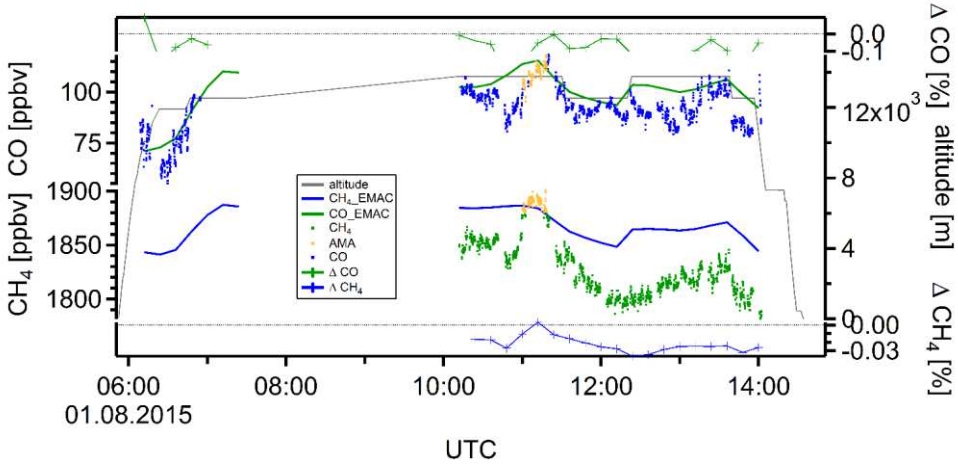

a)

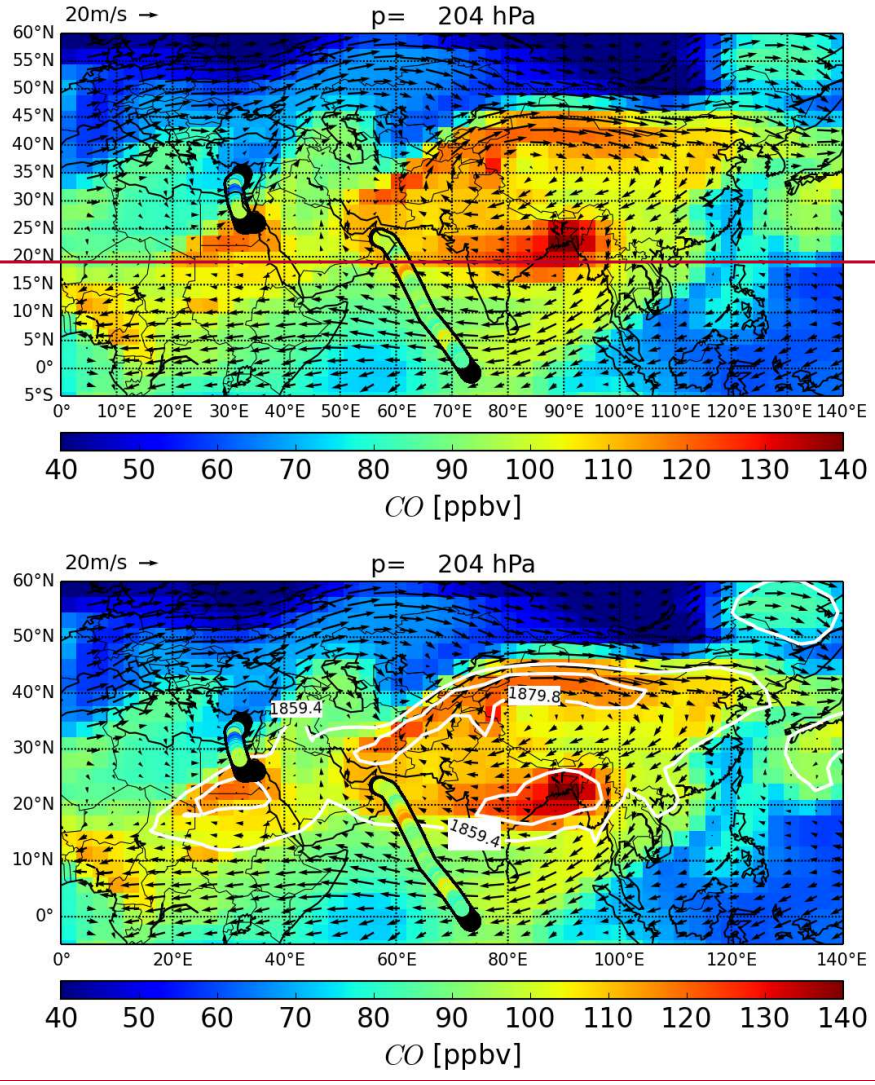
20m/s
p= 204 hPa
60°N
55°N
50°N
45°N
40°N
35°N
30°N
25°N
20°N
15°N
10°N
5°N
0°
5°S
0° 10°E 20°E 30°E 40°E 50°E 60°E 70°E 80°E 90°E 100°E 110°E 120°E 130°E 140°E
40 50 60 70 80 90 100 110 120 130 140
CO [ppbv]
20m/s
p= 204 hPa
60°N
50°N
40°N
30°N
20°N
10°N
0°
1859.4
1879.8
1859.4
0° 20°E 40°E 60°E 80°E 100°E 120°E 140°E
40 50 60 70 80 90 100 110 120 130 140
CO [ppbv]

b)

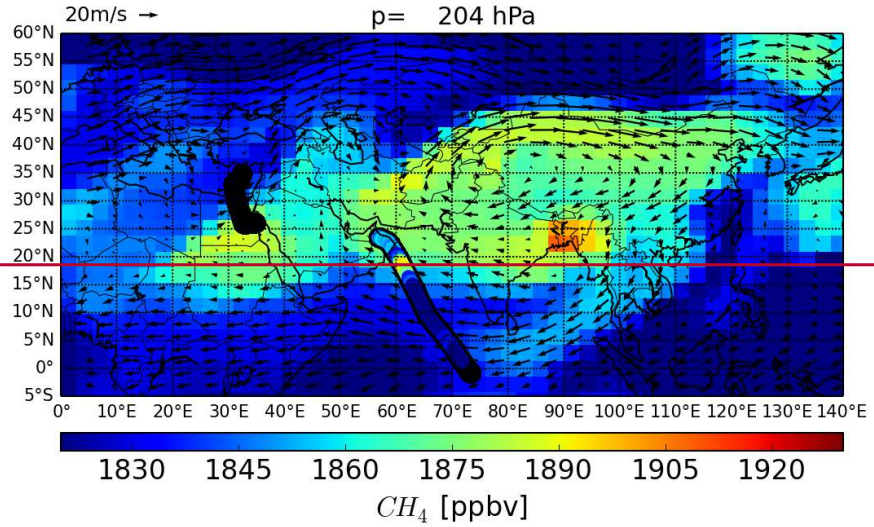
20m/s
p= 204 hPa
60°N
55°N
50°N
45°N
40°N
35°N
30°N
25°N
20°N
15°N
10°N
5°N
0°
5°S
0° 10°E 20°E 30°E 40°E 50°E 60°E 70°E 80°E 90°E 100°E 110°E 120°E 130°E 140°E
1830 1845 1860 1875 1890 1905 1920
CH_4 [ppbv]

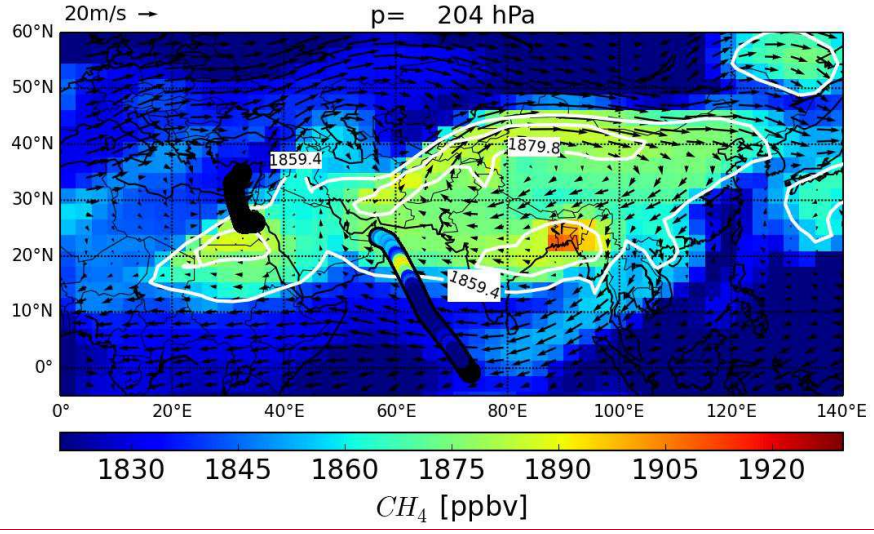
20m/s
p= 204 hPa
60°N
50°N
40°N
30°N
20°N
10°N
0°
1859.4
1879.8
1859.4
0° 20°E 40°E 60°E 80°E 100°E 120°E 140°E
1830 1845 1860 1875 1890 1905 1920
CH_4 [ppbv]

c)

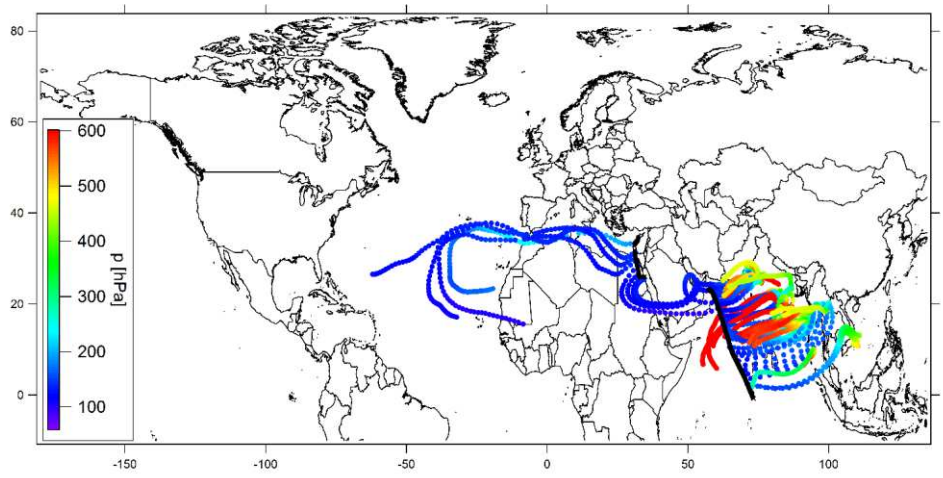

d)

Figure S4: Flight 11 (08.01.2015): transfer flight from Paphos to Gan.

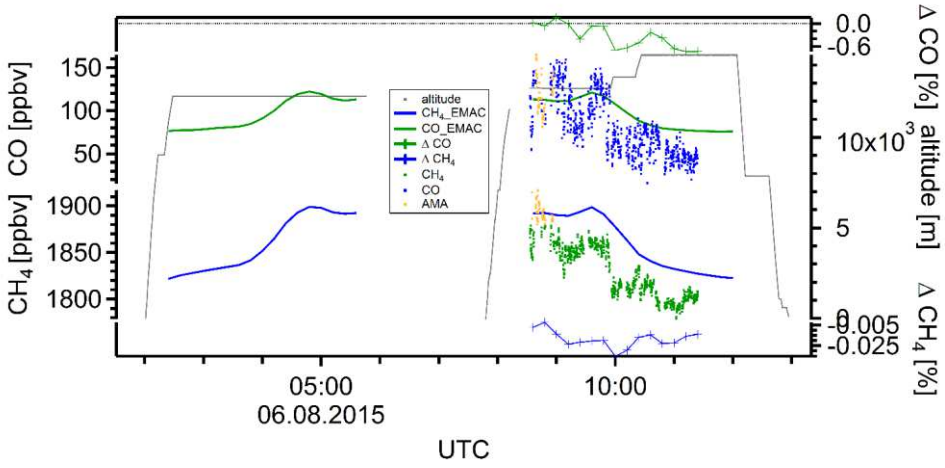

a)

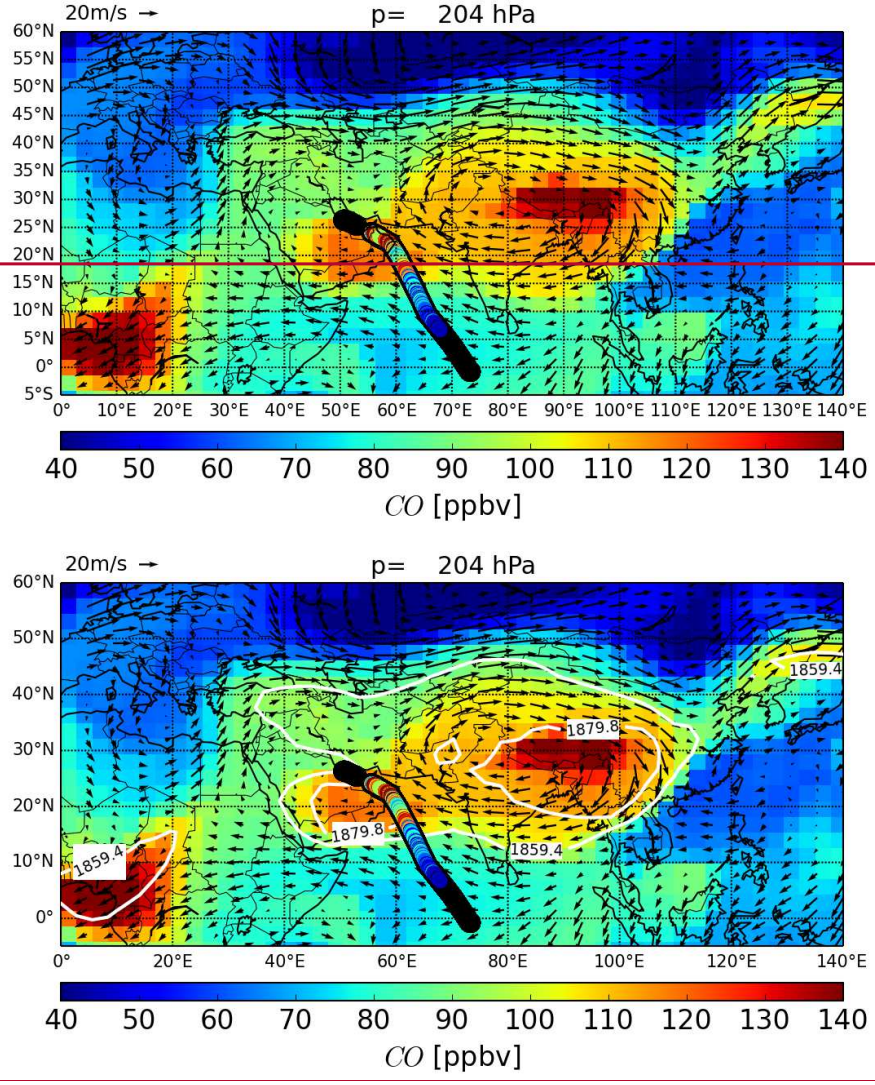
20m/s
p= 204 hPa
60°N
55°N
50°N
45°N
40°N
35°N
30°N
25°N
20°N
15°N
10°N
5°N
0°
5°S
0° 10°E 20°E 30°E 40°E 50°E 60°E 70°E 80°E 90°E 100°E 110°E 120°E 130°E 140°E
40 50 60 70 80 90 100 110 120 130 140
CO [ppbv]
20m/s
p= 204 hPa
60°N
50°N
40°N
30°N
20°N
10°N
0°
1859.4
1879.8
1879.8
1859.4
1859.4
0° 20°E 40°E 60°E 80°E 100°E 120°E 140°E
40 50 60 70 80 90 100 110 120 130 140
CO [ppbv]

b)

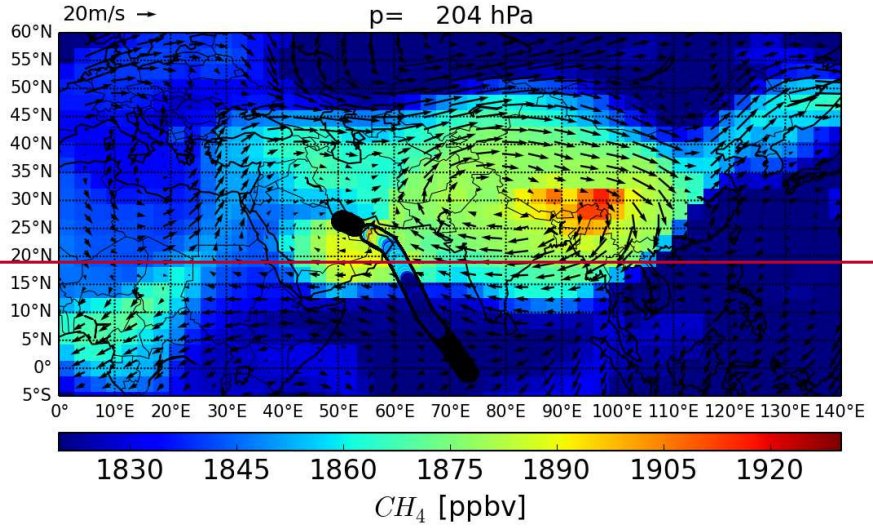
20m/s
p= 204 hPa
60°N
55°N
50°N
45°N
40°N
35°N
30°N
25°N
20°N
15°N
10°N
5°N
0°
5°S
0° 10°E 20°E 30°E 40°E 50°E 60°E 70°E 80°E 90°E 100°E 110°E 120°E 130°E 140°E
1830 1845 1860 1875 1890 1905 1920
CH_4 [ppbv]

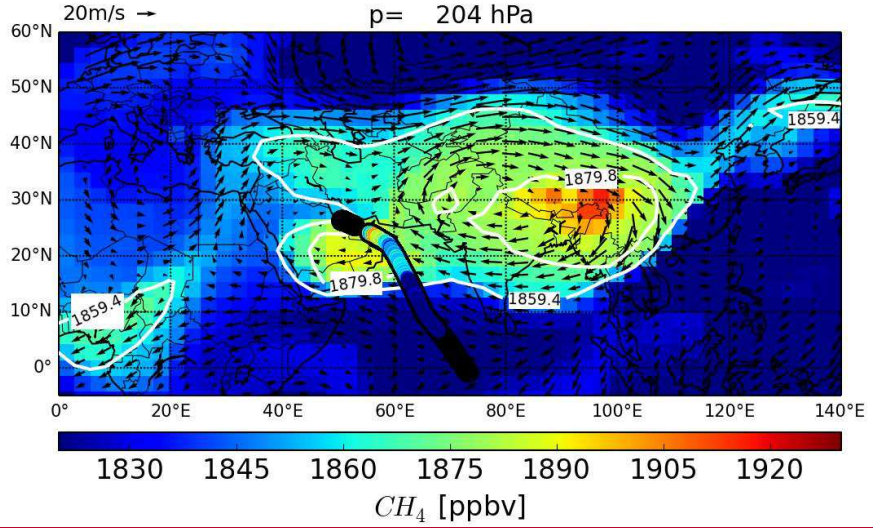
20m/s
p= 204 hPa
60°N
50°N
40°N
30°N
20°N
10°N
0°
1859.4
1879.8
1879.8
1859.4
1859.4
0° 20°E 40°E 60°E 80°E 100°E 120°E 140°E
1830 1845 1860 1875 1890 1905 1920
CH_4 [ppbv]

c)

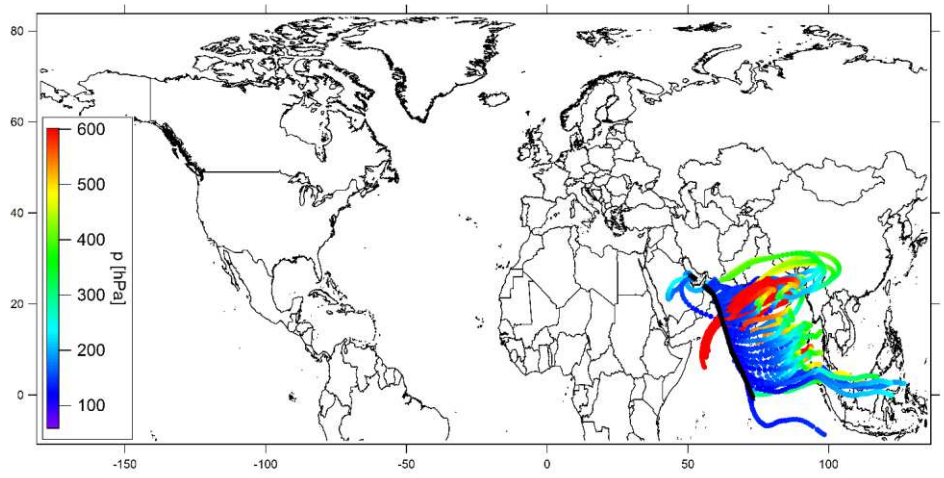

d)

Figure S5: Flight 12/13 (08.06.2015): measurement flight from Gan to Bahrain and return to Gan.

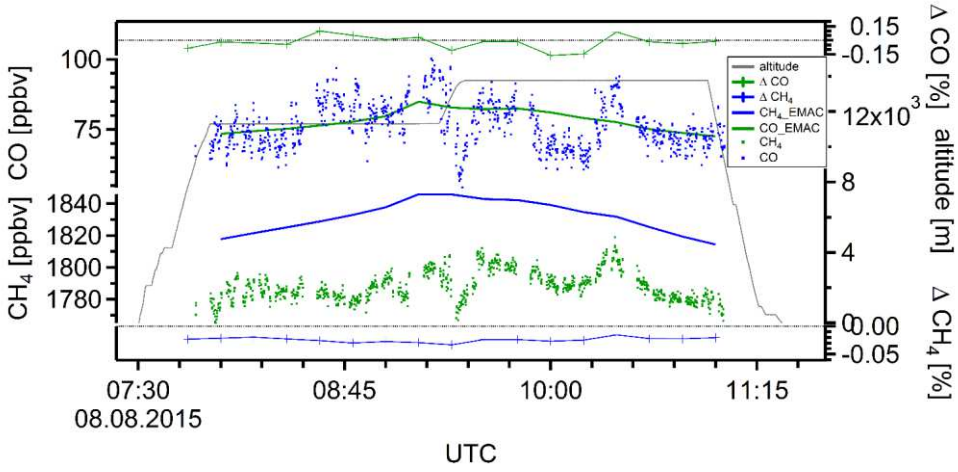

a)

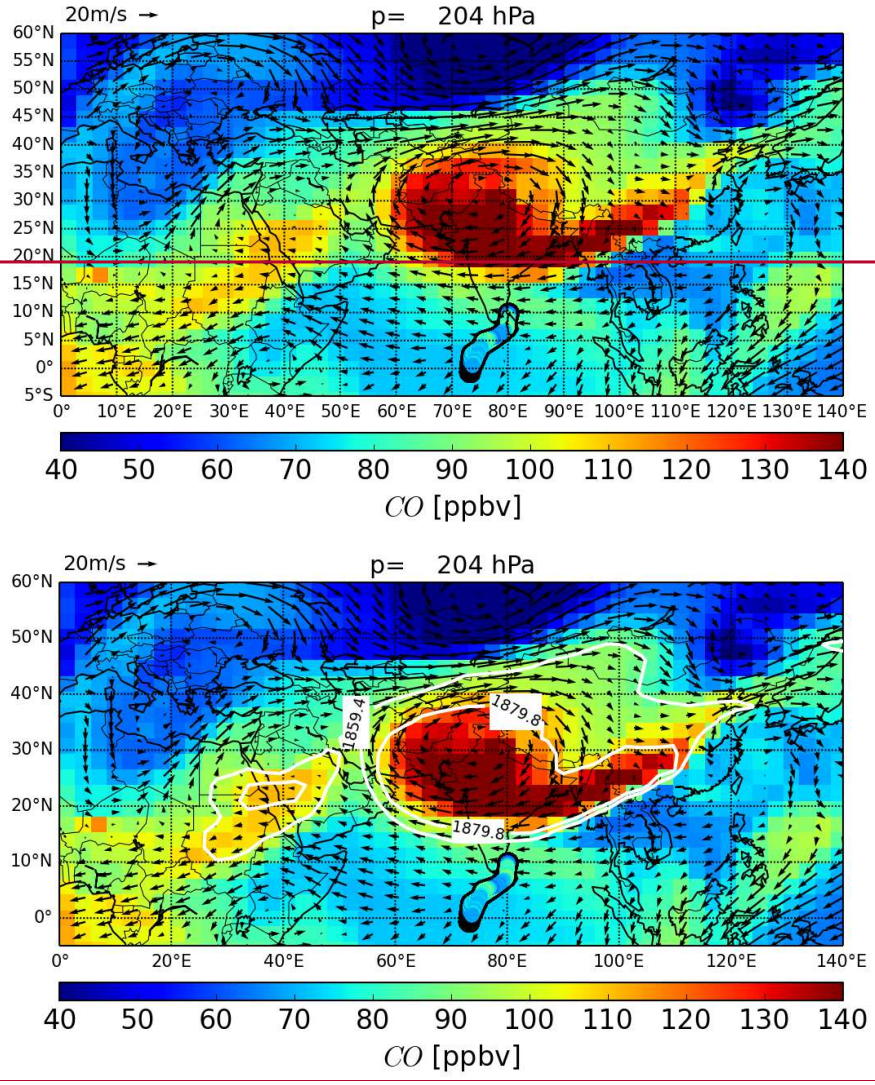
20m/s
p= 204 hPa
60°N
55°N
50°N
45°N
40°N
35°N
30°N
25°N
20°N
15°N
10°N
5°N
0°
5°S
0° 10°E 20°E 30°E 40°E 50°E 60°E 70°E 80°E 90°E 100°E 110°E 120°E 130°E 140°E
40 50 60 70 80 90 100 110 120 130 140
CO [ppbv]
20m/s
p= 204 hPa
60°N
50°N
40°N
30°N
20°N
10°N
0°
1859.4
1879.8
1879.8
0° 20°E 40°E 60°E 80°E 100°E 120°E 140°E
40 50 60 70 80 90 100 110 120 130 140
CO [ppbv]

b)

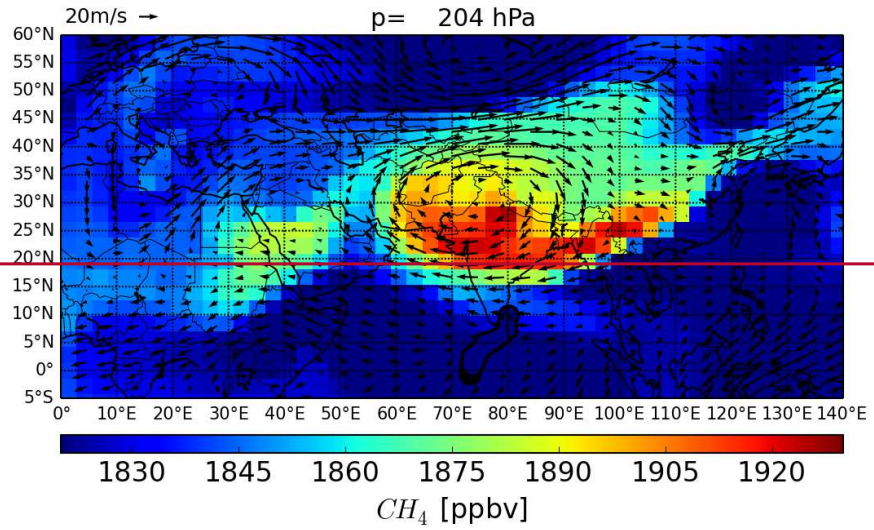
20m/s
p= 204 hPa
60°N
55°N
50°N
45°N
40°N
35°N
30°N
25°N
20°N
15°N
10°N
5°N
0°
5°S
0° 10°E 20°E 30°E 40°E 50°E 60°E 70°E 80°E 90°E 100°E 110°E 120°E 130°E 140°E
1830 1845 1860 1875 1890 1905 1920
CH_4 [ppbv]

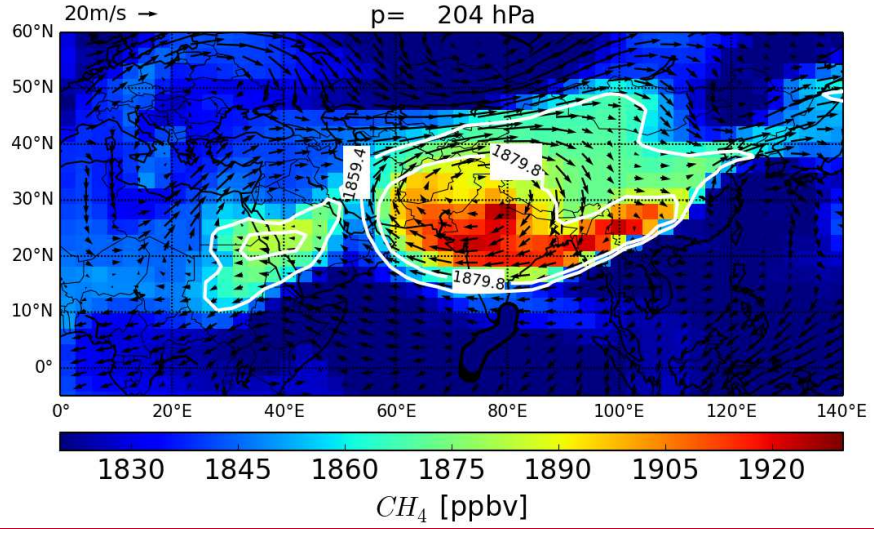
20m/s
p= 204 hPa
60°N
50°N
40°N
30°N
20°N
10°N
0°
0° 20°E 40°E 60°E 80°E 100°E 120°E 140°E
1859.4
1879.8
1879.8
1830 1845 1860 1875 1890 1905 1920
CH_4 [ppbv]

c)

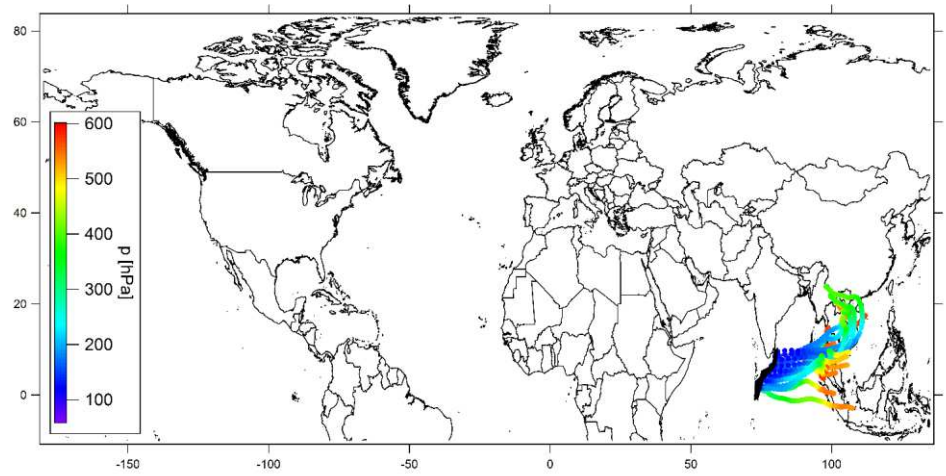

d)

Figure S6: Flight 14 (08.08.2015): measurement flight from Gan to Gan towards Sri Lanka.

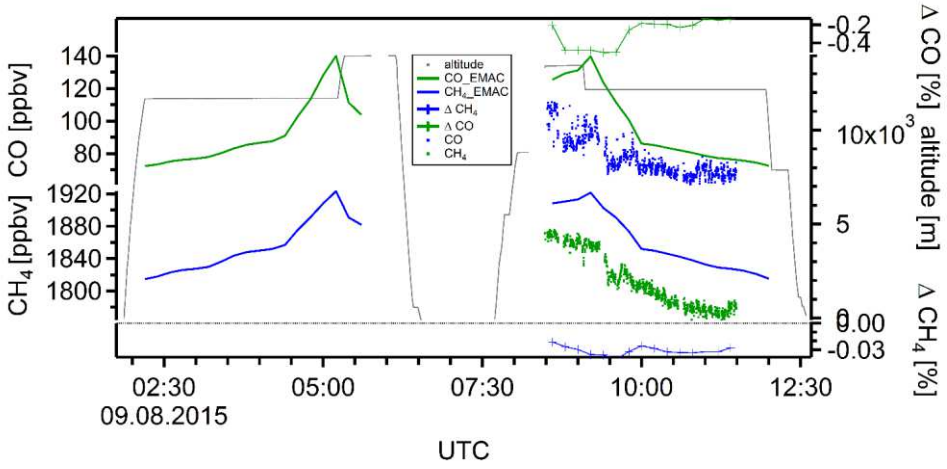

a)

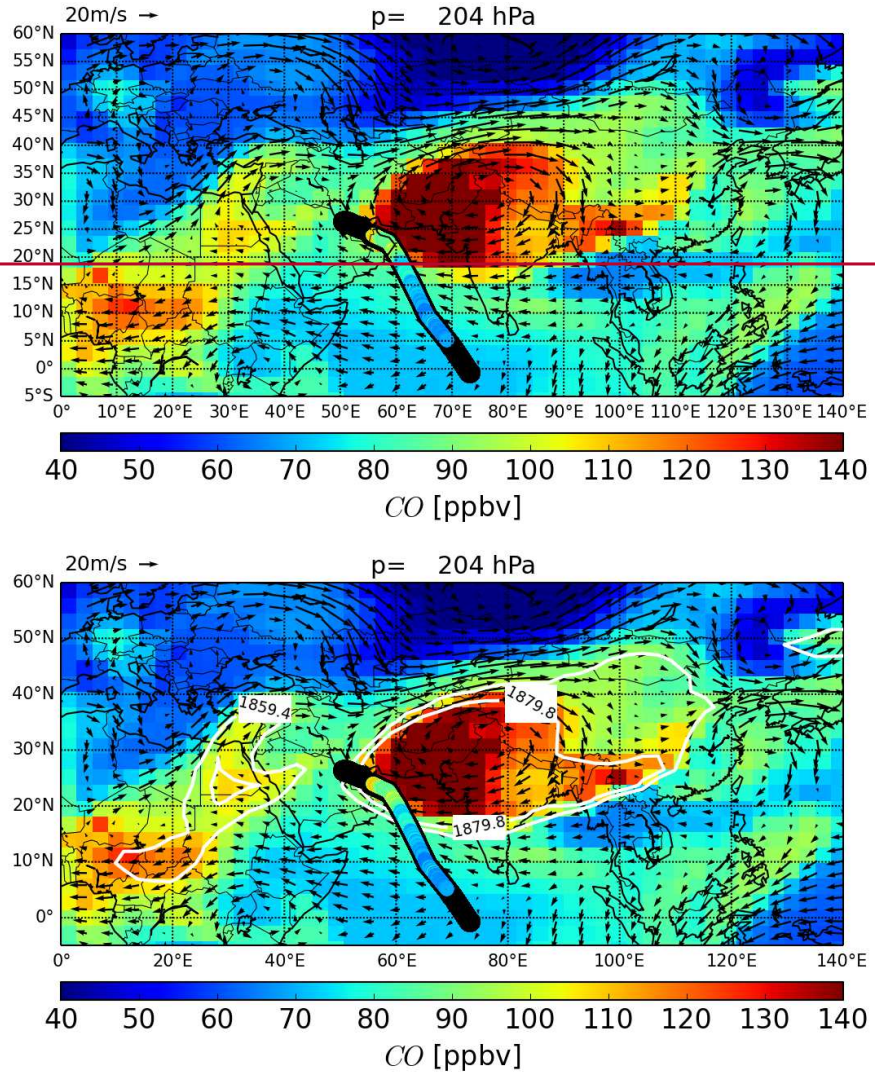
20m/s
p= 204 hPa
60°N
55°N
50°N
45°N
40°N
35°N
30°N
25°N
20°N
15°N
10°N
5°N
0°
5°S
0° 10°E 20°E 30°E 40°E 50°E 60°E 70°E 80°E 90°E 100°E 110°E 120°E 130°E 140°E
40 50 60 70 80 90 100 110 120 130 140
CO [ppbv]
20m/s
p= 204 hPa
60°N
50°N
40°N
30°N
20°N
10°N
0°
1859.4
1879.8
1879.8
0° 20°E 40°E 60°E 80°E 100°E 120°E 140°E
40 50 60 70 80 90 100 110 120 130 140
CO [ppbv]

b)

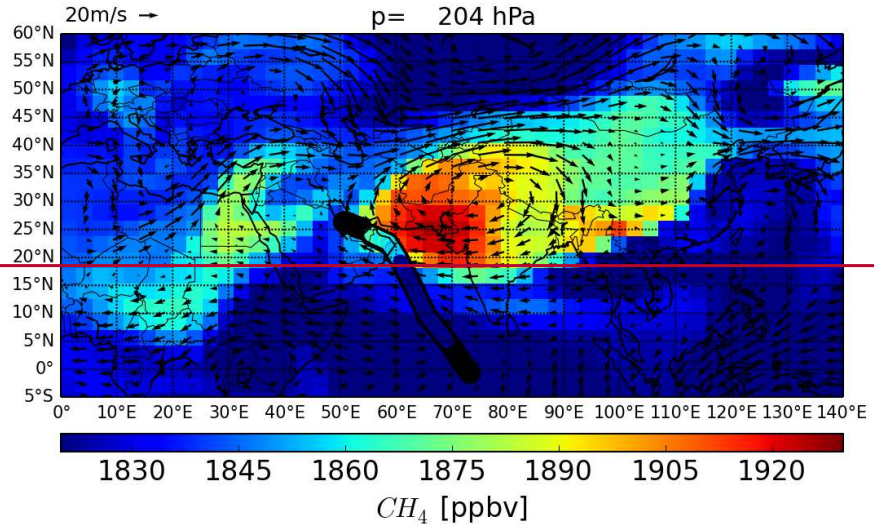
20m/s
p= 204 hPa
60°N
55°N
50°N
45°N
40°N
35°N
30°N
25°N
20°N
15°N
10°N
5°N
0°
5°S
0° 10°E 20°E 30°E 40°E 50°E 60°E 70°E 80°E 90°E 100°E 110°E 120°E 130°E 140°E
1830 1845 1860 1875 1890 1905 1920
CH_4 [ppbv]

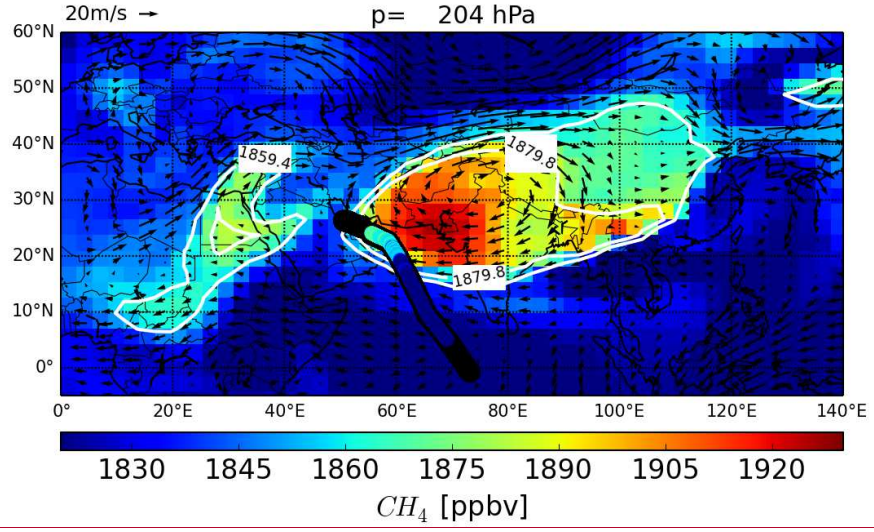
20m/s
p= 204 hPa
60°N
50°N
40°N
30°N
20°N
10°N
0°
1859.4
1879.8
1879.8
0° 20°E 40°E 60°E 80°E 100°E 120°E 140°E
1830 1845 1860 1875 1890 1905 1920
CH_4 [ppbv]

c)

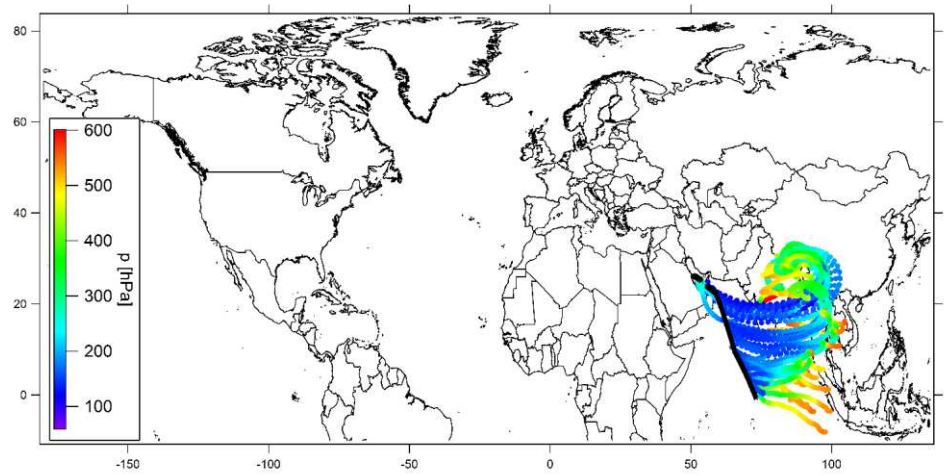

d)

Figure S7: Flight 15/16 (08.09.2015): measurement flight from Gan to Bahrain and return to Gan.

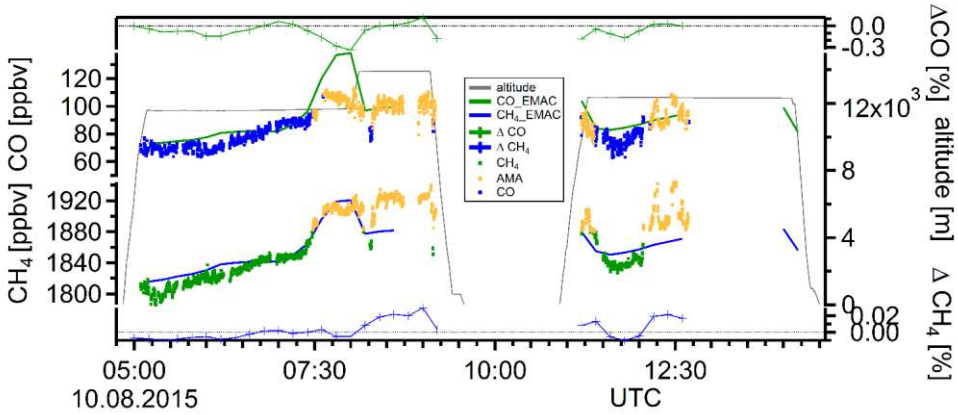

a)

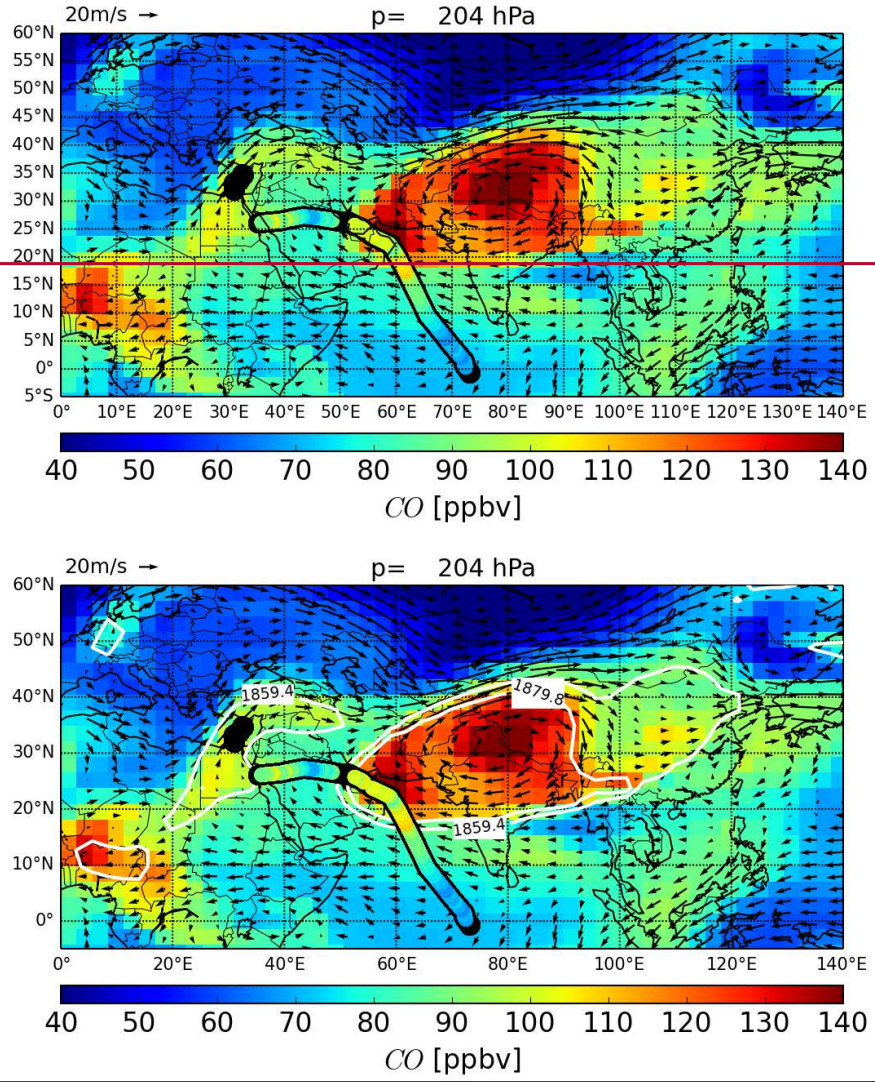
20m/s
p= 204 hPa
60°N
55°N
50°N
45°N
40°N
35°N
30°N
25°N
20°N
15°N
10°N
5°N
0°
5°S
0° 10°E 20°E 30°E 40°E 50°E 60°E 70°E 80°E 90°E 100°E 110°E 120°E 130°E 140°E
40 50 60 70 80 90 100 110 120 130 140
CO [ppbv]
20m/s
p= 204 hPa
60°N
50°N
40°N
30°N
20°N
10°N
0°
1859.4
1879.8
1859.4
0° 20°E 40°E 60°E 80°E 100°E 120°E 140°E
40 50 60 70 80 90 100 110 120 130 140
CO [ppbv]

b)

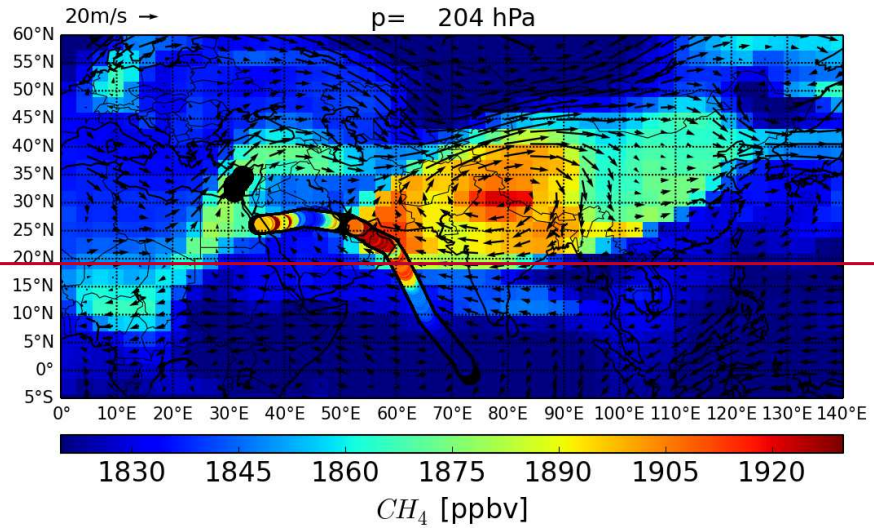
20m/s
p= 204 hPa
60°N
55°N
50°N
45°N
40°N
35°N
30°N
25°N
20°N
15°N
10°N
5°N
0°
5°S
0° 10°E 20°E 30°E 40°E 50°E 60°E 70°E 80°E 90°E 100°E 110°E 120°E 130°E 140°E
1830 1845 1860 1875 1890 1905 1920
CH_4 [ppbv]

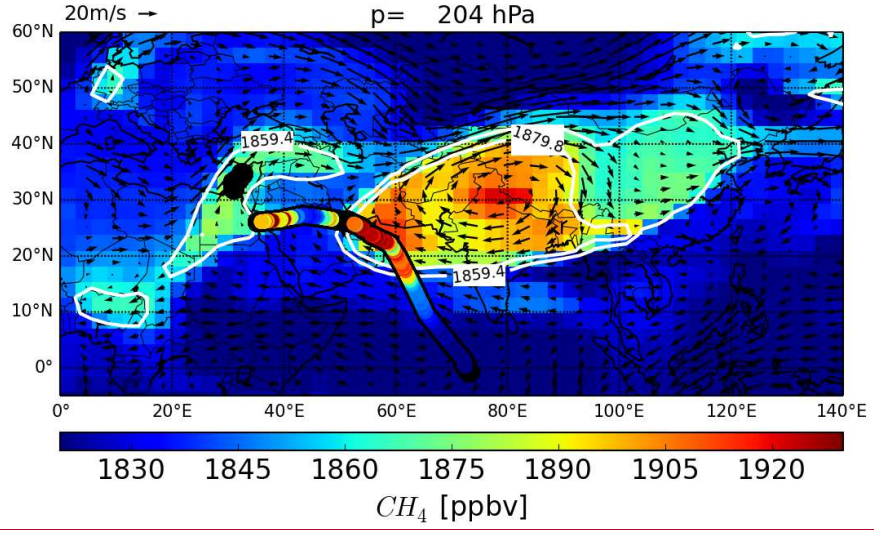
20m/s
p= 204 hPa
60°N
50°N
40°N
30°N
20°N
10°N
0°
1859.4
1879.8
1859.4
0° 20°E 40°E 60°E 80°E 100°E 120°E 140°E
1830 1845 1860 1875 1890 1905 1920
CH_4 [ppbv]

c)

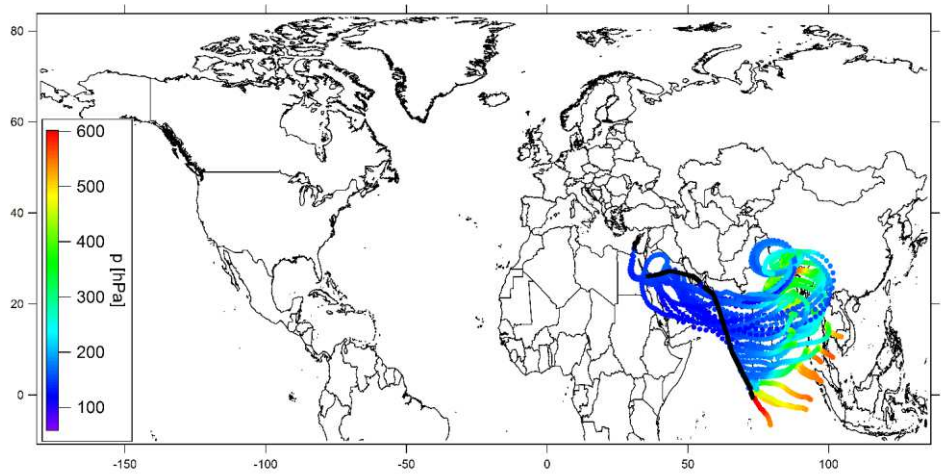

d)

Figure S8: Flight 17/18 (08.10.2015): transfer flight from Gan to Paphos via refuelling stop in Bahrain.

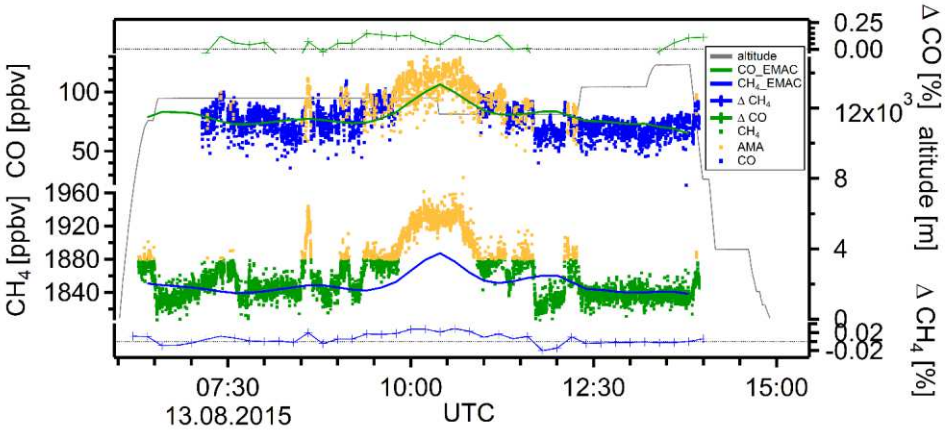

a)

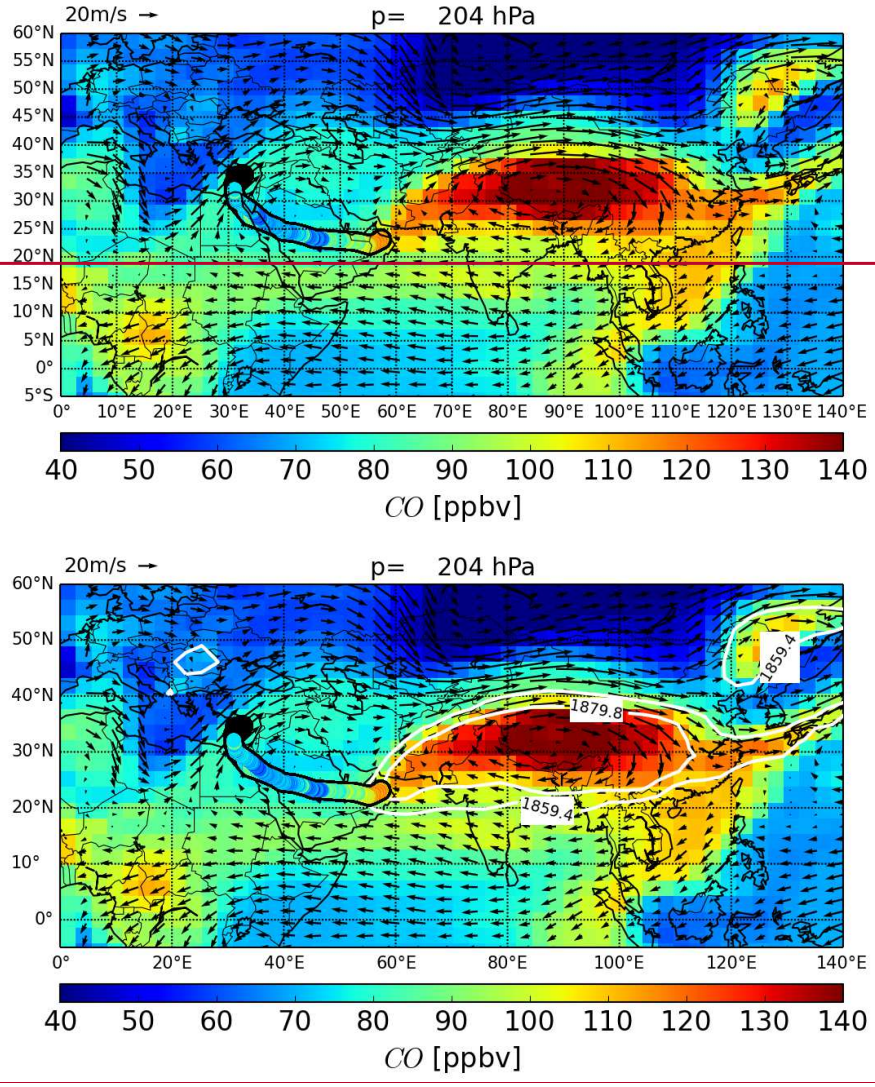
20m/s
p= 204 hPa
60°N
55°N
50°N
45°N
40°N
35°N
30°N
25°N
20°N
15°N
10°N
5°N
0°
5°S
0° 10°E 20°E 30°E 40°E 50°E 60°E 70°E 80°E 90°E 100°E 110°E 120°E 130°E 140°E
40 50 60 70 80 90 100 110 120 130 140
CO [ppbv]
20m/s
p= 204 hPa
60°N
50°N
40°N
30°N
20°N
10°
0°
1859.4
1879.8
1859.4
0° 20°E 40°E 60°E 80°E 100°E 120°E 140°E
40 50 60 70 80 90 100 110 120 130 140
CO [ppbv]

b)

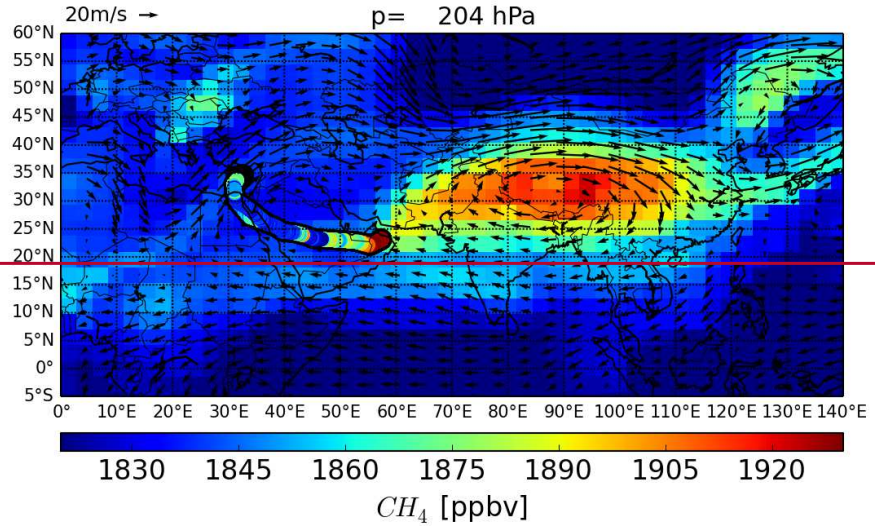
20m/s
p= 204 hPa
60°N
55°N
50°N
45°N
40°N
35°N
30°N
25°N
20°N
15°N
10°N
5°N
0°
5°S
0° 10°E 20°E 30°E 40°E 50°E 60°E 70°E 80°E 90°E 100°E 110°E 120°E 130°E 140°E
1830 1845 1860 1875 1890 1905 1920
CH_4 [ppbv]

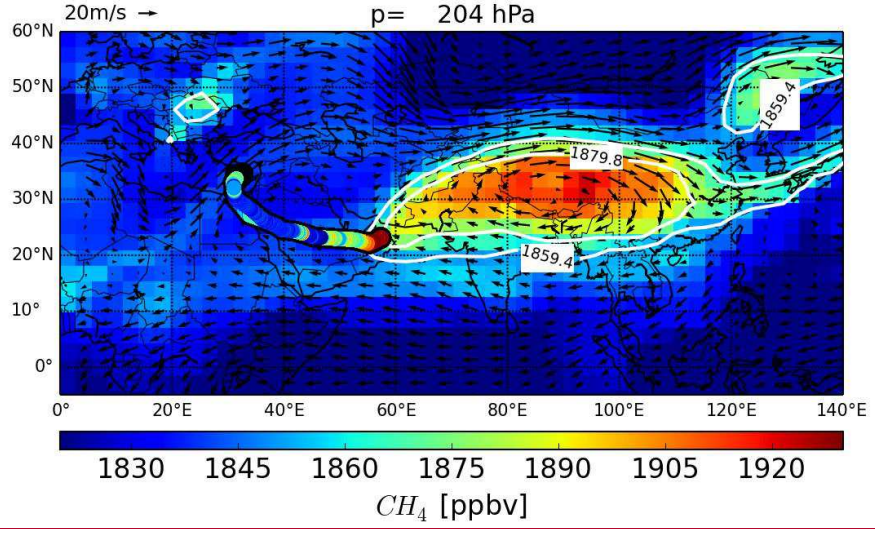
20m/s
p= 204 hPa
60°N
50°N
40°N
30°N
20°N
10°
0°
1879.8
1859.4
1859.4
0° 20°E 40°E 60°E 80°E 100°E 120°E 140°E
1830 1845 1860 1875 1890 1905 1920
CH_4 [ppbv]

c)

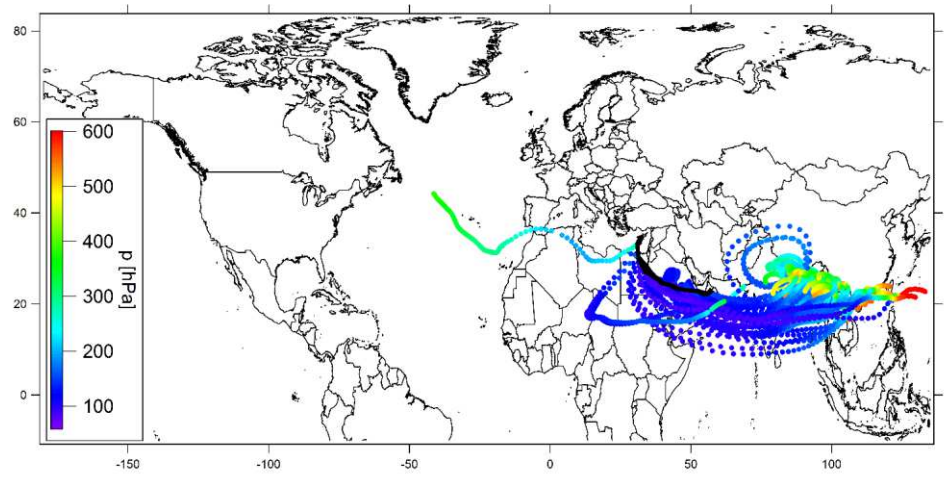

d)

Figure S9: Flight 19 (08.13.2015): measurement flight from Paphos to Paphos towards Oman.

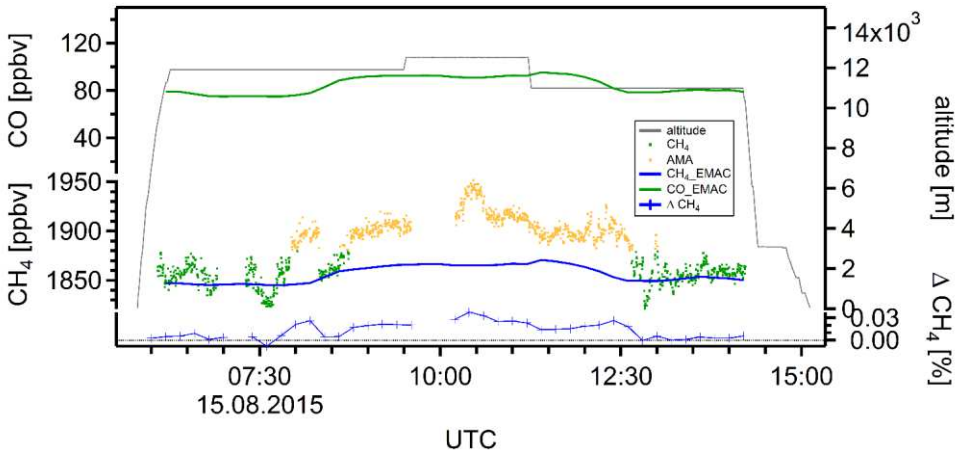

a)

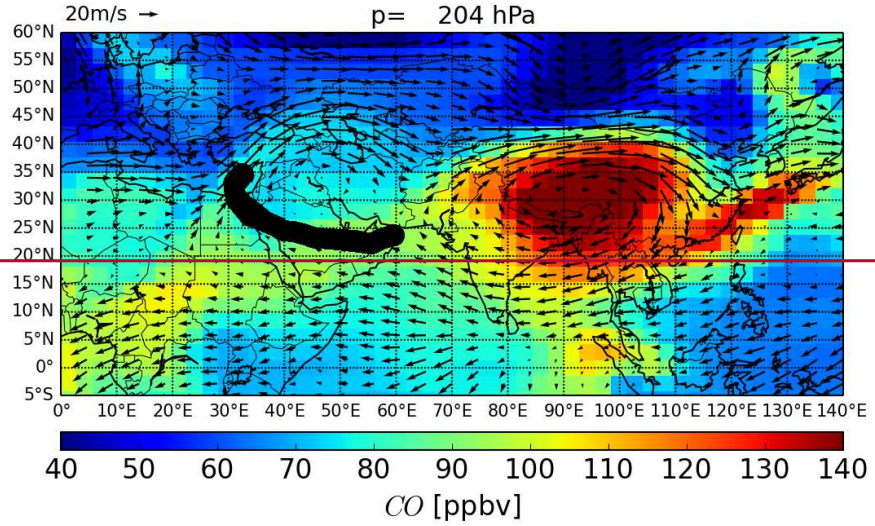
20m/s
p= 204 hPa
60°N
55°N
50°N
45°N
40°N
35°N
30°N
25°N
20°N
15°N
10°N
5°N
0°
5°S
0° 10°E 20°E 30°E 40°E 50°E 60°E 70°E 80°E 90°E 100°E 110°E 120°E 130°E 140°E
40 50 60 70 80 90 100 110 120 130 140
CO [ppbv]

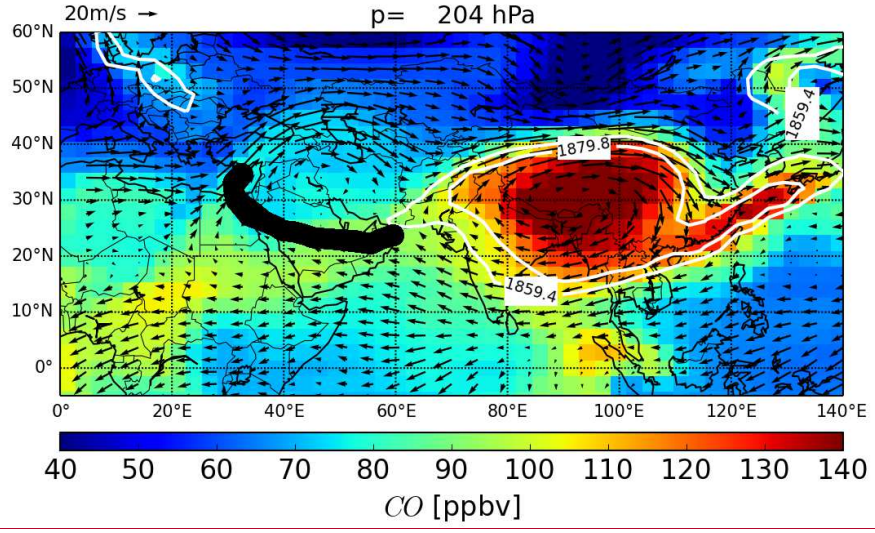
20m/s
p= 204 hPa
60°N
50°N
40°N
30°N
20°N
10°N
0°
1879.8
1859.4
1859.4
0° 20°E 40°E 60°E 80°E 100°E 120°E 140°E
40 50 60 70 80 90 100 110 120 130 140
CO [ppbv]

b)

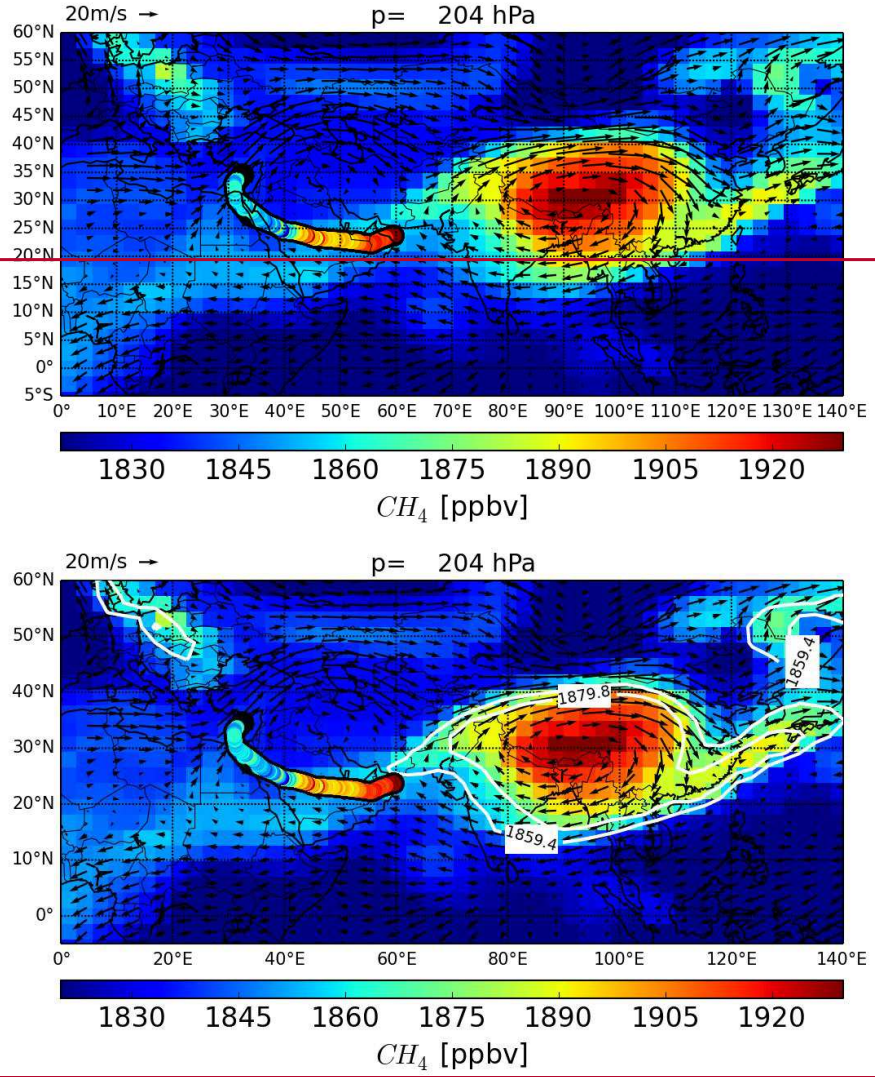
20m/s
p= 204 hPa
60°N
55°N
50°N
45°N
40°N
35°N
30°N
25°N
20°N
15°N
10°N
5°N
0°
5°S
0° 10°E 20°E 30°E 40°E 50°E 60°E 70°E 80°E 90°E 100°E 110°E 120°E 130°E 140°E
1830 1845 1860 1875 1890 1905 1920
CH_4 [ppbv]
20m/s
p= 204 hPa
60°N
50°N
40°N
30°N
20°N
10°N
0°
1879.8
1859.4
1859.4
0° 20°E 40°E 60°E 80°E 100°E 120°E 140°E
1830 1845 1860 1875 1890 1905 1920
CH_4 [ppbv]

c)

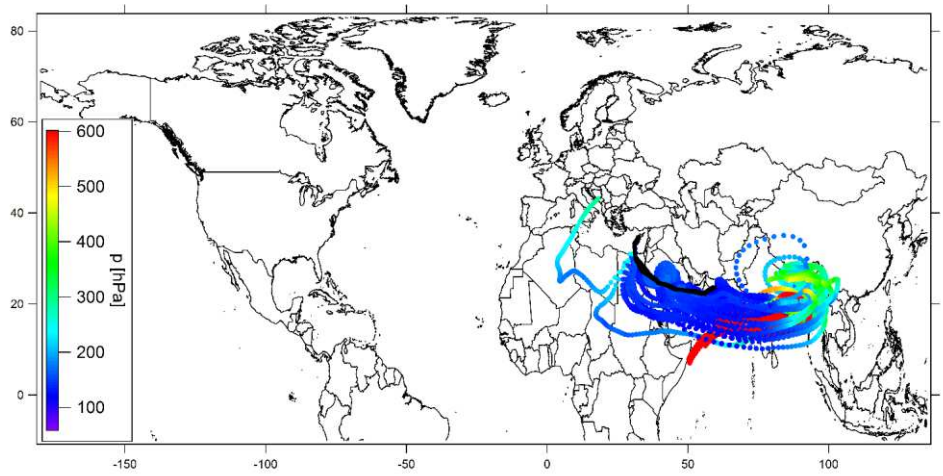

d)

Figure S10: Flight 20 (08.15.2015): measurement flight from Paphos to Paphos towards Oman.

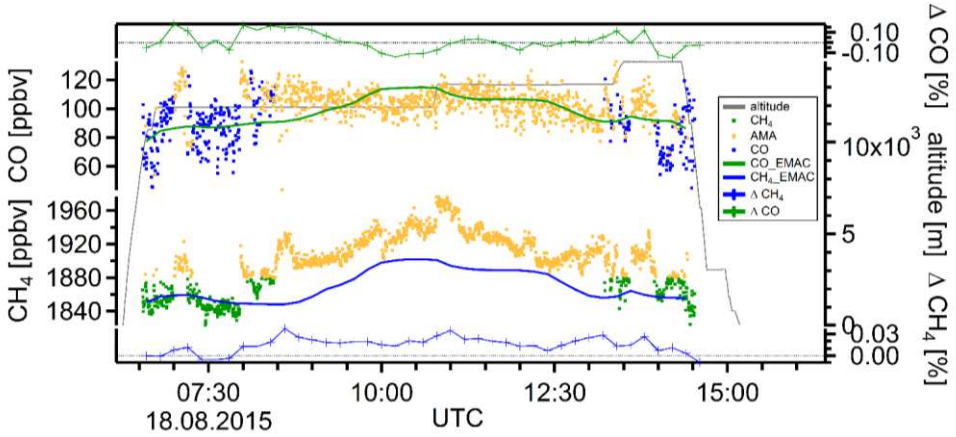

a)

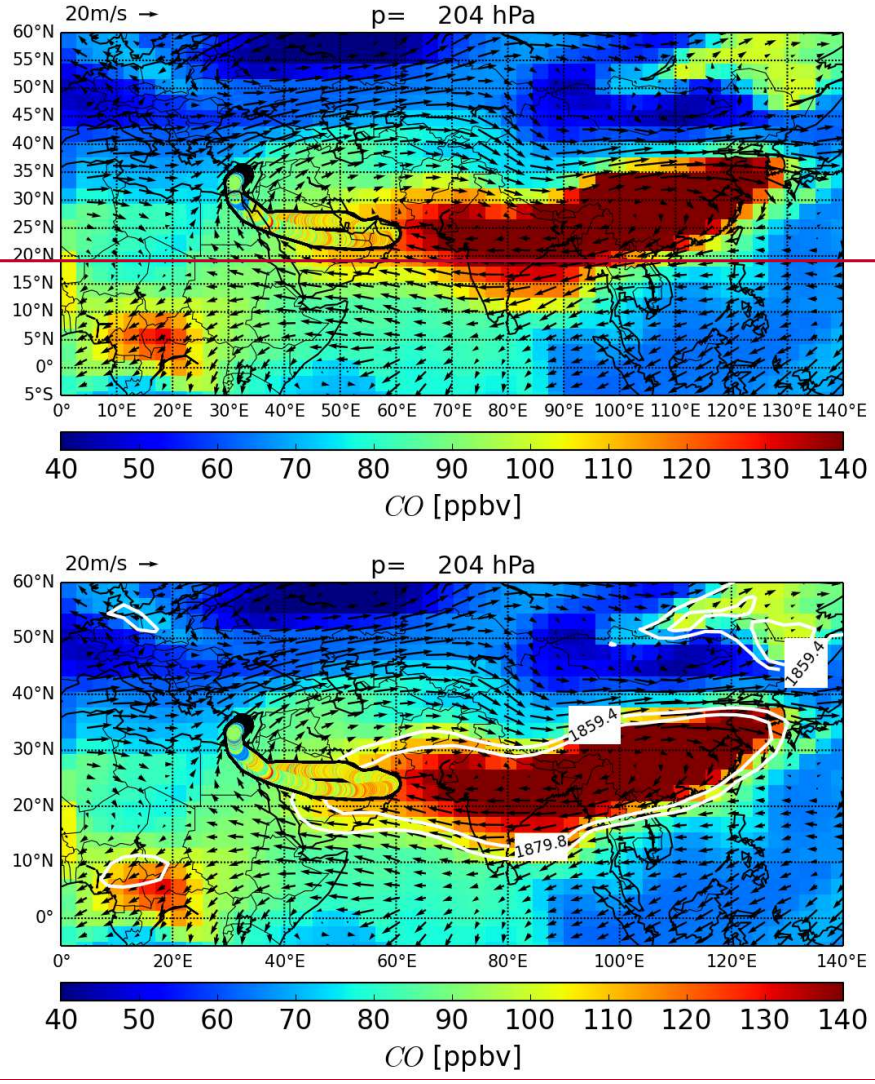
20m/s
p= 204 hPa
60°N
55°N
50°N
45°N
40°N
35°N
30°N
25°N
20°N
15°N
10°N
5°N
0°
5°S
0° 10°E 20°E 30°E 40°E 50°E 60°E 70°E 80°E 90°E 100°E 110°E 120°E 130°E 140°E
40 50 60 70 80 90 100 110 120 130 140
CO [ppbv]
20m/s
p= 204 hPa
60°N
50°N
40°N
30°N
20°N
10°N
0°
1859.4
1859.4
1879.8
0° 20°E 40°E 60°E 80°E 100°E 120°E 140°E
40 50 60 70 80 90 100 110 120 130 140
CO [ppbv]

b)

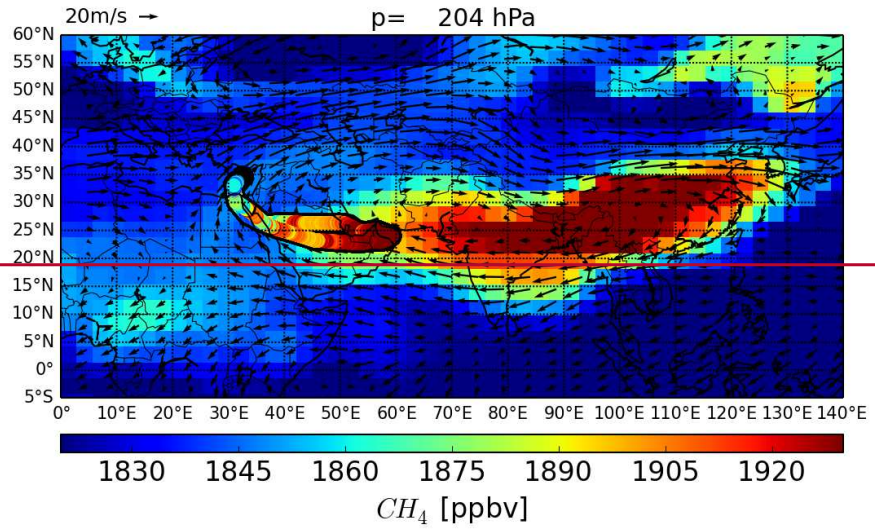
20m/s
p= 204 hPa
60°N
55°N
50°N
45°N
40°N
35°N
30°N
25°N
20°N
15°N
10°N
5°N
0°
5°S
0° 10°E 20°E 30°E 40°E 50°E 60°E 70°E 80°E 90°E 100°E 110°E 120°E 130°E 140°E
1830 1845 1860 1875 1890 1905 1920
CH_4 [ppbv]

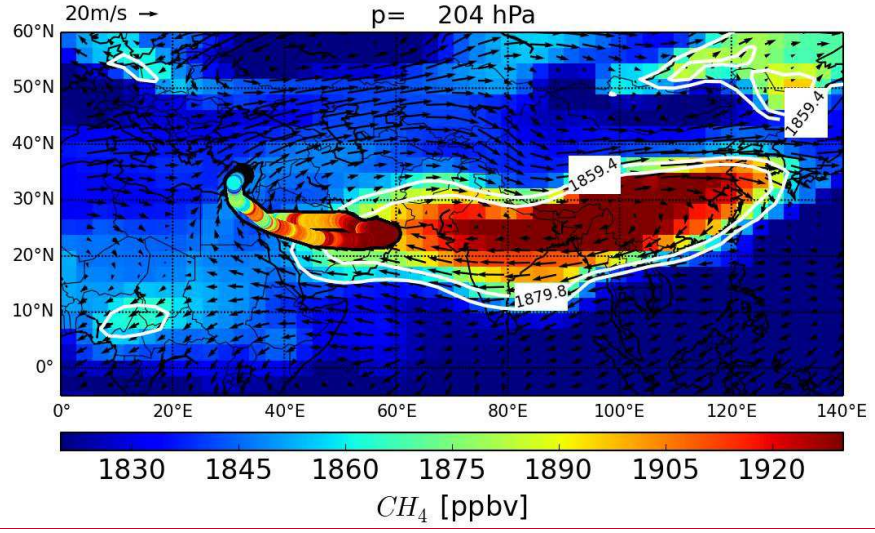
20m/s
p= 204 hPa
60°N
50°N
40°N
30°N
20°N
10°N
0°
1859.4
1859.4
1879.8
0° 20°E 40°E 60°E 80°E 100°E 120°E 140°E
1830 1845 1860 1875 1890 1905 1920
CH_4 [ppbv]

c)

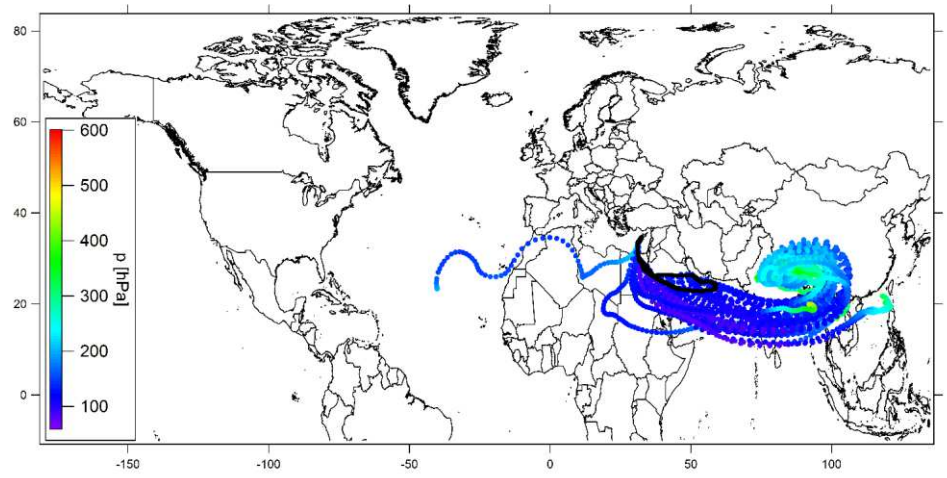

d)

Figure S11: Flight 21 (08.18.2015): measurement flight from Paphos to Paphos towards Oman.

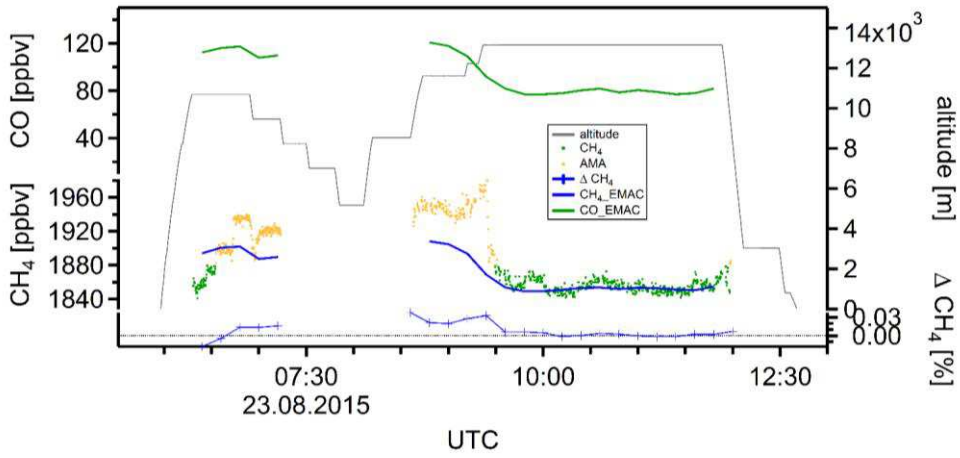

a)

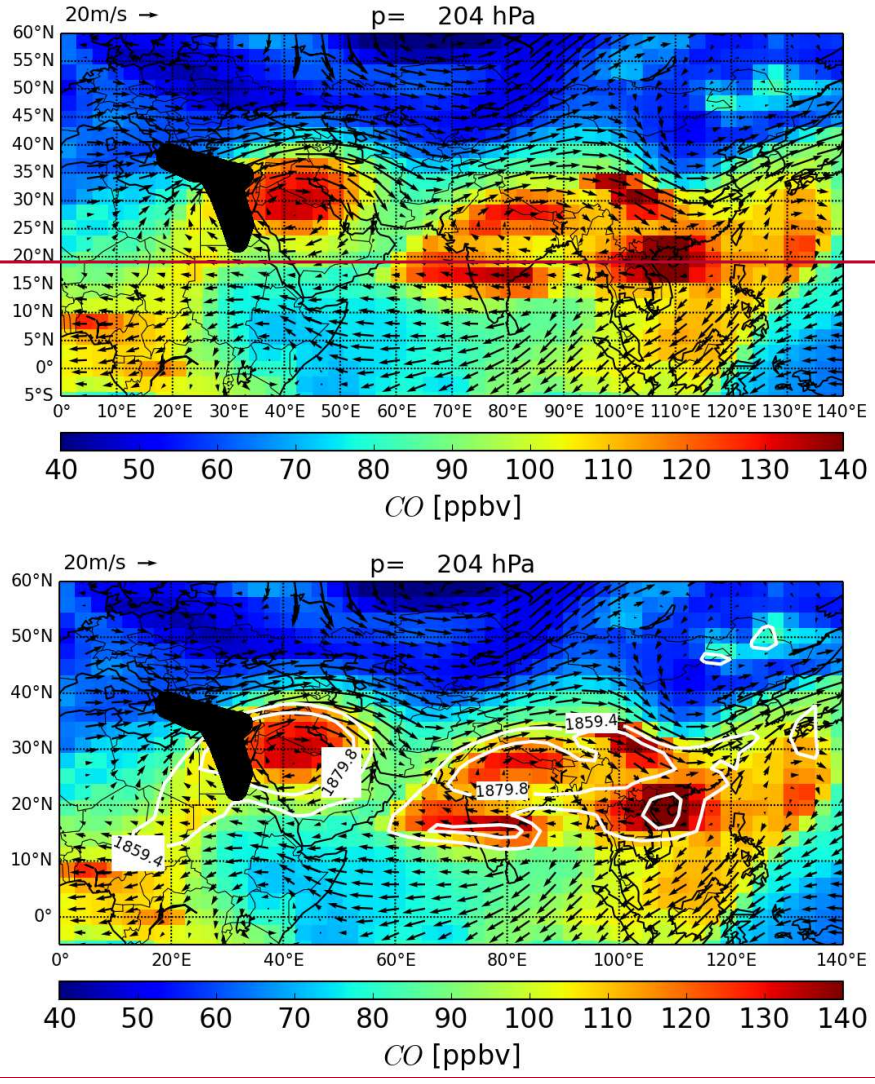
20m/s
p= 204 hPa
60°N
55°N
50°N
45°N
40°N
35°N
30°N
25°N
20°N
15°N
10°N
5°N
0°
5°S
0° 10°E 20°E 30°E 40°E 50°E 60°E 70°E 80°E 90°E 100°E 110°E 120°E 130°E 140°E
40 50 60 70 80 90 100 110 120 130 140
CO [ppbv]
20m/s
p= 204 hPa
60°N
50°N
40°N
30°N
20°N
10°N
0°
1859.4
1879.8
1879.8
1859.4
0° 20°E 40°E 60°E 80°E 100°E 120°E 140°E
40 50 60 70 80 90 100 110 120 130 140
CO [ppbv]

b)

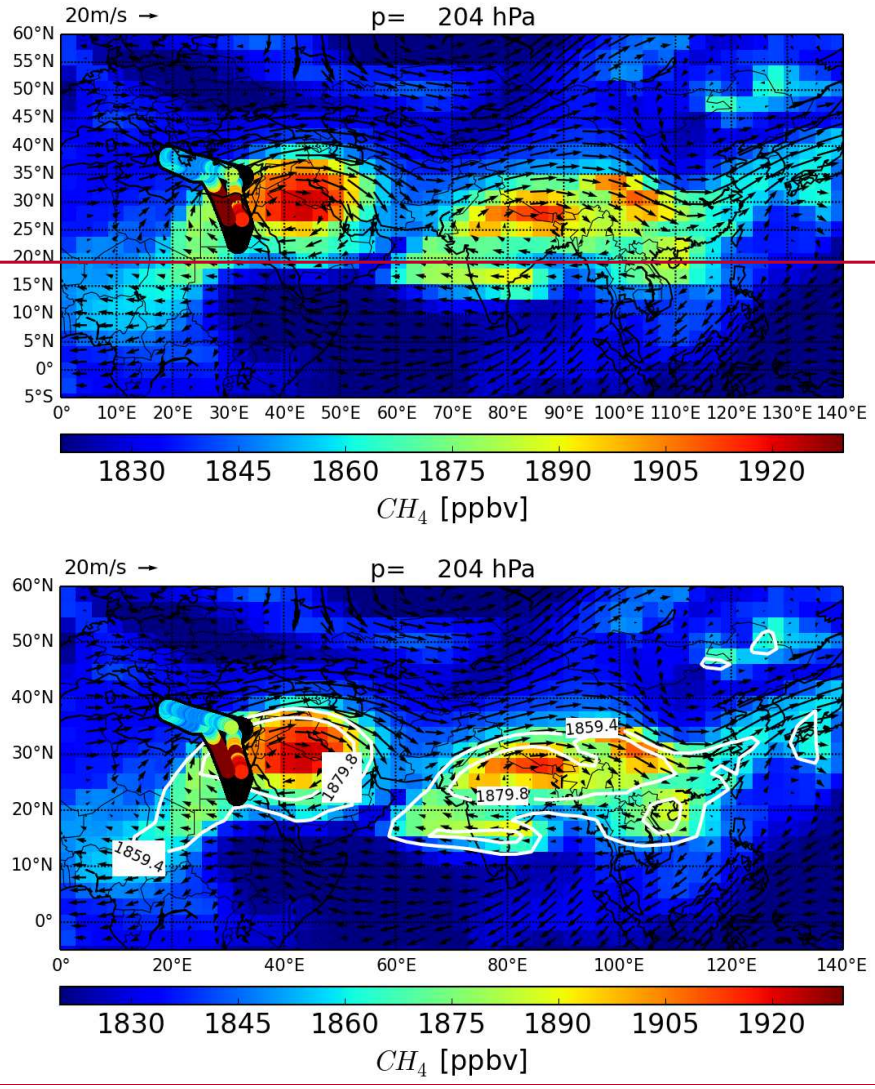
20m/s
p= 204 hPa
60°N
55°N
50°N
45°N
40°N
35°N
30°N
25°N
20°N
15°N
10°N
5°N
0°
5°S
0° 10°E 20°E 30°E 40°E 50°E 60°E 70°E 80°E 90°E 100°E 110°E 120°E 130°E 140°E
1830 1845 1860 1875 1890 1905 1920
CH_4 [ppbv]
20m/s
p= 204 hPa
60°N
50°N
40°N
30°N
20°N
10°N
0°
1859.4
1879.8
1879.8
1859.4
0° 20°E 40°E 60°E 80°E 100°E 120°E 140°E
1830 1845 1860 1875 1890 1905 1920
CH_4 [ppbv]

c)

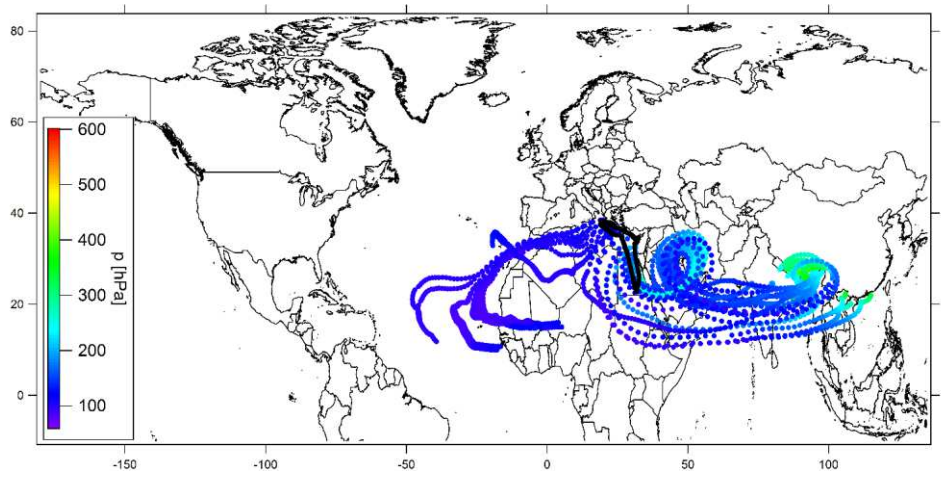

d)

Figure S12: Flight 22 (08.23.2015): measurement flight from Paphos to Paphos over Egypt, Greece, the Mediterranean; with profiles over Egypt.

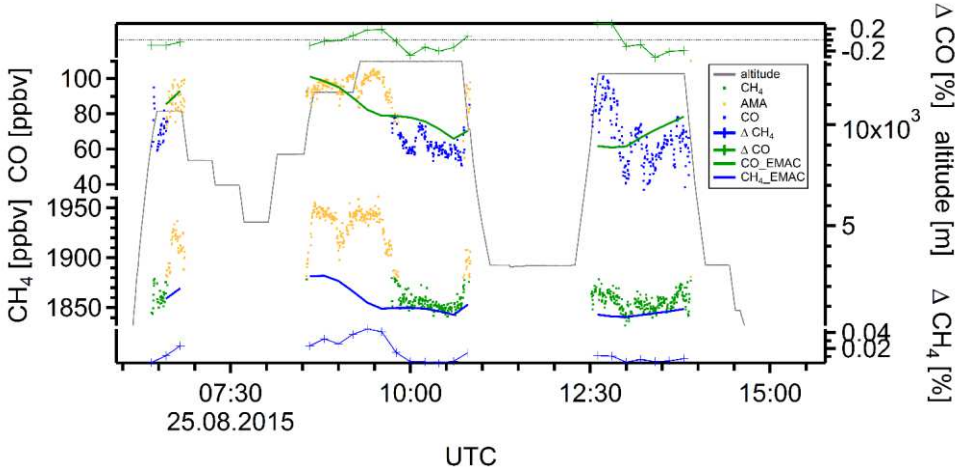

a)

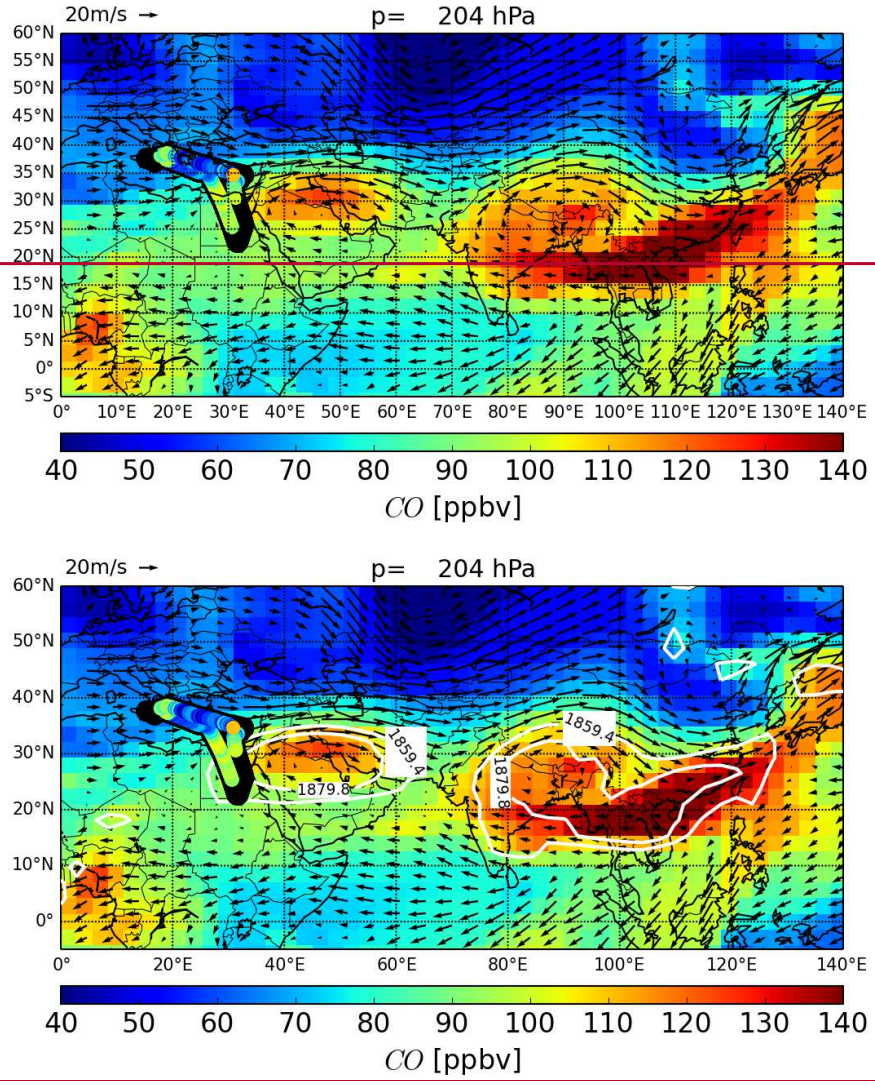
20m/s
p= 204 hPa
60°N
55°N
50°N
45°N
40°N
35°N
30°N
25°N
20°N
15°N
10°N
5°N
0°
5°S
0° 10°E 20°E 30°E 40°E 50°E 60°E 70°E 80°E 90°E 100°E 110°E 120°E 130°E 140°E
40 50 60 70 80 90 100 110 120 130 140
CO [ppbv]
20m/s
p= 204 hPa
60°N
50°N
40°N
30°N
20°N
10°N
0°
1859.4
1879.8
0° 20°E 40°E 60°E 80°E 100°E 120°E 140°E
40 50 60 70 80 90 100 110 120 130 140
CO [ppbv]

b)

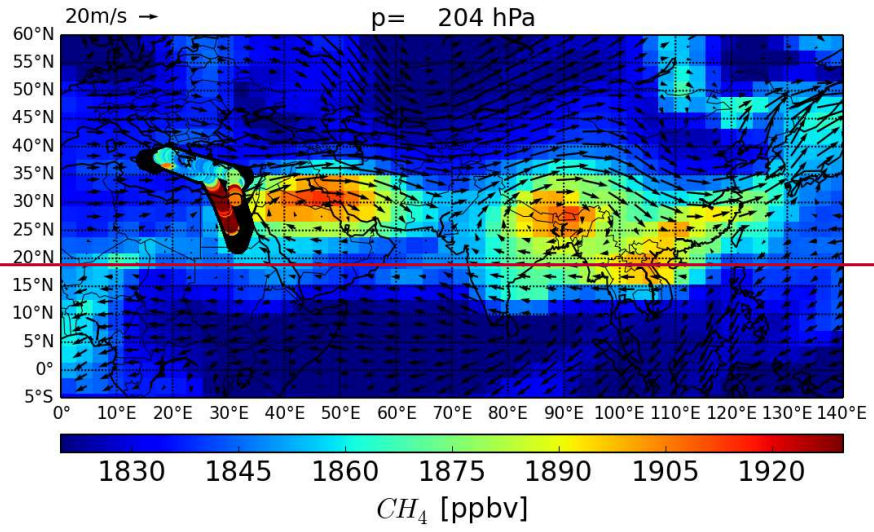
20m/s
p= 204 hPa
60°N
55°N
50°N
45°N
40°N
35°N
30°N
25°N
20°N
15°N
10°N
5°N
0°
5°S
0° 10°E 20°E 30°E 40°E 50°E 60°E 70°E 80°E 90°E 100°E 110°E 120°E 130°E 140°E
1830 1845 1860 1875 1890 1905 1920
CH_4 [ppbv]

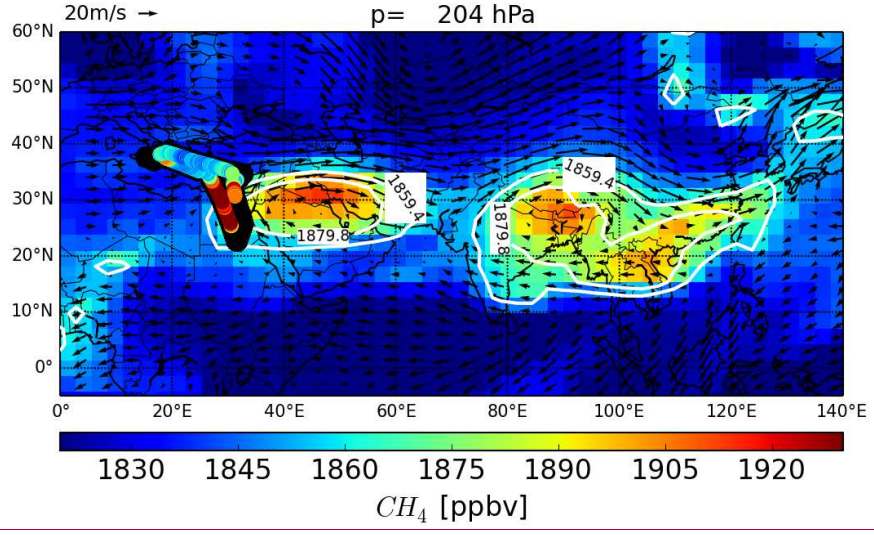
20m/s
p= 204 hPa
60°N
50°N
40°N
30°N
20°N
10°N
0°
1859.4
1879.8
1859.4
1879.8
0° 20°E 40°E 60°E 80°E 100°E 120°E 140°E
1830 1845 1860 1875 1890 1905 1920
CH_4 [ppbv]

c)

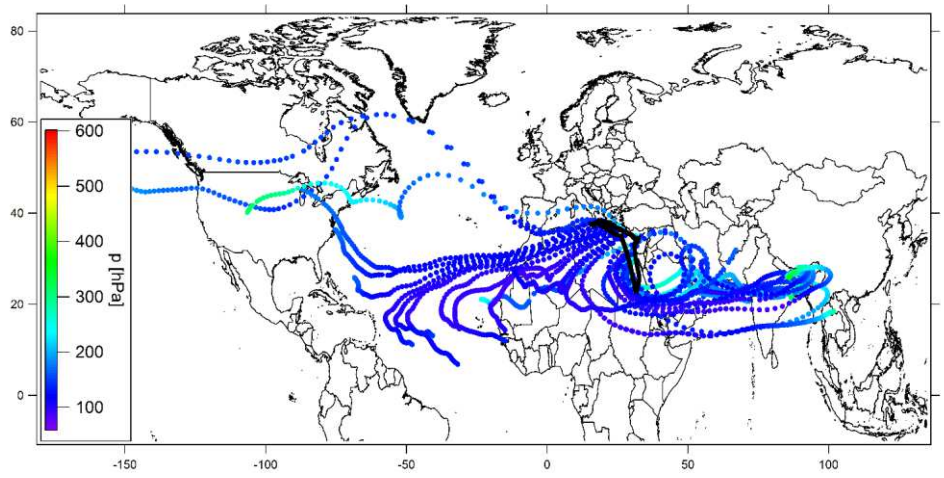

d)

Figure S13: Flight 23 (08.25.2015): measurement flight from Paphos to Paphos over Egypt, Etna, the Mediterranean; with profiles over Egypt and low altitude at the Etna.

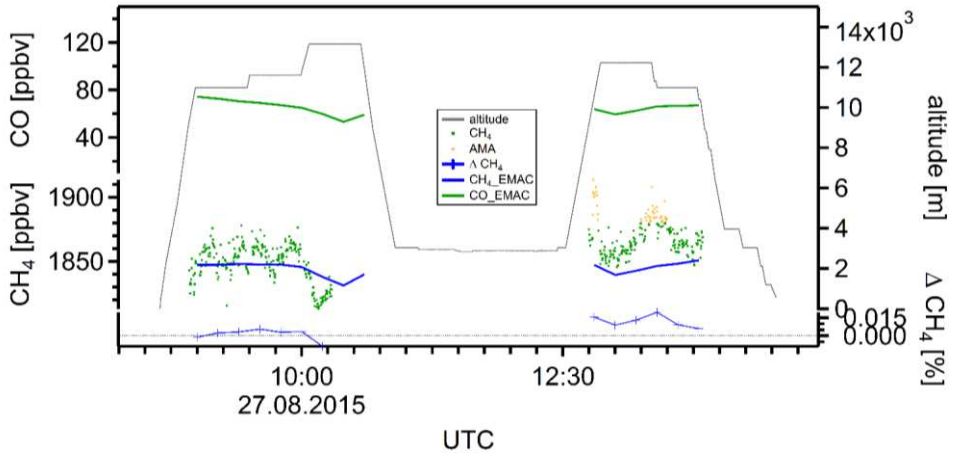

a)

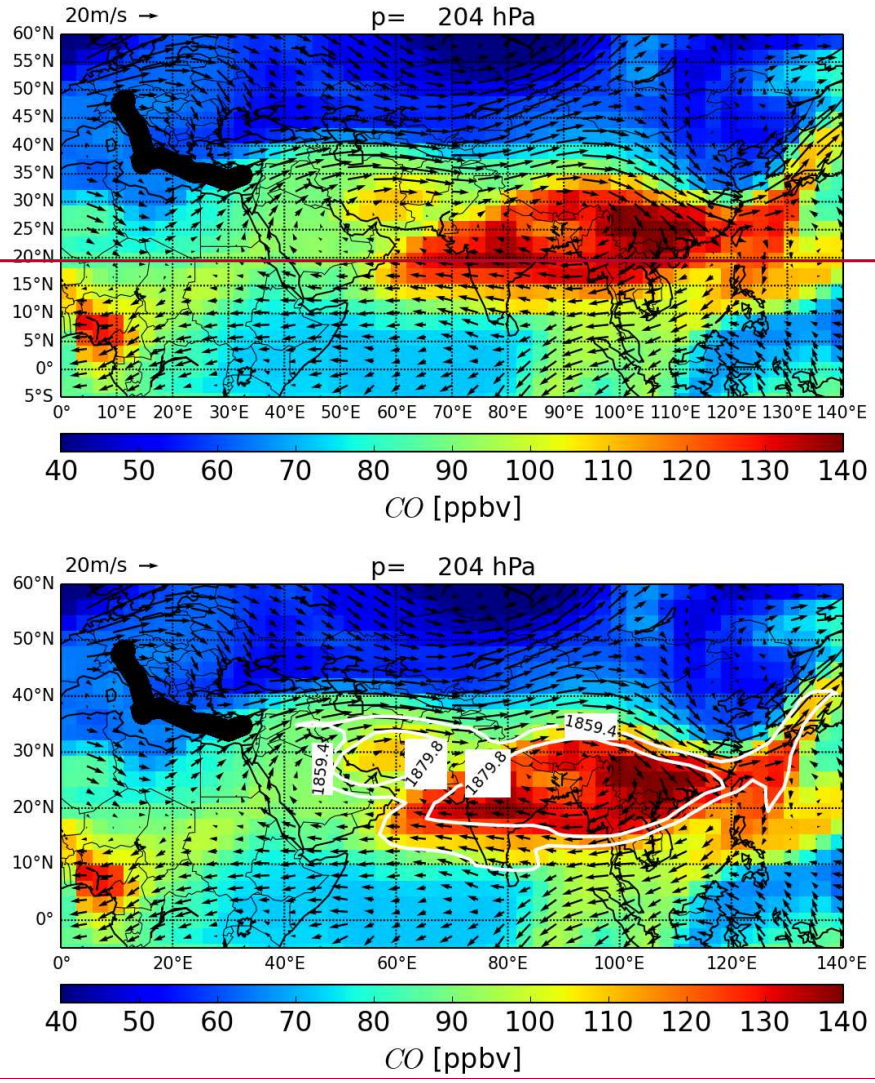
20m/s
p= 204 hPa
60°N
55°N
50°N
45°N
40°N
35°N
30°N
25°N
20°N
15°N
10°N
5°N
0°
5°S
0° 10°E 20°E 30°E 40°E 50°E 60°E 70°E 80°E 90°E 100°E 110°E 120°E 130°E 140°E
40 50 60 70 80 90 100 110 120 130 140
CO [ppbv]
20m/s
p= 204 hPa
60°N
50°N
40°N
30°N
20°N
10°N
0°
0° 20°E 40°E 60°E 80°E 100°E 120°E 140°E
1859.4
1879.8
1879.8
1859.4
40 50 60 70 80 90 100 110 120 130 140
CO [ppbv]

b)

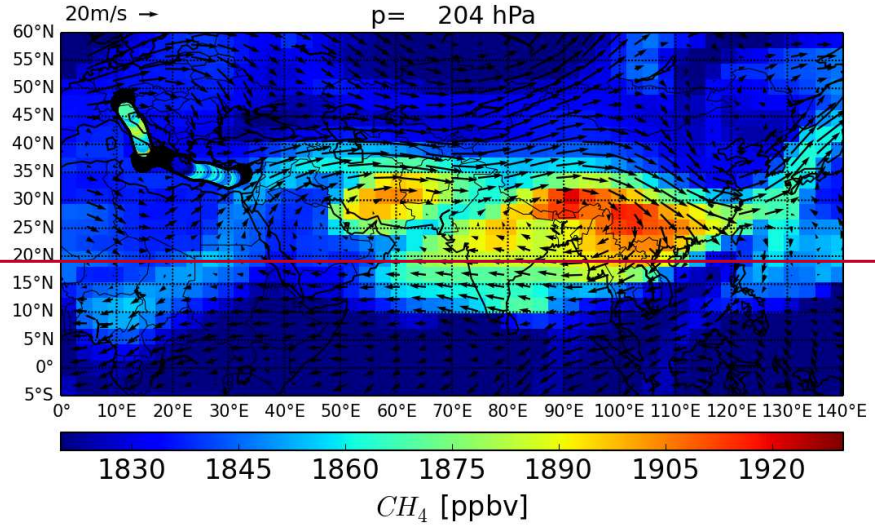
20m/s
p= 204 hPa
60°N
55°N
50°N
45°N
40°N
35°N
30°N
25°N
20°N
15°N
10°N
5°N
0°
5°S
0° 10°E 20°E 30°E 40°E 50°E 60°E 70°E 80°E 90°E 100°E 110°E 120°E 130°E 140°E
1830 1845 1860 1875 1890 1905 1920
CH_4 [ppbv]

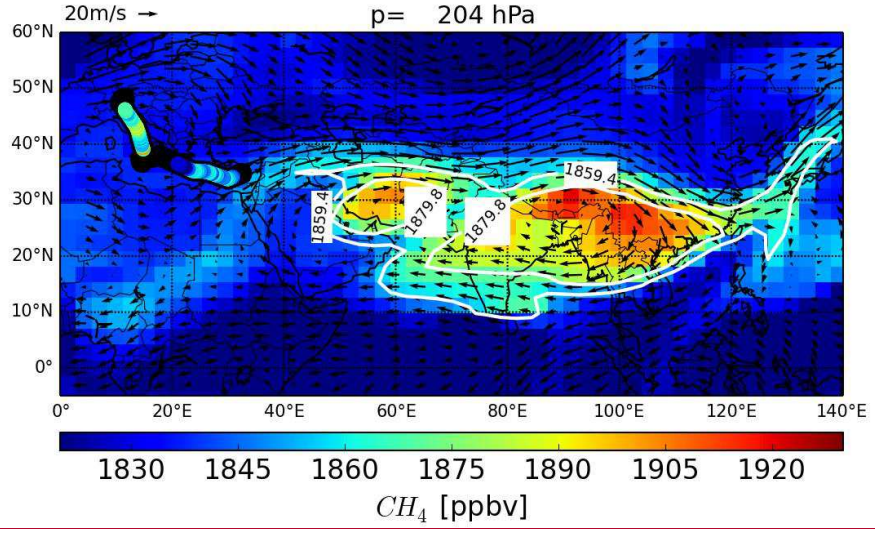
20m/s
p= 204 hPa
60°N
50°N
40°N
30°N
20°N
10°N
0°
1859.4
1879.8
1879.8
1859.4
0° 20°E 40°E 60°E 80°E 100°E 120°E 140°E
1830 1845 1860 1875 1890 1905 1920
CH_4 [ppbv]

c)

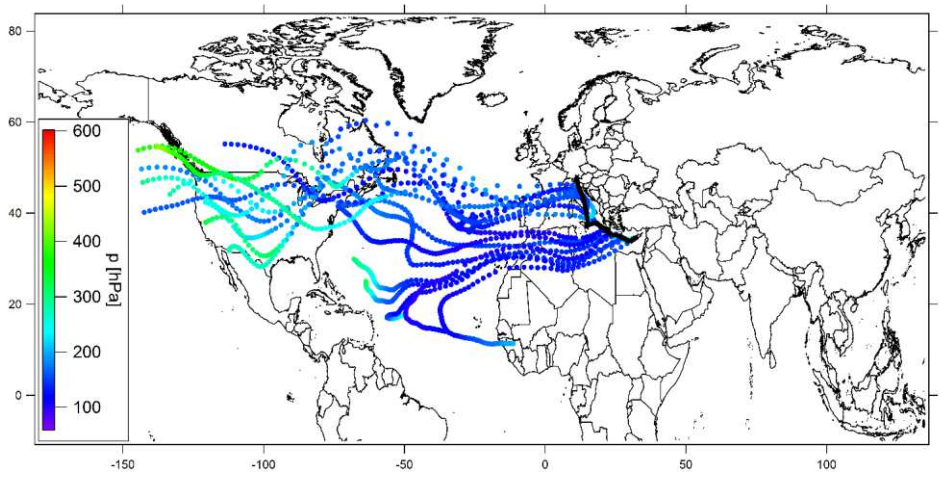

d)

Figure S14: Flight 24 (08.27.2015): transfer flight from Paphos to Oberpfaffenhofen via Etna with low altitude.